AgRISTARS

A Joint Program for Agriculture and Resources Inventory Surveys Through Aerospace Remote Sensing

Supporting Research

November 1981

MARS X-BAND SCATTEROMETER

Paul F. Gabel, Jr., Fawwaz T. Ulaby, and David R. Brunfeldt

University of Kansas Center for Research Inc.
Remote Sensing Laboratory
Campus West
Lawrence, Kansas 66045

Lyndon B. Johnson Space Center
Houston, Texas 77058

1. Report No.	2. Government Accession No.	3. Recipient's Catalog No.
RSL TR 360-14		

4. Title and Subtitle	5. Report Date
MARS X-BAND SCATTEROMETER	November 1981
	6. Performing Organization Code

7. Author(s)	8. Performing Organization Report No.
Paul F. Gabel, Jr., Fawwaz T. Ulaby, David R. Brunfeldt	
	10. Work Unit No.

9. Performing Organization Name and Address	11. Contract or Grant No.
Remote Sensing Laboratory University of Kansas Center for Research, Inc. 2291 Irving Hill Drive - Campus West Lawrence, Kansas 66045	NAS9-15427
	13. Type of Report and Period Covered
12. Sponsoring Agency Name and Address	Interim Report
NATIONAL AERONAUTICS AND SPACE ADMINISTRATION Lyndon B. Johnson Space Center Houston, Texas 77058 Technical Monitor: Jack F. Paris	14. Sponsoring Agency Code

15. Supplementary Notes

16. Abstract

This document describes the design, construction, and data-collection procedures of the Mobile Agricultural Radar Sensor (MARS) X-band scatterometer. This system is an inexpensive, highly mobile, truck-mounted FM-CW radar operating at a center frequency of 10.2 GHz. The antennas, which allow for VV and VH polarizations, are configured in a side-looking mode that allows for drive-by data collection. This configuration shortens fieldwork time considerably while increasing statistical confidence in the data. Both internal calibration, via a delay line, and external calibration with a Luneberg lens are used to calibrate the instrument in terms of σ°. The radar scattering cross-section per unit area, σ°, is found using the radar equation.

17. Key Words (Suggested by Author(s))	18. Distribution Statement
Radar, Scatterometer, Remote Sensing, Earth Resources, Agriculture, Microwaves	

19. Security Classif. (of this report)	20. Security Classif. (of this page)	21. No. of Pages	22. Price*
Unclassified	Unclassified	131	

*For sale by the National Technical Information Service, Springfield, Virginia 22161

RSL Remote Sensing Laboratory

The University of Kansas Center for Research, Inc.
2291 Irving Hill Drive-Campus West, Lawrence, Kansas 66045

Telephone: (913) 864-4832

MARS X-BAND SCATTEROMETER

Remote Sensing Laboratory
RSL Technical Report 360-14

Paul F. Gabel, Jr.

Fawwaz T. Ulaby

David R. Brunfeldt

November 1981

Fawwaz T. Ulaby, Principal Investigator

Supported by:
NATIONAL AERONATUICS AND SPACE ADMINISTRATION
Lyndon B. Johnson Space Center
Houston, Texas 77058

CONTRACT NAS 9-15421

ABSTRACT

This document describes the design, construction, and data-collection procedures of the Mobile Agricultural Radar Sensor (MARS) X-band scatterometer. This system is an inexpensive, highly mobile, truck-mounted FM-CW radar operating at a center frequency of 10.2 GHz. The antennas, which allow for VV and VH polarizations, are configured in a side-looking mode that allows for drive-by data collection. This configuration shortens fieldwork time considerably while increasing statistical confidence in the data. Both internal calibration, via a delay line, and external calibration with a Luneberg lens are used to calibrate the instrument in terms of σ^{o}. The radar scattering cross-section per unit area, σ^{o}, is found using the radar equation.

Page intentionally left blank

TABLE OF CONTENTS

LIST OF SYMBOLS

$\Delta f = B$	Peak-to-peak RF frequency deviation
f_{IF}	Mixer output frequency
f_M	Modulation frequency
Δf_D	Decorrelation bandwidth for independence
f_d	Doppler frequency shift
R_t	Range to target
R_c	Range to lens during calibration
Δr	Range resolution
σ	Radar scattering cross-section
σ^o	Radar scattering cross-section per unit area
σ_c	Radar scattering cross-section of Luneberg lens
A_e	Antenna effective area
A_{ill}	Target illuminated area
P_t	Output power from transmit antenna
P_r	Received power at the receive antenna output
G_t	Transmit antenna gain
G_r	Receive antenna gain
G_D	Dish antenna gain
G_{HN}	Gain of standard-gain horn antenna
c	Velocity of light
λ	Wavelength
$B = \Delta f$	RF bandwidth
τ	Time delay from radar to target and back

D	Difference between mimimum and maximum distance to the scatterers in the illuminated area
β_{3dB}	Antenna half-power beamwidth
d	Antenna aperture effective diameter
θ	Angle of incidence
V^t	Receiver output voltage of target as measured by digit panel meter
V^c	Receiver output voltage of lens as measured by digit panel meter
K^t	System transfer function, V^t/P_t
K^c	System transfer function, V^c/P_t
C_{VV}, C_{VH}	System calibration constant for VV-polarization, cross-polarization
L	Delay-line loss
P_{dl}	Power measured with delay line calibration
R_{ff}	Antenna far-field range
N_s	Number of independent samples due to spatial averaging
N_f	Number of independent samples due to frequency averaging
N_t	Total number of independent samples
h	Height of antennas above ground

LIST OF FIGURES

LIST OF TABLES

Page intentionally left blank

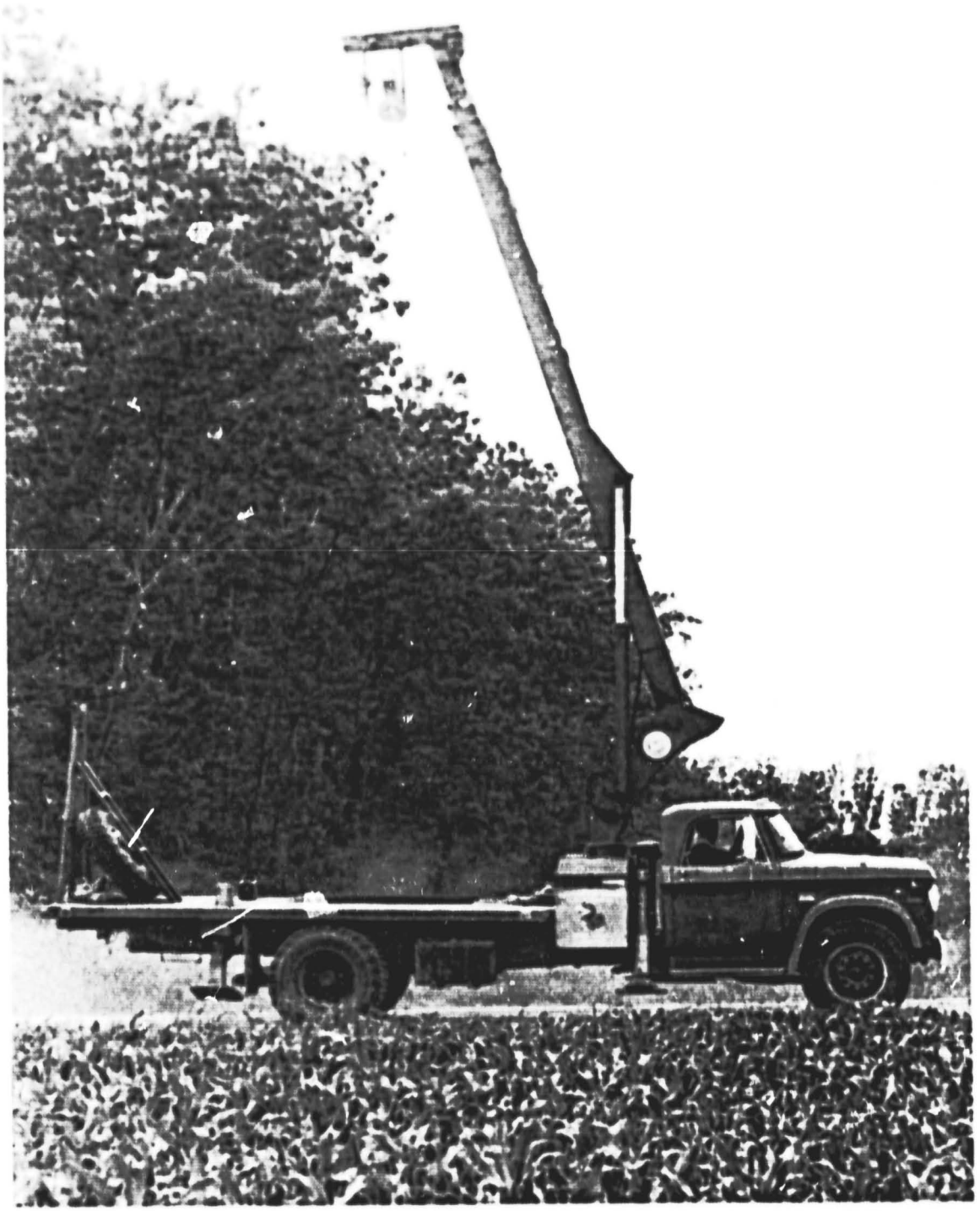

MARS X-band scatterometer in use.

1.0 INTRODUCTION

Understanding the relationships between the radar backscattering coefficient of vegetation and the physical parameters of the vegetation volume and underlying soil surface is a key step in the evolution process of radar remote sensing techniques towards their use on an operational basis for monitoring agricultural productivity. These relationships are determined through the development of theoretical models and experimental investigations. Although extensive experimental studies have been conducted over the past two decades [1-27], most of the work has been performed by only a few institutions. This is due, in part, to the high cost and complexity of microwave scatterometers [28-32] when compared, for example, to optical radiometers.

The purpose of this investigation is to design, construct and test a prototype model of a microwave scatterometer that meets the following four basic criteria: it is (a) suitable for crop observations, (b) calibrated, (c) simple to operate, and (d) low cost (≈ $10 K). These objectives were indeed realized, as discussed in the following sections, which describe the operation of the system and provide a guide for duplicating it and testing its sub-sections. For the purpose of easy reference, the system has been named MARS, an acronym for Mobile Agricultural Radar System.

2.0 GENERAL THEORY AND SYSTEM OPERATION

The MARS system is a calibrated FM-CW scatterometer designed for measuring the scattering properties of targets at X-band. The scattering properties are a function of the complex dielectric constant and roughness of the target, as well as local angle of incidence, polarization, and frequency. This system works in the X-band region at a center frequency of 10.2 GHz. Results from the MARS system can be readily compared to data measured by other radars, or they may be used to calibrate an uncalibrated system. Table 1 gives a brief listing of the system parameters. Figures 1 and 2 show the RF- and control-sections, respectively.

2.1 Design Objectives

The MARS system was designed to meet the following objectives:

a. allow operation in the X-band region,

b. allow for 40 dB dynamic range of σ^{o},

c. be operationally simple,

d. have dual-polarization capabilities (VV and VH),

e. offer an inexpensive construction cost,

f. be capable of 30° - 70° angular range from the vertical,

g. be highly mobile and able to take data from a moving vehicle,

h. have internal and external calibration capabilities,

i. have the ability to determine range,

j. provide reasonable frequency averaging,

k. be operable by a single individual.

TABLE 1

MARS System Parameters

Type		FM-CW
Modulation		Triangular
Frequency: f_0		10.2 GHz
RF Bandwidth: Δf		420 MHz
Transmitter Power		60 mW
IF Frequency: f_{IF}		22 kHz
Antennas:		
Height above ground		9.3 m
Transmit antenna diameter		30 cm
Cross-polarization antenna		standard gain horn
Transmit feed		dual dipole
Beamwidths of product patterns $(G_T(\theta,\phi) \cdot G_R(\theta,\phi))$		
	VV Elevation :	3.96°
	Azimuth :	4.31°
	VH Elevation :	5.44°
	Azimuth :	5.14°
Look Angle Range:	θ	20°- 80° from vertical
Dynamic Range:		50 dB

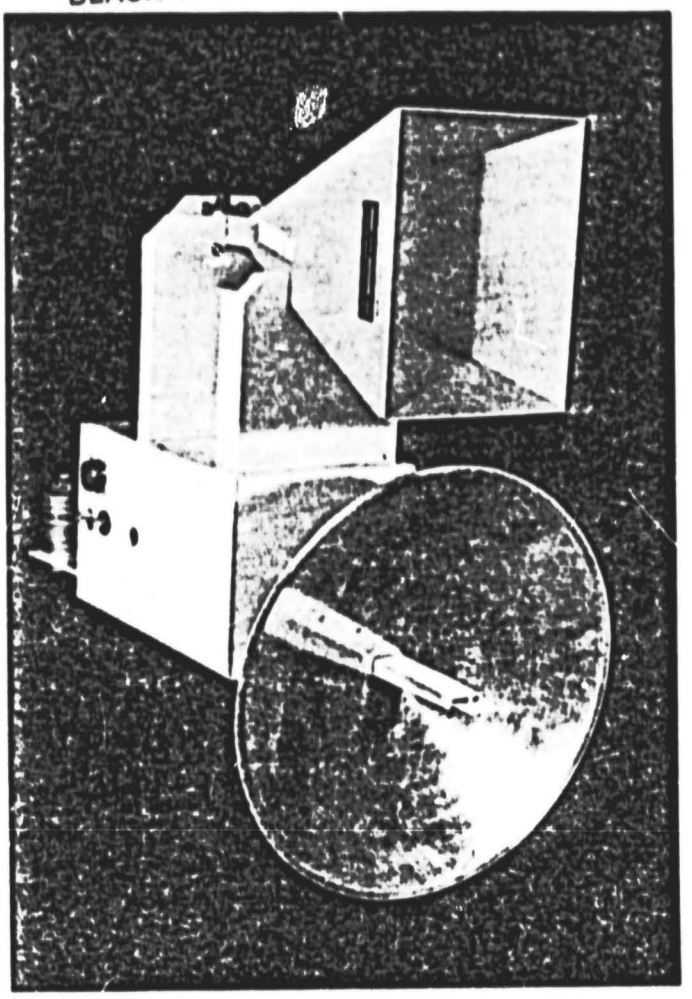

Figure 1. MARS RF section.

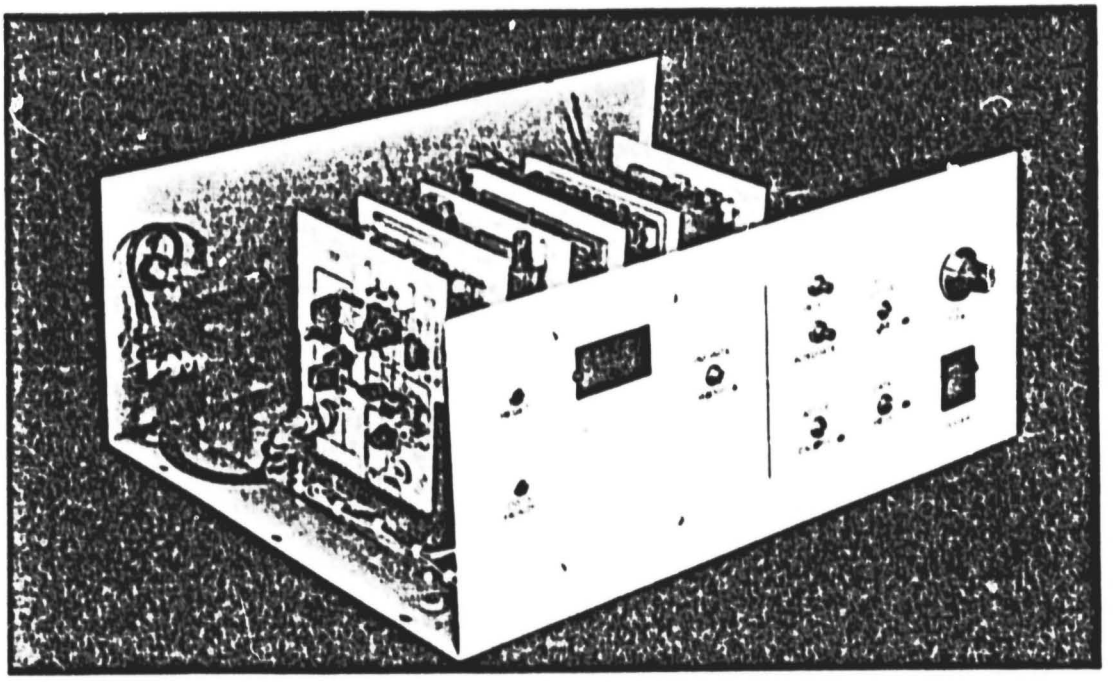

Figure 2. MARS IF/control section.

2.2 General FM-CW Radar

Figure 3 depicts a simplified block-diagram of an FM-CW radar. A triangle generator is used to frequency modulate an oscillator to produce an FM-CW signal. A small portion of the transmitted signal is tapped off by the coupler to provide a reference local-oscillator (LO) signal to the mixer. The transmitted signal illuminates the target, part of it is backscattered, and then received by the receive antenna after a delay of 2 R/c seconds. The signal enters the RF port of the mixer, is mixed with the LO signal, and the intermediate frequency (IF) signal is generated at the mixer output. Knowledge of the FM rate and the propagation velocity provides the information necessary to determine the range to target.

2.3 Derivation of IF Equation

A simplified representation of the transmitted and received signals in the time domain is shown in Figure 4. Arbitrarily beginning the transmit signal at time t = 0, we know from propagation theory that the received signal is delayed by 2 R/c seconds and that one full cycle of the transmit wave occurs every $(f_M)^{-1}$ seconds. As a point of interest, the delay time is typically less than 0.01% of the total cycle time, so the figure shown is exaggerated. The vertical displacement or difference, if we think in terms of the mixing process, between the two signals is the IF frequency, f_{IF}, and is a function of the FM rate. The center frequency, f_0, is set at 10.2 GHz and is modulated about that point by $\pm \Delta f/2$ where Δf is 420 MHz.

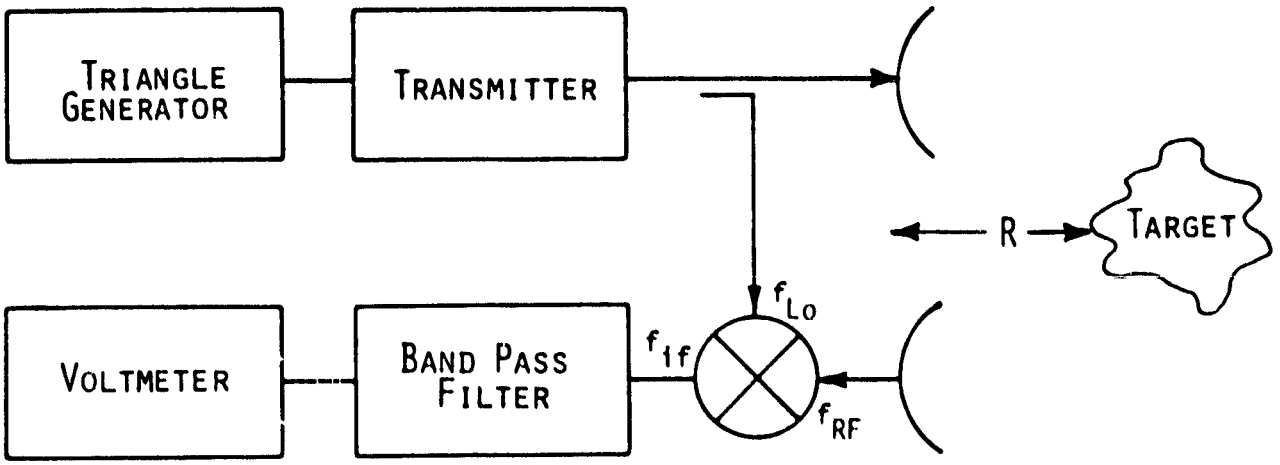

Figure 3. Block diagram of a simple FM-CW radar.

Figure 5 shows the relationship of all the parameters laid out in the form of similar triangles. From this representation we can derive the IF equation as:

$$\frac{f_{IF}}{\Delta f/2} = \frac{2\ R/c}{1/4\ f_M} \quad . \tag{1}$$

Solving Equation (1) for f_{IF} yields a simple expression for the IF frequency:

$$f_{IF} = \frac{4R\Delta f f_M}{C} \quad . \tag{2}$$

The MARS system uses a bandpass filter to fix f_{IF} at 22 kHz while Δf and c are known constants. With this in mind, we see that there is a deterministic relationship between the range to target and the modulation rate. Equation (2) does not take into account delays due to propagation between the antennas and the mixer. A more exact form determined through measurements is given by (28).

2.4 Radar Equation

For a narrow-beam antenna observing a distributed target, the radar equation is given by:

$$P_r = \frac{P_t\ G_t\ G_r\ \lambda^2\ A_{ill}\ \sigma^o}{(4\pi)^3\ R^4} \quad . \tag{3}$$

In calculating σ^o from this equation, a few assumptions are made.

1. Antenna gains are constant over the area of illumination.
2. The range to target is constant over the illuminated area.
3. The illuminated area is relatively homogeneous.

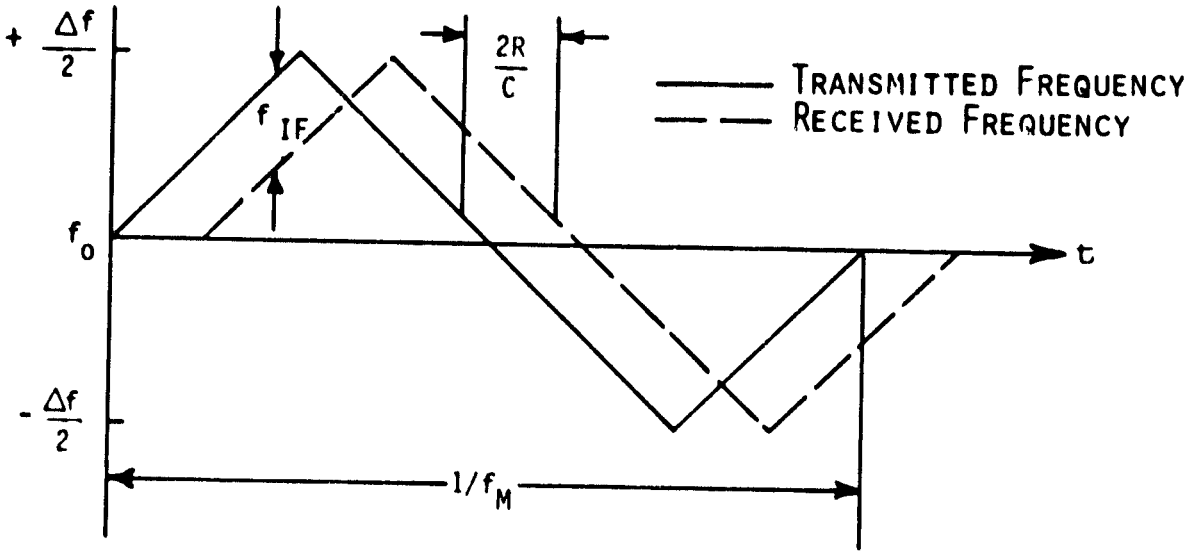

Figure 4. Transmitted and received frequency versus time.

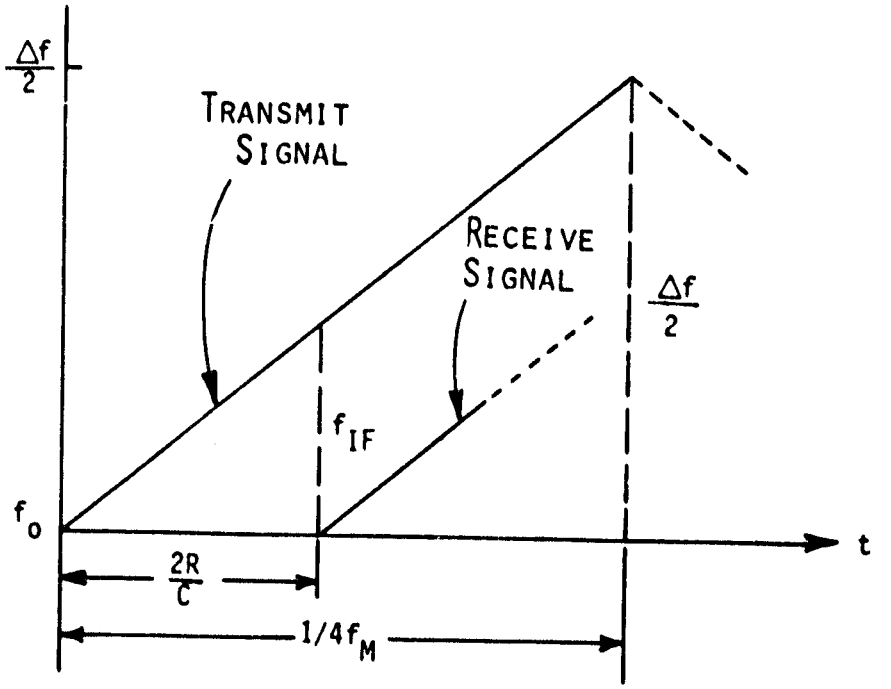

Figure 5. Similar triangle representation used to determine f_{IF}.

All of these assumptions are reasonable for narrow-beam antennas. The widest beamwidth for the MARS system is less than 5.5°, therefore these assumptions are valid for this system as well.

2.5 Statistical Properties

Since a calibrated scatterometer is a fully coherent instrument, fading can be a serious problem unless some means to minimize it is exercised. Fading is a result of constructive and destructive interference of the signals backscattered from scattering elements within the illuminated area (or volume). In radar images, fading shows up as speckle and is a result of the coherent nature of the receiver.

The process of averaging can be used to minimize the effects of fading and therefore increase the statistical confidence associated with the measured data. Frequency and spatial averaging, which together serve to increase the number of independent samples averaged into each value of σ^o, are employed in the MARS system. The importance of averaging is evident in Figure 6, where the 5% and 95% confidence levels are plotted as a function of the number of independent samples for a fading signal described by the Rayleigh distribution. The total number of independent samples N_t is given by

$$N_t = N_s \cdot N_f \qquad (4)$$

where

N_s = number of independent samples due to spatial averaging

N_f = number of independent samples due to frequency averaging

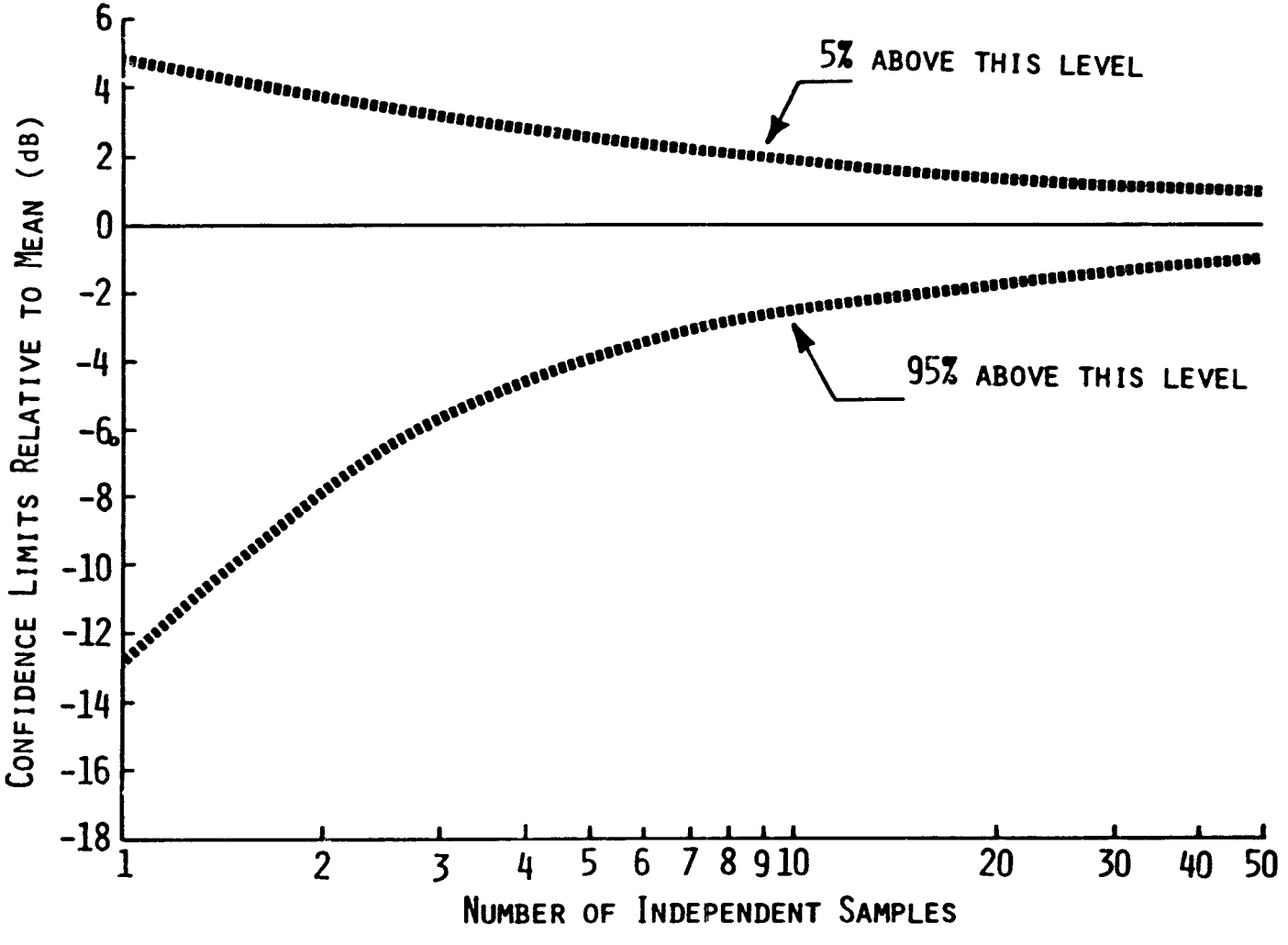

Figure 6. Ninety-percent confidence interval for Rayleigh distribution.

N_f takes on a simple expression

$$N_f = \frac{B}{\Delta f_D} \tag{5}$$

where

B = system RF bandwidth (= Δf for the MARS)

Δf_D = decorrelation bandwidth for independence.

In terms of the geometry of Figure 7,

$$\Delta f_D = \frac{150\ (10^6)}{D} \quad , \text{Hz} \tag{6}$$

where

$$D = h\ [\sec\ (\theta + \beta/2) - \sec\ (\theta - \beta/2)] \tag{7}$$

β = antenna elevation plane half-power beamwidth.

For the MARS system, B = 420 MHz which when substituted into (5) and (6) leads to:

$$N_f = 2.8D \tag{8}$$

Table 2 lists values of N_f for various angles of incidence assuming a platform height of 9 meters. Note that this expression is valid only if the IF spectrum is not filter-limited by the band-pass filter. In the event filter limiting occurs, the range resolution is given by

$$\Delta r = \frac{r\Delta f_{IF}}{f_{IF}} \tag{9}$$

where

Δf_{IF} = bandwidth of IF filter; set at 6.6 kHz

F_{IF} = IF center frequency; set at 22 kHz.

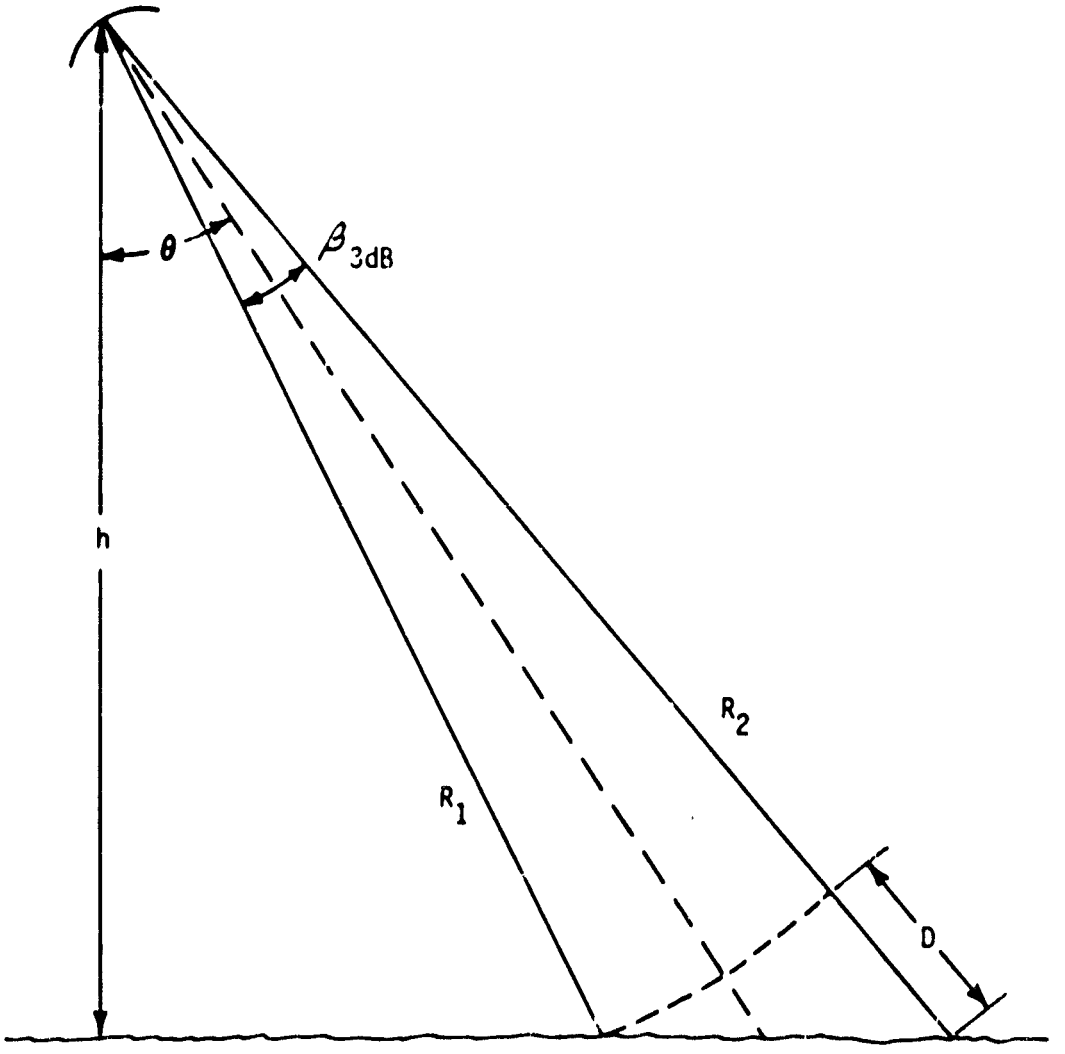

Figure 7. Geometry used to calculate Δf_D.

TABLE 2

Number of Independent Samples
Due to Frequency Averaging, N_f

θ	N_f
20°	1.00
30°	1.17
40°	1.9[illegible]
50°	3.27
60°	6.12
70°	14.28

So long as D is less than Δr, Equation (19) is valid, but if D becomes larger than Δr, the value of Δr calculated from (9) should be used for D in (8). At a height of 9.0 meters, the MARS IF spectrum does not filter-limit until the angle of incidence exceeds 75°.

Spatial independence is achieved when a new area of illumination on the target is shifted from the previous one by d/2, where d is the aperture diameter. Table 3 lists values of N_s for various driving speeds when taking data, using an integration time of 17 seconds.

Table 4 lists the total number of independent samples N_t obtained for various driving speeds and angles of incidence.

2 6 Data Collection Procedure

The design of the MARS system was conceived with the idea of making data acquisition a simple and straightforward process. The first step involves external calibration against the Luneberg lens and is described thoroughly in the section on calibration. The last two steps, internal calibration and actual backscattering measurements, are performed at the site of the experiment. The following procedure was developed at the University of Kansas and has proved to be an effective method of data collection.

2.6.1 Internal Calibration

Procedure:

1. Upon arrival at a site, be sure the system has had 30 minutes of warm-up time before use. This can be accomplished while driving to the site or upon arrival, whichever is most

TABLE 3

Number of Independent Samples
Due to Spatial Averaging, N_s

Speed (MPH)	N_s
5	249
10	498
15	748
20	997

TABLE 4

Total Number of Independent Samples
$N_t = N_s \cdot N_f$

N_t

Speed (MPH)

θ	5	10	15
20°	249	498	748
30°	291	582	875
40°	480	961	1443
50°	814	1628	2445
60°	1523	3047	4577
70°	3555	7111	10,681

convenient. Position the vehicle/radar near the field to be measured and set the angle of incidence to the desired level. Set the following switches as specified.

mode - "CALIBRATE"
polarization - "LIKE"
data - "PEAK"
display - "RADAR"

2. Adjust the "FM Rate" dial until the displayed value is maximized. Care should be taken to make sure the level is at its peak value - hence the term "peaking" the radar is used.
3. Set display switch to "FM RATE," record display on data sheet, (see Appendix C) and return switch to "RADAR" position.
4. Return data switch to "DATA" mode and depress "RESET" button, making sure the "RESET" LED comes on.
5. Depress "INTEGRATE" button. "RESET" LED should go off and display value should ramp up.
6. After one integration period (17 seconds) the "DATA READY" LED will come on and the data should be recorded promptly.

2.6.2 Backscatter Measurement

The actual backscatter measurement process is the same as for internal calibration with only a few minor differences.

1. After internal calibration, set the mode switch to "ACTIVE" and data switch to "PEAK."
2. Depress the "RESET" button to remove the stored charge from the integrator. Check "RESET" LED.
3. Making sure the radar is pointed intc a representative portion of the target and that the proper angle of incidence is set, peak the display as before. A random fluctuation in the display reading will now be noticeable. This is due to

fading, which was described earlier, and makes the peaking process more tedious. However, if care is taken to watch the envelope range of the fade, accurate signal maximizing is possible.

4. Once again record the FM RATE and return the display switch to "RADAR."

5. Return data switch to "DATA" mode and begin driving the truck until a constant speed between 5 - 10 MPH is reached.

6. When a constant speed is reached depress the "INTEGRATE" button. Be sure to maintain speed till "DATA READY" LED comes on, or all portions of the target will not have a uniform weighting in terms of averaging.

7. After one integration period the "DATA READY" LED will come on. Record the data promptly and stop.

8. Set the polarization switch to "CROSS" (VH) and repeat steps 1 - 7 for the cross-polarization. This process should be done over the same area of the target as before to get a true like-cross relationship.

2.7 Doppler Contribution

There may be some concern about contributions due to Doppler shift, since the data are taken in a moving mode and the signal is peaked in a stationary state. Significant Doppler shift would cause a portion of the spectrum to move out of the IF band and yield a lower power value than was actually present. Table 5 shows the Doppler shift for various truck speeds; clearly, the contributions are negligible (the IF bandwidth is 6.6 kHz). This is due to the use of narrow-beam antennas, and look-direction that is orthogonal to the truck-velocity vector.* Figure 8 shows the geometry involved in finding the Doppler contributions.

TABLE 5

IF Spectral Shift Due to Doppler Contribution, f_d

Speed (MPH)	f_d (HZ)
5	5.7
10	11.4
15	17.1
20	22.8

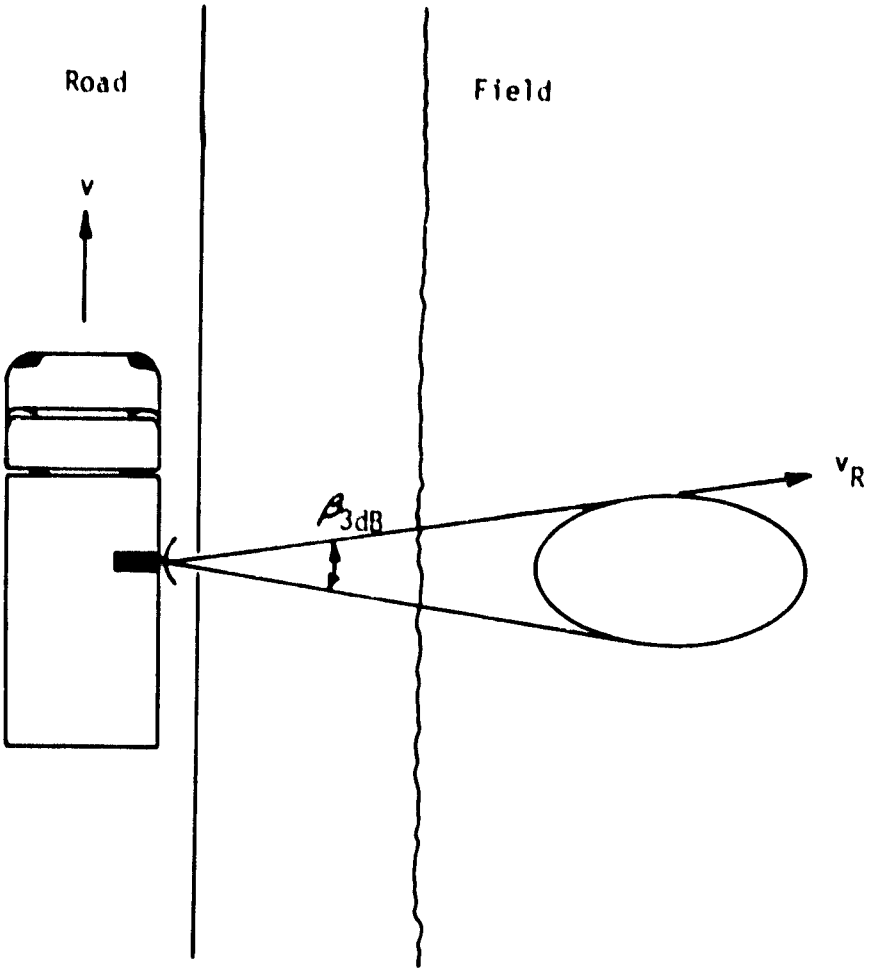

Figure 8: Geometry to determine Doppler shift frequency, f_d.

3.0 CALIBRATION

To obtain a meaningful and reliable value for σ^o, two modes of calibration must be employed. By measuring the return from a target of known radar cross-section, an absolute scale can be determined for values of σ^o. The Luneberg lens provides a good reference for this mode because it not only has a large known radar cross-section but also has a beamwidth of the order of 140°. Figure 9 shows the lens radar cross-section, σ_c, as a function of frequency for VV polarization.

System stability is established by periodically replacing the transmit antenna with a short-circuited delay line in order to perform an internal calibration. This step is accomplished by the Active/Calibrate switch shown in Figure 14. Fluctuations in transmitter power, cable loss, etc., can be monitored in this way and removed later when σ^o is calculated.

3.1 Derivation of σ^o_{VV} and σ^o_{VH} Equations

Previously, the radar equation was defined for a target with a given scattering cross-section per unit area σ^o,

$$P_r = \frac{P_t\, G_t\, G_r\, \lambda^2\, A_{111}\, \sigma^o}{(4\pi)^3\, R^4} \quad . \tag{3}$$

Since the measurements are performed for two polarizations, VV and VH, and two separate mixers are used, there will be two distinct system transfer constants in the σ^o calculations.

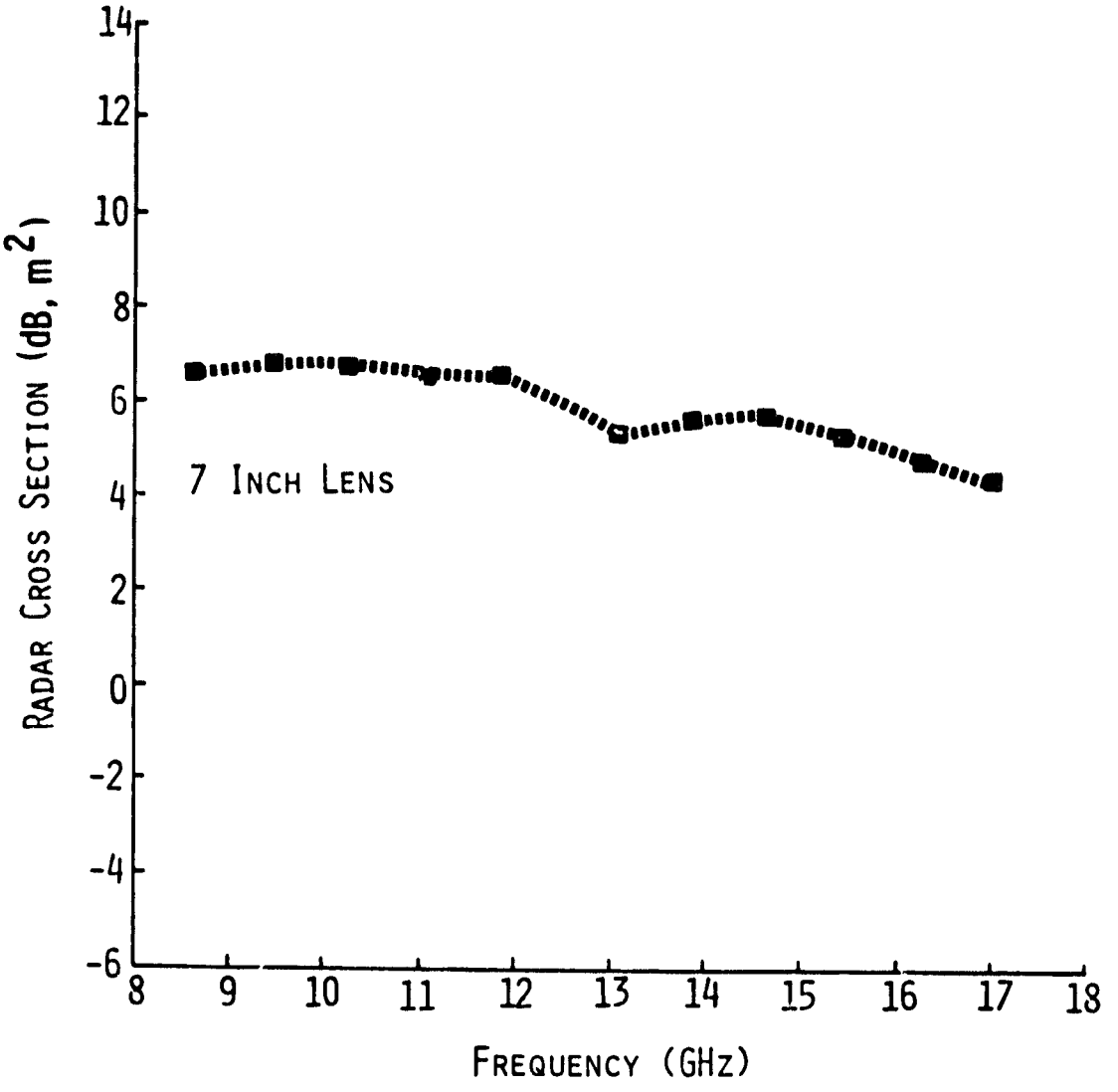

Figure 9. Measured cross-section of the Luneberg lenses calibrated against the cross-section of a metallic sphere with a 12-inch diameter.

3.1.1 Calibration Equation for σ^o_{VV}

For the like-polarization (VV), let K^t_{VV} be the system-transfer constant relating the received power P_r and the measured voltage V^t_{VV}. This voltage is given by

$$V^t_{VV} = K^t_{VV} \left[\frac{P_t \, G_D^2 \, \lambda^2 \, \sigma^o_{VV} \, A_{ill_{VV}}}{(4\pi)^3 \, R_t^4} \right]^{\frac{1}{2}} \tag{10}$$

where G_D is the gain of the dish antenna.

When the transmit antenna is replaced by a delay line (10) becomes

$$V^t_d = K^t_{VV} \, [P_t \, L]^{\frac{1}{2}} \tag{11}$$

where L represents the two-way loss through the short-circuited delay line.

Taking the ratio of the target-received voltage to the delay-line voltage eradicates dependence on K^t_{VV} and P_t,

$$M^t_{VV} = \frac{V^t_{VV}}{V^t_d} = \left[\frac{G_D^2 \, \lambda^2 \, \sigma^o \, A_{ill_{VV}}}{(4\pi)^3 \, R_t^4 \, L} \right]^{\frac{1}{2}} . \tag{12}$$

In the external calibration mode, the radar looks at the Luneberg lens, which is a point source, and Equation (10) takes the form:

$$V^c_{VV} = K^c_{VV} \left[\frac{P_t \, G_D^2 \, \lambda^2 \, \sigma_c}{(4\pi)^3 \, R_c^4} \right]^{\frac{1}{2}} . \tag{13}$$

Again switching to the delay line yields

$$V^c_d = K^c_{VV} \, [P_t \, L]^{\frac{1}{2}} . \tag{14}$$

The ratio of (13) and (14) again removes the dependence on K_{VV} and P_t,

$$M^c_{VV} = \frac{V^c_{VV}}{V^c_d} = \left[\frac{G_D^2 \lambda^2 \sigma_c}{(4\pi)^3 R_c^4 L}\right]^{\frac{1}{2}} . \tag{15}$$

If the ratio of M^t_{VV} to M^c_{VV} is taken, the following expression for σ^o_{VV} is obtained.

$$\begin{aligned}\sigma^o_{VV}(dB) = {} & 20 \log M^t_{VV} - 20 \log M^c_{VV} \\ & + \sigma_c(dB) - 10 \log A_{ill_{VV}} \\ & + 40 \log R_t - 40 \log R_c \quad .\end{aligned} \tag{16}$$

For computational purposes, the above equation may be written in the form:

$$\sigma^o_{VV}(dB) = A - B + C_{VV}(R_t, \theta) \tag{17}$$

where

$$\begin{aligned}A = M^t_{VV}(dB) &= 20 \log M^t_{VV} \\ &= V^t_{VV}(dB) - V^t_{d\ell}(dB)\end{aligned} \tag{18}$$

$$B = V^c_{VV}(dB) - V^c_{d\ell}(dB) \tag{19}$$

$$C_{VV}(R_t, \theta) = \sigma_c(dB) - 10 \log A_{ill_{VV}} + 40 \log R_t - 40 \log R_c . \tag{20}$$

The four voltages are read from the system panel meter during observation of (a) the target ($V^t_{VV}(dB)$), (b) the delay line ($V^t_{d\ell}(dB)$), prior to observing the target, (c) the Luneberg lens ($V^c_{VV}(dB)$), and (d) the delay-line ($V^c_{d\ell}(dB)$) prior to observing the Luneberg lens. With $\sigma_c(dB)$ and R_c known, $C_{VV}(R_t, \theta)$ is a function of only the range

to target R_t and the angle of incidence θ (for a given antenna pattern). Hence, for a given system configuration (platform height and antenna pattern), $C_{VV}(R_t, \theta)$ can be readily computed as shown in Appendix C.

3.1.2 Calibration Equation for σ^o_{VH}

The previous derivation is not applicable for σ^o_{VH} for two basic reasons. The first is that the lens is not a calibrated reference for cross-polarized measurements. Secondly, the delay line is configured in the like-polarization mode only, so the ratio method is not applicable. Therefore a different approach must be employed to calculate σ^o_{VH}.

The radar equation for the cross-polarized case takes the form

$$V^t_{VH} = K^t_{VH} \left[\frac{P_t \, G_D \, G_{HN} \, \lambda^2 \, \sigma^o_{VH} \, A_{ill_{VH}}}{(4\pi)^3 \, R_t^4} \right]^{\frac{1}{2}} \qquad (21)$$

where G_{HN} is the gain of the standard-gain horn antenna.

Comparison of (10) and (21) shows three main differences. One is that the areas of illumination for VV and VH are different because the antenna beamwidths are not the same. Secondly, the transmit and receive antenna gain products are different because G_D = 28.8 dB and G_{HN} = 22.4 dB. Finally, the values of K^t_{VV} and K^t_{VH}, which take into account cable losses, mixer conversion loss, etc., may be different due to the use of separate mixers for the two polarizations.

To arrive at a calibration equation for σ^o_{VH}, a two step procedure was configured. The first step involved measuring the

received voltage for each of two antenna configurations. In the first configuration, V^c_{VV} due to the Luneberg lens was measured using the dish antenna. In the second configuration, the horn antenna, which usually is H-polarized since it is used for making the VH-polarization measurements, was turned 90° and a measurement was made observing the Luneberg lens. Thus, in both of these configurations, the VV-polarized returns from the lens was measured. In this case, the ratio of the two measurements is:

$$C_1 = \frac{V^c_{VV} \text{ (Dish antenna for transmit and receive)}}{V^c_{VV} \text{ (Dish antenna for transmit, horn antenna for receive)}}$$

$$= \frac{K_{VV}\,(G_D^2)^{\frac{1}{2}}}{K_{VH}\,(G_D\,G_{HN})^{\frac{1}{2}}} = \frac{K_{VV}}{K_{VH}}\left(\frac{G_D}{G_{HN}}\right)^{\frac{1}{2}} . \qquad (22)$$

Now, consider the ratio of (21) to (10),

$$C_2 = \frac{V^t_{VH}}{V^t_{VV}} = \frac{K^t_{VH}}{K^t_{VV}} \left[\frac{G_D\,G_{HN}\,\sigma^o_{VH}\,A_{ill_{VH}}}{G_D^2\,\sigma^o_{VV}\,A_{ill_{VV}}}\right]^{\frac{1}{2}} . \qquad (23)$$

Using (22), the above expression reduces to:

$$C_2 = C_1 \left[\frac{\sigma^o_{VH}\,A_{ill_{VH}}}{\sigma^o_{VV}\,A_{ill_{VV}}}\right]^{\frac{1}{2}} , \qquad (24)$$

which may be rewritten as:

$$\sigma^o_{VH}\,(dB) = C_2\,(dB) - C_1\,(dB) + \sigma^o_{VV}\,(dB)$$

$$+ 10 \log A_{ill_{VV}} - 10 \log A_{ill_{VH}} \qquad (25)$$

where C_1 (dB) = 20 log C_1 ($\triangleq$ DIFF in Appendix C)

C_2 (dB) = 20 log C_2

= 20 log V^t_{VH} - 20 log V^t_{VV}

= V^t_{VH} (dB) - V^t_{VV} (dB) .

For computational purposes, (25) may be put in the form:

$$\sigma^o_{VH}\ (dB) = V^t_{VH}\ (dB) - V^t_{VV}\ (dB) + \sigma^o_{VV}\ (dB) + C_{VH}\ (R_t, \theta) \tag{26}$$

where,

$$C_{VH}\ (R_t, \theta) = 10 \log A_{111_{VV}} - 10 \log A_{111_{VH}} - C_1\ (dB). \tag{27}$$

Hence, having found σ^o_{VV} (dB) through its calibration Equation (17), σ^o_{VH} may be calculated from the measured values of the voltages V^t_{VH} and V^t_{VV} and the angle-dependent constant C_{VH} (R_t, θ), as indicated in Appendix C.

Table 6 shows representative values for C_{VV} (R_t) and C_{VH} (R_t) at $\theta = 50°$. The program used for their generation, as well as sample calculation forms for σ^o_{VV} and σ^o_{VH}, can be found in Appendix C.

3.2 Range Equation

The range to the target is measured indirectly by the FM tuning rate displayed on the console. The measured FM rate is inversely proportional to the total range between the mixer and the target which includes a short distance between the mixer and the antenna. The range calibration equation was determined experimentally by measuring the FM rate at each of several ranges to the Luneberg lens. These measurements led to the simple expression:

TABLE 6

Representative values of $C_{VV}(R_t)$ and $C_{VH}(R_t)$ at $\theta = 50°$.

INCIDENCE ANGLE : 50.
POLARIZATION:VV

C(R) AS A FUNCTION OF FM RATE

RANGE(M)	FM RATE	C(R):(DB)	RANGE(M)	FM RATE	C(R):(DB)
14.46	235	5.37	11.91	285	4.68
14.16	240	5.10	11.70	290	4.53
13.87	245	5.00	11.50	295	4.38
13.57	250	5.03	11.31	300	4.23
13.32	255	5.05	11.12	305	4.08
13.06	260	5.40	10.91	310	3.94
12.81	265	5.32	10.70	315	3.80
12.57	270	5.15	10.57	320	3.65
12.34	275	4.99	10.43	325	3.53
12.12	280	4.83	10.27	330	3.37

INCIDENCE ANGLE : 50.
POLARIZATION:VH

C(R) AS A FUNCTION OF FM RATE

RANGE(M)	FM RATE	C(R):(DB)	RANGE(M)	FM RATE	C(R):(DB)
14.46	235	12.05	11.91	285	12.05
14.16	240	12.05	11.70	290	12.05
13.87	245	12.05	11.50	295	12.05
13.57	250	12.05	11.31	300	12.05
13.32	255	12.05	11.12	305	12.05
13.06	260	12.05	10.94	310	12.05
12.81	265	12.05	10.76	315	12.05
12.57	270	12.05	10.59	320	12.05
12.34	275	12.05	10.43	325	12.05
12.12	280	12.05	10.27	330	12.05

$$\text{RANGE} = \frac{3423.5}{FM} - 0.106, \text{ meters} \qquad (28)$$

where FM is the FM rate in Hz.

3.3 Calibration Procedure

The MARS scatterometer is a calibrated instrument that requires periodic calibration to maintain a high degree of accuracy. As mentioned in the previous section, short-term fluctuations are tracked by monitoring the return from a shorted delay line. This section deals with the process of absolute calibration from the Luneberg lens.

A routine process is necessary if results from one calibration date are to be compared with another. This is desirable because long-term system stability can be mapped from results obtained under the same set of test conditions. This type of history can then help to build confidence in the measured data and can describe possible anomalies. Figure 10 shows the MARS system when set up for calibration and the procedure for taking a lens set follows.

3.3.1 Lens Set Procedure

1. With the antennas approximately 3 meters above the ground, point them slightly above the horizon and in a direction clear of all obstructions.
2. Set the lens pole at a distance approximately 15 meters from the antenna. Be sure the pole is made of a non-reflective material such as fiberglass or wood.
3. Peak the signal return while in the "ACTIVE" mode.
4. Adjust the radar azimuth position so as to peak the power in that plane.

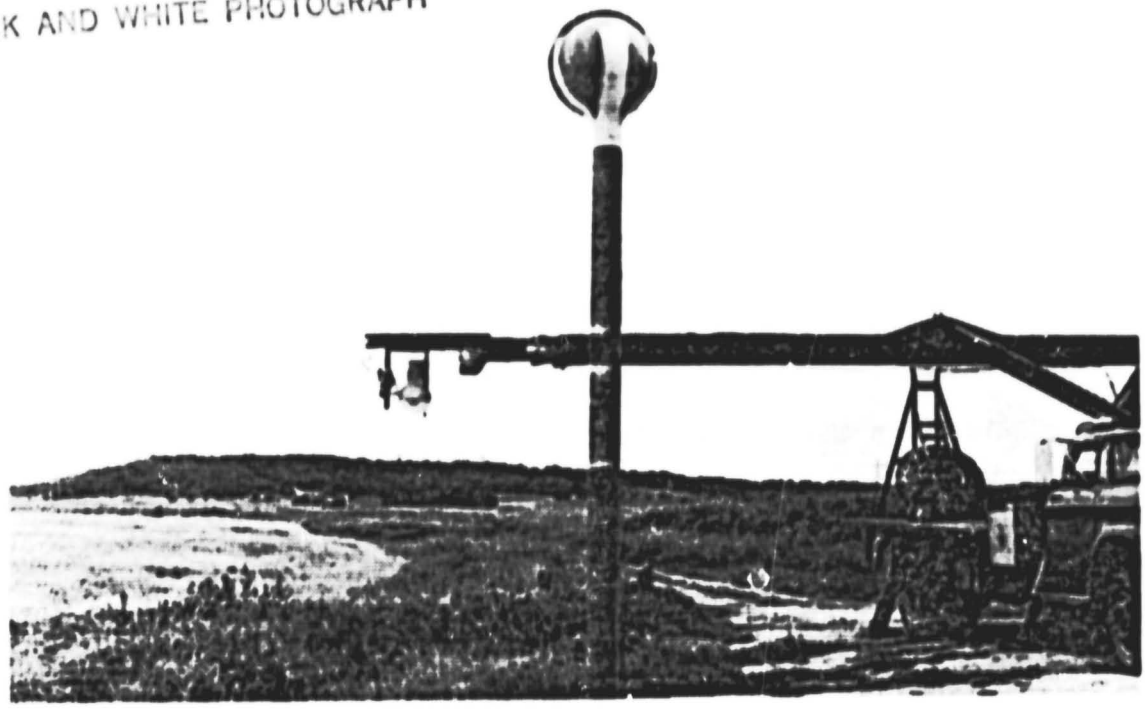

Figure 10A. View of radar during calibration.

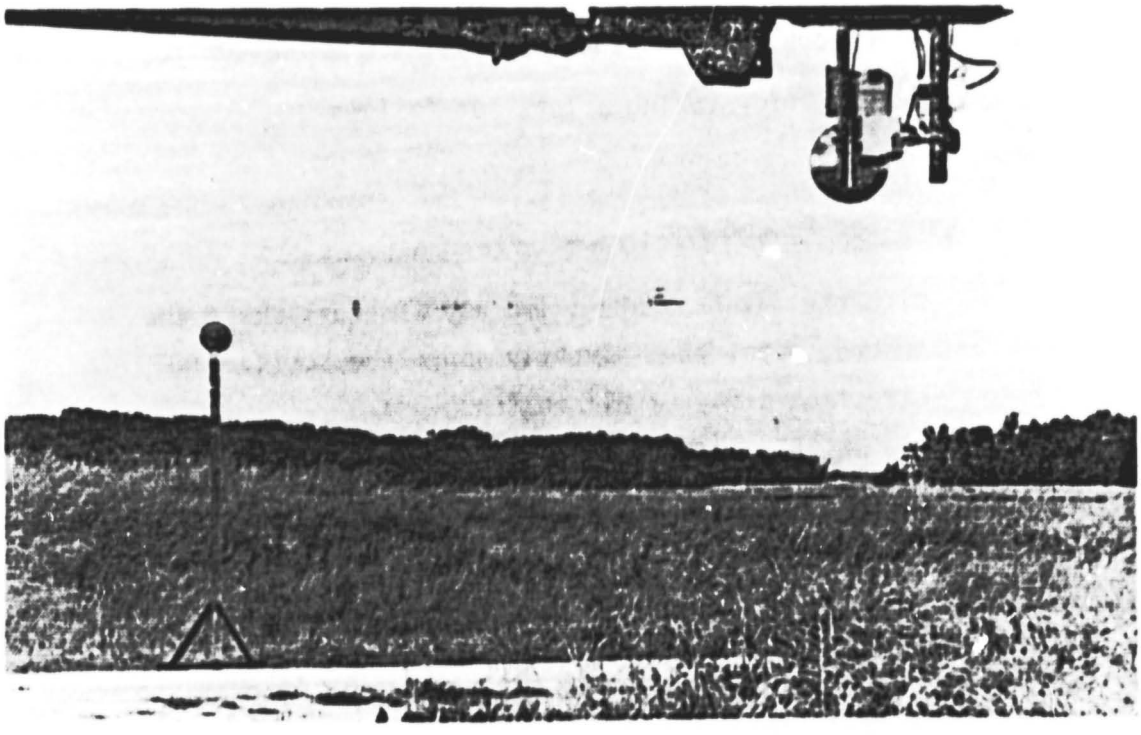

Figure 10B. View of Luneberg lens during calibration.

5. Adjust the radar vertical position so as to peak the power in that plane. Steps 4 and 5 should be done with great care because this establishes the absolute calibration of the instrument.

6. Re-peak the system with the FM tuning dial.

7. Take a data set as described earlier.

8. Repeat steps 6 and 7 for the cross-polarization mode. Although the lens is not a calibrated reference for the cross-polarized mode, it depolarizes the incident wave only very slightly. This slight depolarization is comparable to the depolarization of the antenna itself and thus the VH measurement serves as a system check for cross-polarization stability and as a figure of merit.

9. Repeat steps 3 through 8 two times and average the like- and cross-returns.

10. Check to see if V^c_{VV} (dB) is close to the previously acquired data set. If not, determine the problem, and repeat entire process.

11. If V^c_{VV} (dB) is close to earlier set, calculate V^c_{VV} (dB) - $V^c_{d\ell}$ (dB) for σ^o_{VV} calculations. (This equals B in Equation (17)).

Confidence in the measured return from the lens is a function of the background return (in this case the lens pole and/or the ground returns through a sidelobe). Figure 11 shows the relationship between measurement uncertainty and the ratio of target power to background return power. A typical ratio for the MARS system is 25 dB, which implies an uncertainty of ± 0.5 dB.

A thorough discussion of measurement uncertainty is given by Ulaby, et al. [30].

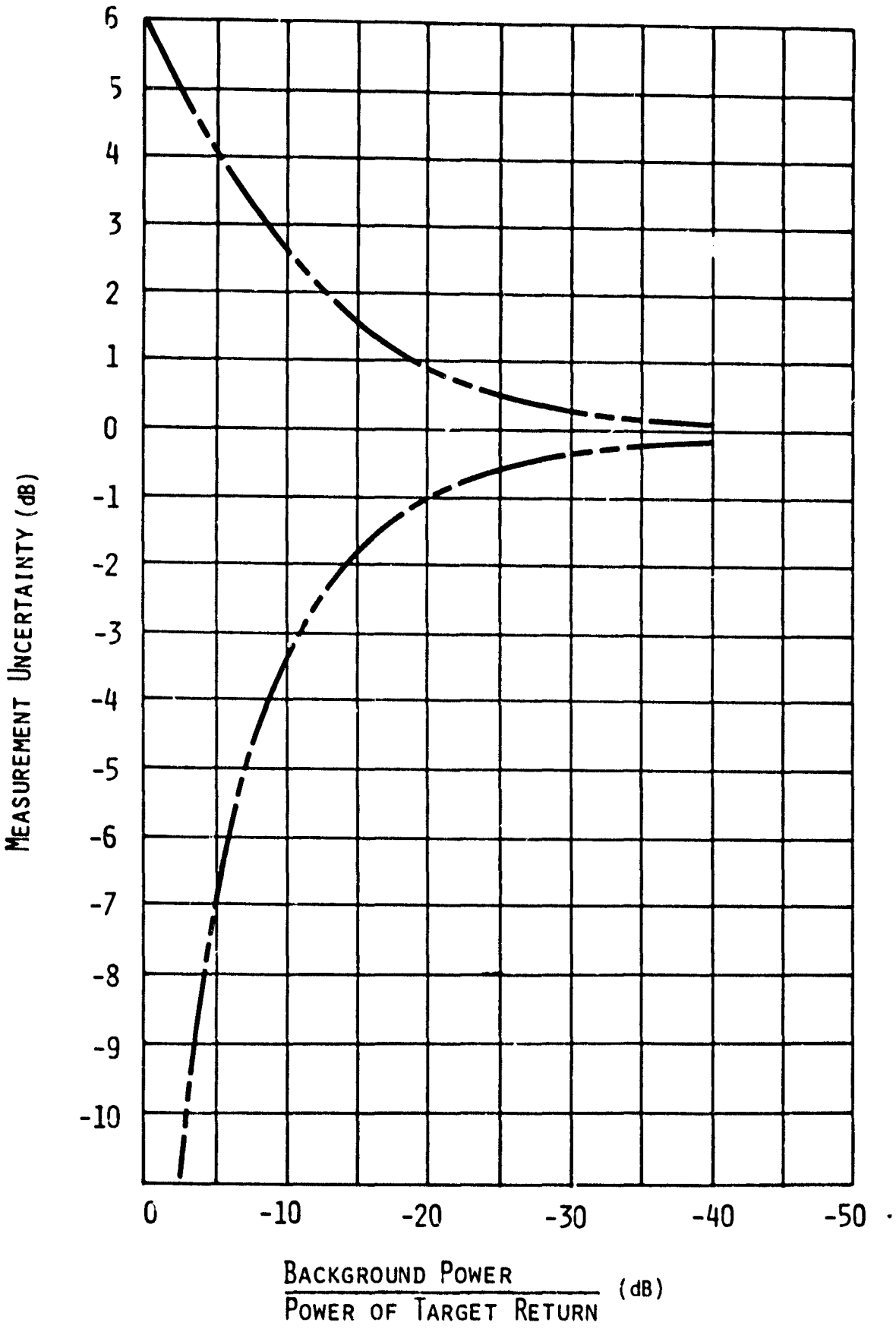

Figure 11. Measurement uncertainty with background contributions.

3.3.2 Sky Noise Test

The final step in the MARS calibration procedure is the determination of system noise and minimum detectable signal. This is most easily accomplished by pointing the antennas toward the sky and measuring the return at several FM rates. These rates should correspond to typical values used at the various data-set angles of incidence. Since the return from the sky is essentially negligible, the measured value is system noise and represents a threshold of the minimum detectable signal. This noise power can be used along with the FM rate to calculate a minimum σ^o. An offset factor, typically 4 - 6 dB, is added to this value of σ^o_{min} to define a minimum acceptable value, $\sigma^o_{critical}$. When calculating σ^o from data results, values falling below $\sigma^o_{critical}$ are discarded, while values above it are accepted as good data. Table 7 shows typical sky-noise test results with σ^o_{min} calculated to the right.

4.0 GENERAL HARDWARE CONCEPTS AND LAYOUT

Design Concepts

The MARS scatterometer is divided into two subsystems: an RF section and an IF/control section. The RF subsystem is mounted on a positioning unit atop an 8-meter boom and is connected to the control subsystem via two RG-58 coax lines and one 7 conductor cable. The control section is mounted in the cab of the truck such that one individual can simultaneously drive the truck and operate the radar. A simple remote position controller and angle indicator was configured and placed in the cab. Figure 12 shows the control section mounted in the truck.

TABLE 7

Minimum detectable σ^o with signal-to-noise ratio of 1. Noise level determined by pointing the antennas towards the sky.

Effective θ	FM Rate (Hz)	V^t_{VV} (dB)	V^t_{VH} (dB)	$\sigma^o_{min\ VV}$ (dB)	$\sigma^o_{min\ VH}$ (dB)
30°	365	- 8.4	-26.2	-32.6	-37.6
40°	335	- 9.1	-26.5	-33.5	-38.0
50°	285	-11.0	-26.8	-34.7	-37.7
60°	230	-15.3	-27.2	-38.3	-37.3
70°	160	-16.6	-28.0	-38.1	-36.7

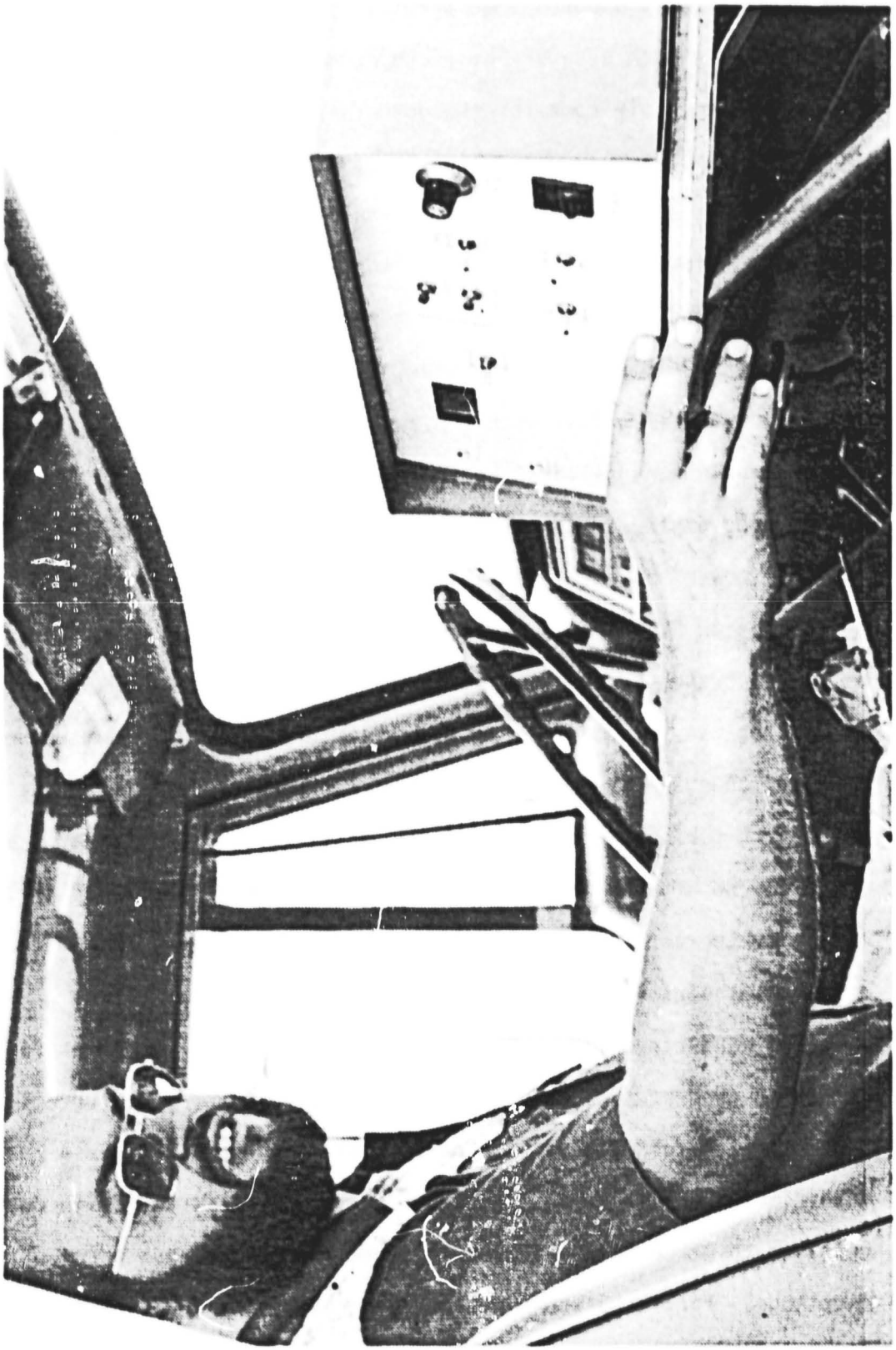

Figure 12. Cab view of radar controls during operation.

Several features enhance the overall utility of this system: The small size is a bonus that permits system operation from a small vehicle such as a van or pickup truck. A large rack space is not needed; only room for the downstairs control unit and a simple tripod assembly upon which to mount the RF subsystem. The system is easily operated by a single individual, a feature that allows for savings in manpower costs. All critical components, such as ICs and adjustment potentiometers, are indicated on the board itself. This self-documentation trait minimizes confusion for someone not familiar with the system and reduces time spent on routine tuning and calibration procedures. Careful examination of photographs of the system will reveal that there are no visible external power sources. This is so because the entire system is powered by an RV grade power inverter operating from the vehicle battery. System-power demands are low enough that a standard alternator can maintain the necessary battery charge without undue loading, thus the expense of an external generator is eliminated. Aside from further reducing the total cost, this also eliminates a major source of annoying noise common to field experiments of this type. Furthermore, data collection can be accomplished in a matter of a few minutes rather than a few hours, which allows for more frequent measuring of a variety of targets. This is important for gaining a good statistical base for the data. A final feature of this system is its relatively inexpensive cost. Appendix G gives a cost analysis in 1981 dollars. As seen from this, the reduction in cost compared to other more elaborate systems is at least one order of magnitude. Figure 13 shows a block diagram of the MARS scatterometer.

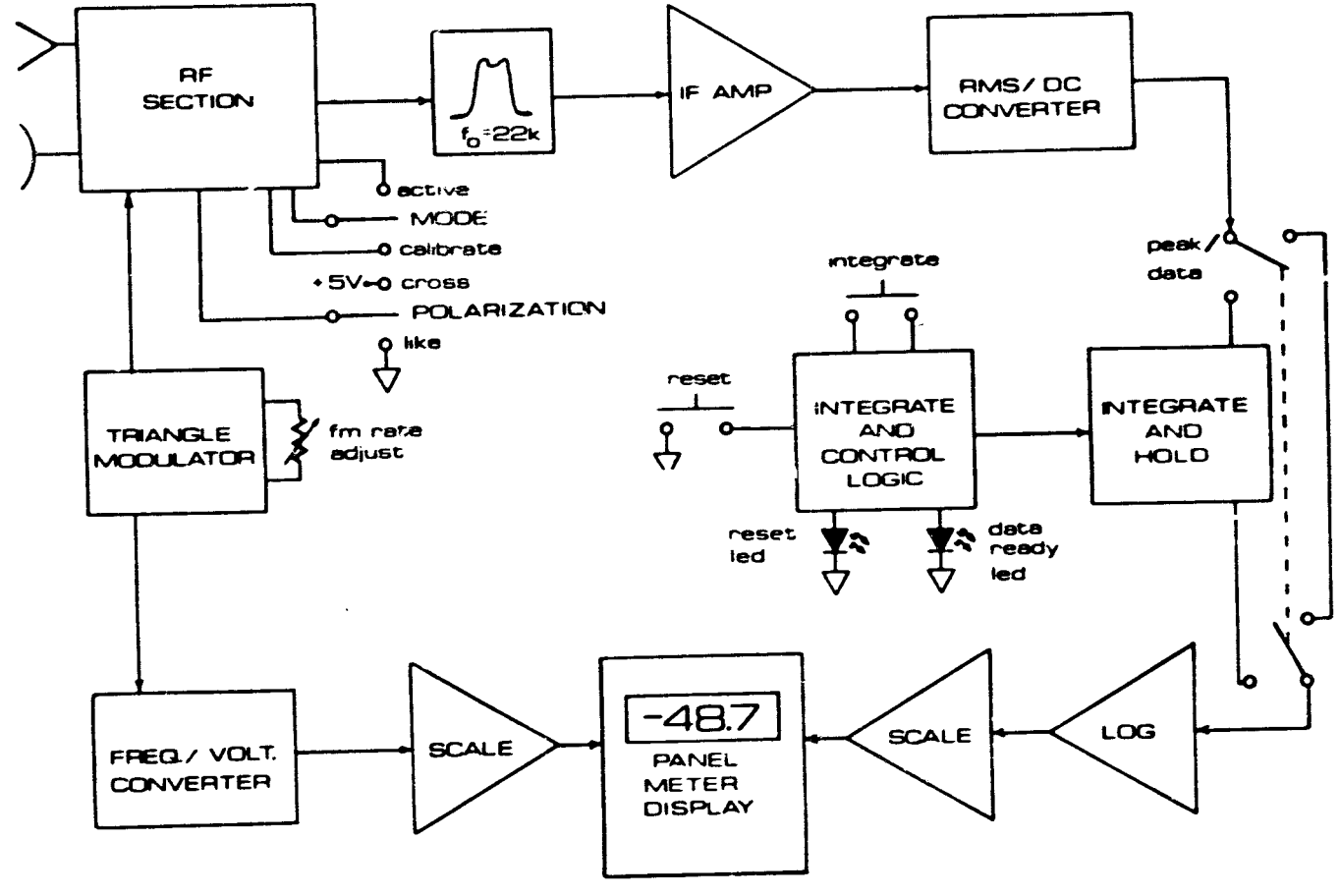

Figure 13. MARS block diagram.

4.1 RF Subsystem

The MARS RF section is shown in Figure 14. The entire subsystem is contained in the RF box shown in Figure 15 and together with the antennas is mounted atop an 8-meter boom. Figure 16 shows the entire microwave assembly. Power for the YIG oscillator and IF switch comes from the downstairs control box via the 7 conductor cable. All components are firmly mounted in the box to avoid shock effects while the system is in motion. Connections between microwave components are made with either semi-rigid cable or standard SMA prefabricated connectors. Due to the temperature-sensitive nature of the microwave components, a warm-up time of half an hour is necessary for system stability during cool to warm ambient conditions. Very cold conditions require a longer warming time. This can be monitored by periodically checking the delay line power until a constant level is achieved.

The delay line is a 5.1-meter-long length of semi-rigid coax coiled around the oscillator. Its electrical length is approximately 7.65 meters and was chosen to correspond to slightly less than the shortest range to be encountered. This serves as a measure of the system's worst noise performance since the noise spectrum decreases as the tuned range increases. This is because most noise in the receiver is a function of internal reflections which have short ranges and high FM rates. The equation to describe the loss through 100 feet of delay line is [30],

$$A = .347\ (.96 + 2(10^{-3})T)\ f^{\frac{1}{2}} + 88(10^{-5})\ f \quad , (dB) \tag{29}$$

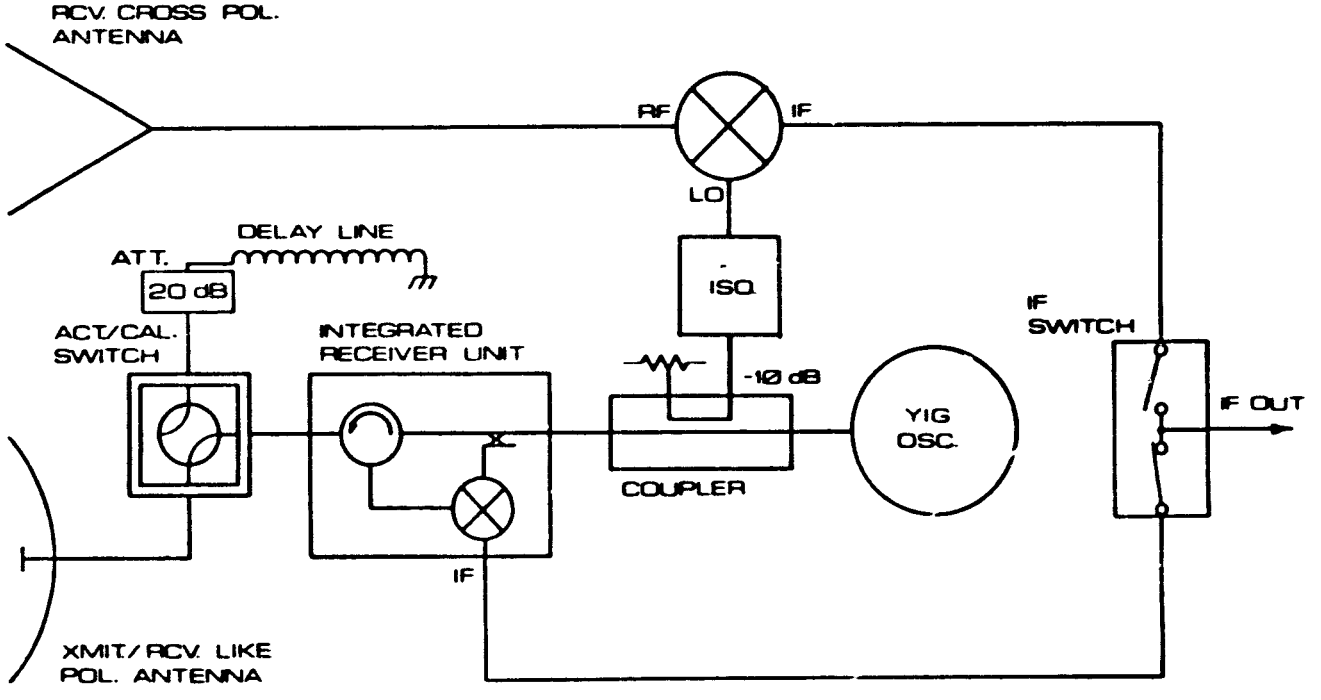

Figure 14. MARS RF section.

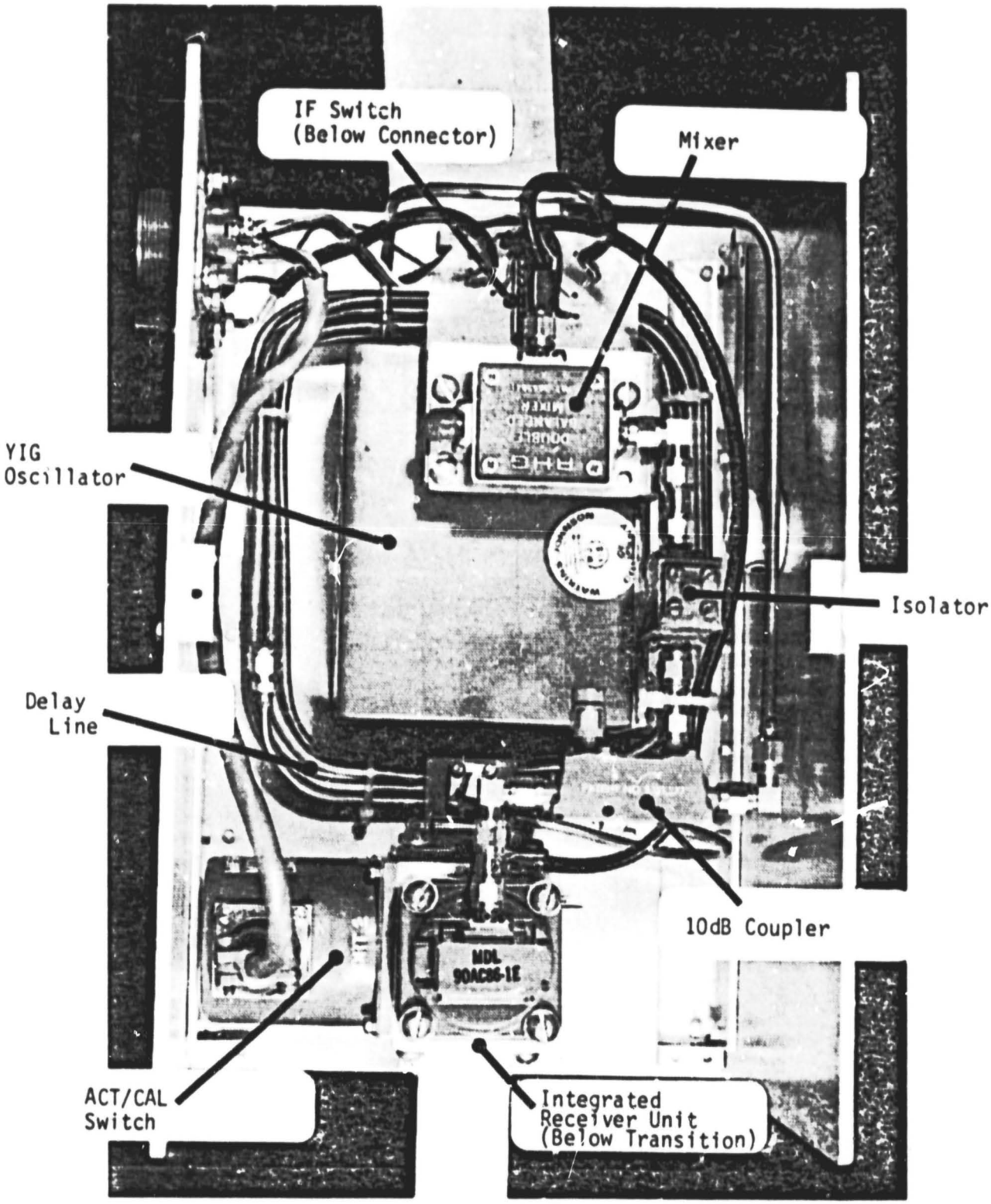

Figure 15. Microwave component layout in RF box.

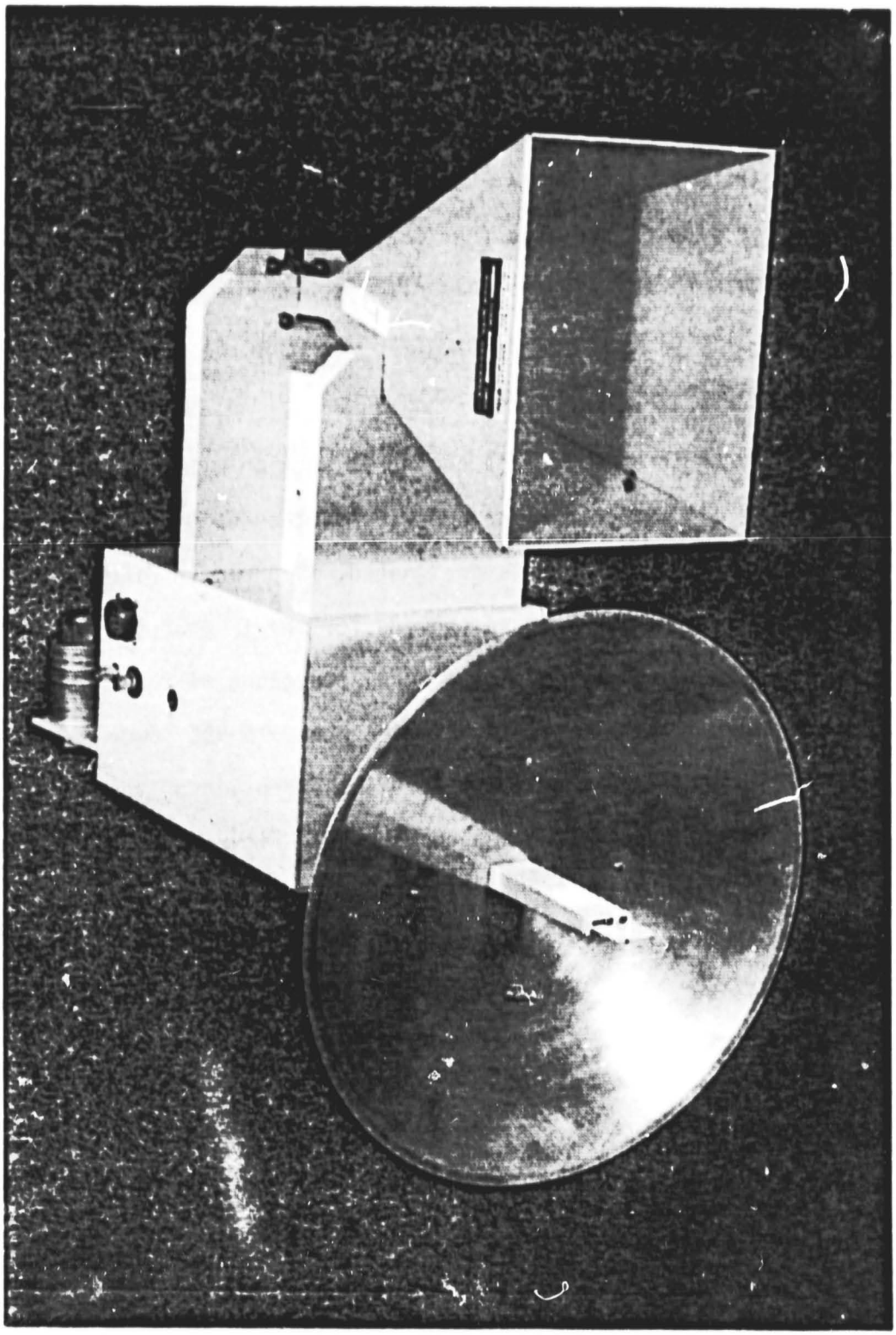

Figure 16. Complete RF assembly.

where

f = frequency in MHz

T = temperature in °C.

For the MARS delay line at 30°C, A = 7.5 dB one way or 15 dB for the case of the shorted line.

The transmit antenna is a 30-cm parabolic reflector illuminated by a double dipole waveguide feed. The cross-polarized antenna is a standard-gain horn. The antennas are discussed in detail in Appendix A.

4.2 IF/Control Subsystem

Figure 17 is a photograph of the IF section with its cover removed and all cards in place. A view of the top of the console, with boards removed and parts designated, is shown in Figure 18. The purpose of this assembly is to provide for the IF processing of the radar signal and to perform the control functions of the RF subsystem, integrator, and panel indicator lights. One ±15 VDC power supply powers all the active components with the exception of the ACT/CAL waveguide switch which operates on 110 VAC. Figure 19 shows a front view of the console and identifies the various controls, while Figure 20 shows a rear view and points out the cable connections.

A detailed explanation of each board and its function is contained in Appendix B.

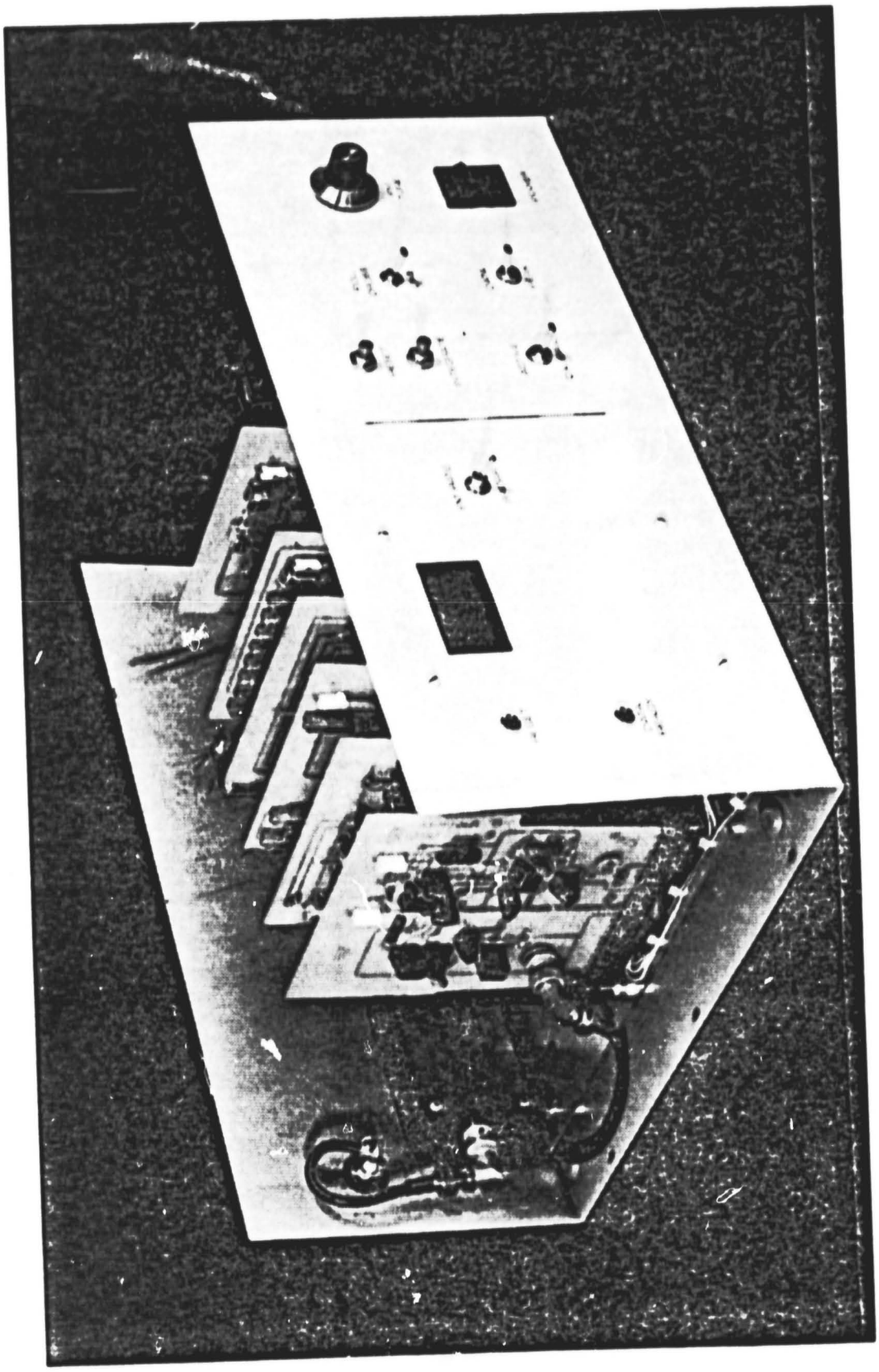

Figure 17. MARS IF/controller section.

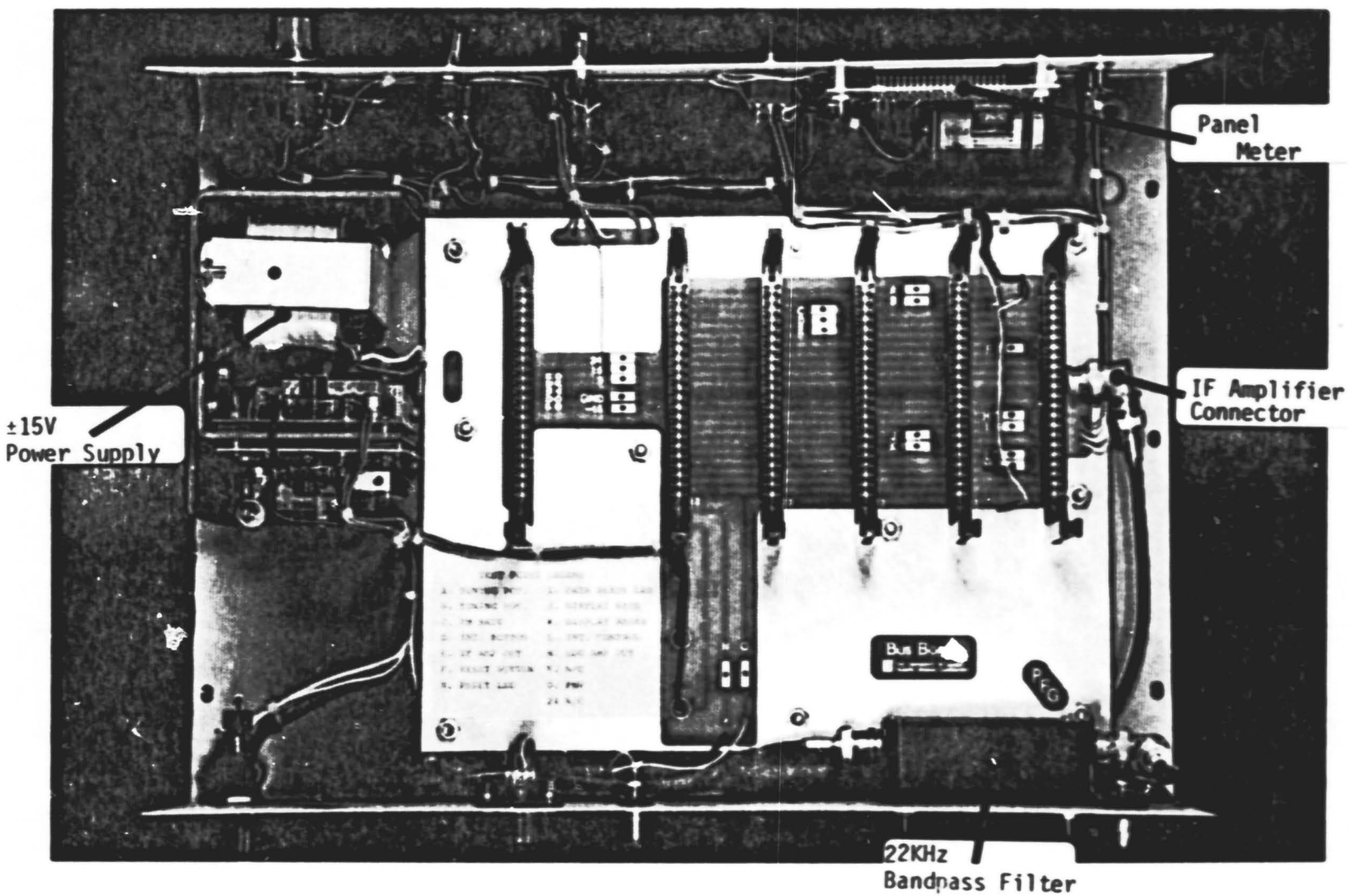

ORIGINAL PAGE
BLACK AND WHITE PHOTOGRAPH

Figure 18. Controller section layout.

Figure 19. Console front layout with switch designations.

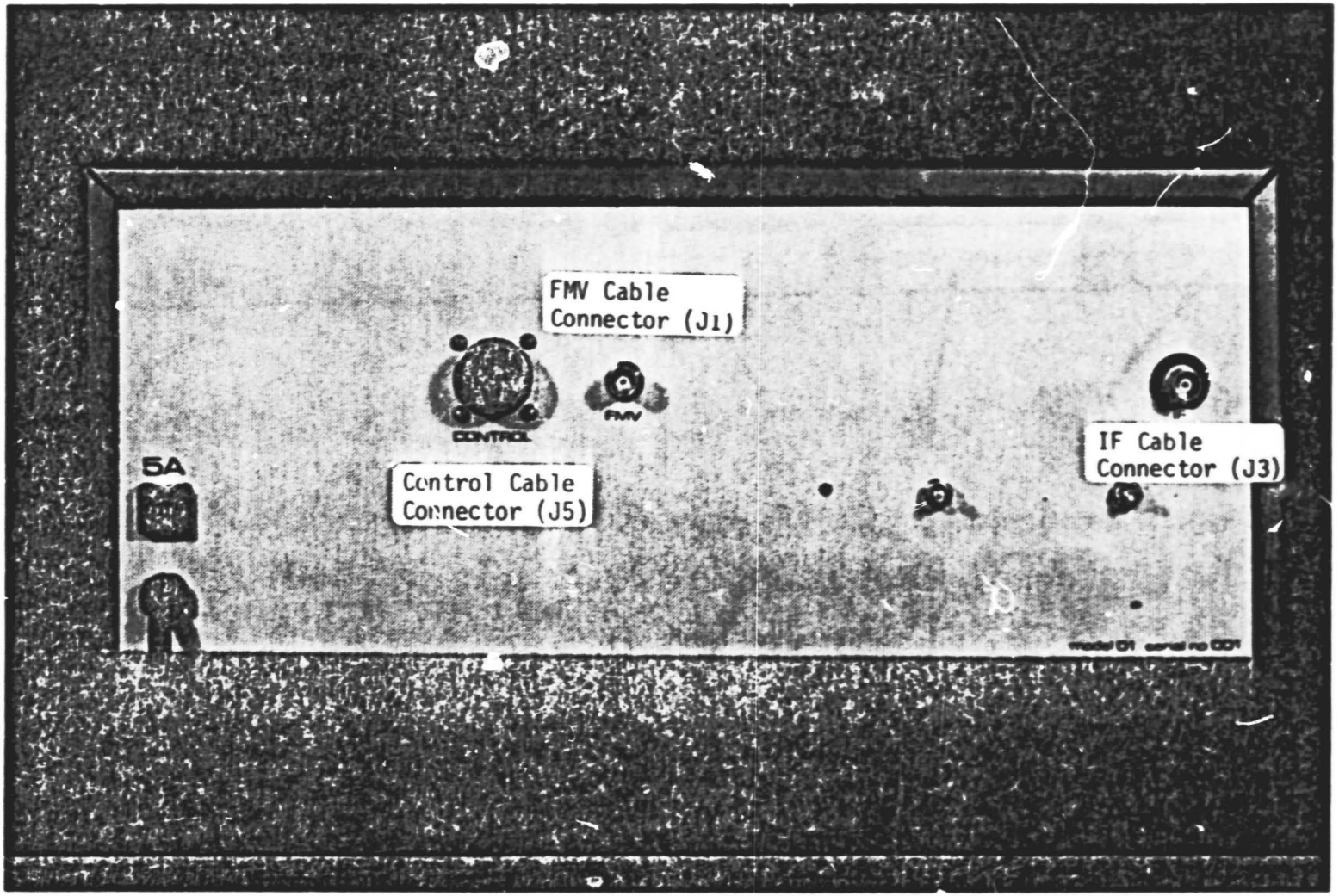

Figure 20. Console back layout with connector designations.

REFERENCES

[1] Ulaby, F. T., "Radar Measurements of Soil Moisture Content," IEEE Transactions on Antennas and Propagation, Vol. AP-22, No. 2, pp. 257-265, March, 1974.

[2] Ulaby, F. T., "Radar Response to Vegetation," IEEE Transactions on Antennas and Propagation, Vol. AP-23, No. 1, pp. 36-45, January, 1975.

[3] Ulaby, F. T., J. Cihlar and R. K. Moore, "Active Microwave Measurement of Soil Water Content," Remote Sensing of Environment, Vol. 3, pp. 185-203, 1974.

[4] Ulaby, F. T., T. F. Bush and P. P. Batlivala, "Radar Response to Vegetation II: 8-18 GHz Band," IEEE Transactions on Antennas and Propagation, Vol. AP-23, No. 5, pp. 608-618, September, 1975.

[5] Bush, T. F. and F. T. Ulaby, "Fading Characteristics of Panchromatic Radar Backscatter from Selected Agricultural Targets," IEEE Transactions on Geoscience Electronics, Vol. GE-13, No. 4, pp. 149-157, October, 1975.

[6] Bush, T. F. and F. T. Ulaby, "On the Feasibility of Monitoring Croplands with Radar," Proceedings Tenth International Symposium on Remote Sensing of Environment, University of Michigan, Ann Arbor, pp. 1111-1121, October, 1975.

[7] Ulaby, F. T. and P. P. Batlivala, "Diurnal Variations of Radar Backscatter from a Vegetation Canopy," IEEE Transactions on Antennas and Propagation, Vol. AP-24, No. 1, pp. 11-17, January, 1976.

[8] Batlivala, P. P. and F. T. Ulaby, "Radar Look Direction and Row Crops," Photogrammetric Engineering and Remote Sensing, Vol. 42, No. 2, pp. 233-238, February, 1976.

[9] Ulaby, F. T. and T. F. Bush, "Monitoring Wheat Growth with Radar," Photogrammetric Engineering and Remote Sensing, Vol. 42, No. 4, pp. 557-568, April, 1976.

[10] Bush, T. F. and F. T. Ulaby, "Radar Return from a Continuous Vegetation Canopy," IEEE Transactions on Antennas and Propagation, Vol. AP-24, No. 3, pp. 269-276, May, 1976.

[11] Ulaby, F. T. and P. P. Batlivala, "Optimum Radar Parameters for Mapping Soil Moisture," IEEE Transactions on Geoscience Electronics, Vol. GE-14, No. 2, pp. 81-93, April, 1976.

[12] Ulaby, F. T. and T. F. Bush, "Corn Growth as Monitored by Radar," IEEE Transactions on Antennas and Propagation, Vol. AP-24, No. 6, pp. 819-828, November, 1976.

[13] Bush, T. F. and F. T. Ulaby, "Variability in the Measurement of Radar Backscatter," IEEE Transactions on Antennas and Propagation, Letters, Vol. AP-24, No. 5, pp. 896-899, November, 1976.

[14] Ulaby, F. T., W. H. Stiles, L. F. Dellwig and B. C. Hanson, "Experiments on the Radar Backscatter of Snow," IEEE Transactions on Geoscience Electronics, Vol. GE-15, No. 4, pp. 185-189, October, 1977.

[15] Fung, A. K. and F. T. Ulaby, "A Scatter Model for Leafy Vegetation," IEEE Transactions on Geoscience Electronics, Vol. GE-16, No. 4, pp. 281-286, October, 1978.

[16] Attema, E. P. W. and F. T. Ulaby, "Vegetation Modeled as a Water Cloud," Radio Science, Vol. 13, No. 2, pp. 357-364, March-April, 1978.

[17] Bush, T. F. and F. T. Ulaby, "An Evaluation of Radar as a Crop Classifier," Remote Sensing of Environment, Vol. 7, pp. 15-36, 1978.

[18] Ulaby, F. T., P. P. Batlivala and M. C. Dobson, "Microwave Backscatter Dependence on Surface Roughness, Soil Moisture and Soil Texture, Part I: Bare Soil," IEEE Transactions on Geoscience Electronics, Vol. GE-16, No. 4, pp. 286-295, October, 1978.

[19] Ulaby, F. T., G. A. Bradley and M. C. Dobson, "Microwave Backscatter Dependence on Surface Roughness, Soil Moisture and Soil Texture, Part II: Vegetation-Covered Soil," IEEE Transactions on Geoscience Electronics, Vol. GE-17, No. 2, pp. 33-40, April, 1979.

[20] Ulaby, F. T. and J. E. Bare, "Look Direction Modulation Function of the Radar Backscattering Coefficient of Agricultrual Fields," Photogrammetric Engineering and Remote Sensing, Vol. 45, pp. 1495-1506, November, 1979.

[21] Stiles, W. H. and F. T. Ulaby, "The Active and Passive Microwave Response to Snow Parameters, Part I: Wetness," Journal of Geophysical Research, Vol. 85, No. C2, pp. 1037-44, February 20, 1980.

[22] Ulaby, F. T. and W. H. Stiles, "The Active and Passive Microwave Response to Snow Parameters, Part II: Water Equivalent of Dry Snow," Journal of Geophysical Research, Vol. 85, No. C2, pp. 1045-1049, February 20, 1980.

[23] Dobson, M. C. and F. T. Ulaby, "Microwave Backscatter Dependence on Surface Roughness, Soil Moisture and Soil Texture: Part III -- Soil Tension," IEEE Transactions on Geoscience and Remote Sensing, Vol. GE-19, No. 1, January, 1981.

[24] Ulaby, F. T., F. Kouyate and A. K. Fung, "A Backscatter Model for a Randomly Perturbed Periodic Surface," IEEE International Geoscience and Remote Sensing Symposium (IGARSS '81), Washington, D.C., June 8-10, 1981.

[25] Peake, W. H., "Interaction of Electromagnetic Waves with Some Natural Surfaces, IRE Transactions on Antennas and Propagation, AP-7, pp. 5324-5329, 1959.

[26] Peake, W. H. and T. L. Oliver, "The Response of Terrestrial Surfaces at Microwave Frequencies," Ohio State University Technical Report 2440-7, Columbus, Ohio, 1971.

[27] LeToan T. and G. Flouzat, "Multifrequency Radar Measurements of Soil Parameters," Proc. 23rd Plenary Meeting, COSPAR, Budapest, Hungary, p. 318, 1980.

[28] Ulaby, F. T., W. H. Stiles, D. Brunfeldt and E. Wilson, "1-35 GHz Mocrowave Scatterometer," IEEE/MTT-S International Microwave Symposium, Orlando, Florida, April 30 - May 2, 1979.

[29] Brunfeldt, D., F. T. Ulaby and H. Stiles, "System Description and Hardware Specification of MAS 1-8," RSL Technical Report 264-17, University of Kansas Center for Research, Inc., February, 1979.

[30] Ulaby, F. T., W. H. Stiles and D. Brunfeldt, "Performance Analysis of the MAS (Microwave Active Spectrometer) Systems: Calibration, Precision and Accuracy," RSL Technical Report 360-4, University of Kansas Center for Research, Inc., February, 1979.

[31] Ulaby, F. T., W. H. Stiles, D. R. Brunfeldt and M. E. Lubben, "MAS 8-18/35 Scatterometer," RSL Technical Report 360-5, University of Kansas Center for Research, Inc., December, 1978.

[32] Attema, E. P. W. and F. T. Ulaby, "35 GHz Radar Scatterometer System," RSL Technical Report 330-3, University of Kansas Center for Research, Inc., December, 1976.

[33] Silver, S., Microwave Antenna Theory and Design, Chapter 8, Dover Publications, Inc., New York, pp. 253-255, 1965.

[34] Brunfeldt, D. R. and V. Frost, "Design and Construction of a Parabolic Antenna," St*AR Technical Report 4001-1, Lawrence, Kansas, January, 1980.

APPENDIX A

ANTENNAS

ANTENNAS

Overview

The MARS scatterometer uses two antennas, one for the like-polarization mode (VV) and the other for cross-polarization mode (VH). The like-polarization antenna is comprised of a 30-cm parabolic reflector illuminated by a double dipole waveguide feed. The receiving antenna for the cross-polarization mode is a standard gain horn. Both are operated at a center frequency of 10.2 GHz. Table A1 lists the antennas' specifications.

TABLE A1
MARS Antenna Specifications

	Dish	Horn
Gain: (dB)	28.8	22.4
Beamwidth:		
Elevation	5.6°	12.0°
Azimuth	6.1°	13.0°
Far Field Range: R_{ff}	6.3 m	2.5 m
Center Frequency: f_o	10.2 GHz	10.2 GHz
VSWR	1:1.30	1:1.05
Sidelobe Level	21 dB	~17 dB

Figure A1 shows the reflector antenna and feed assembly that is used to transmit in the vertical polarization mode.

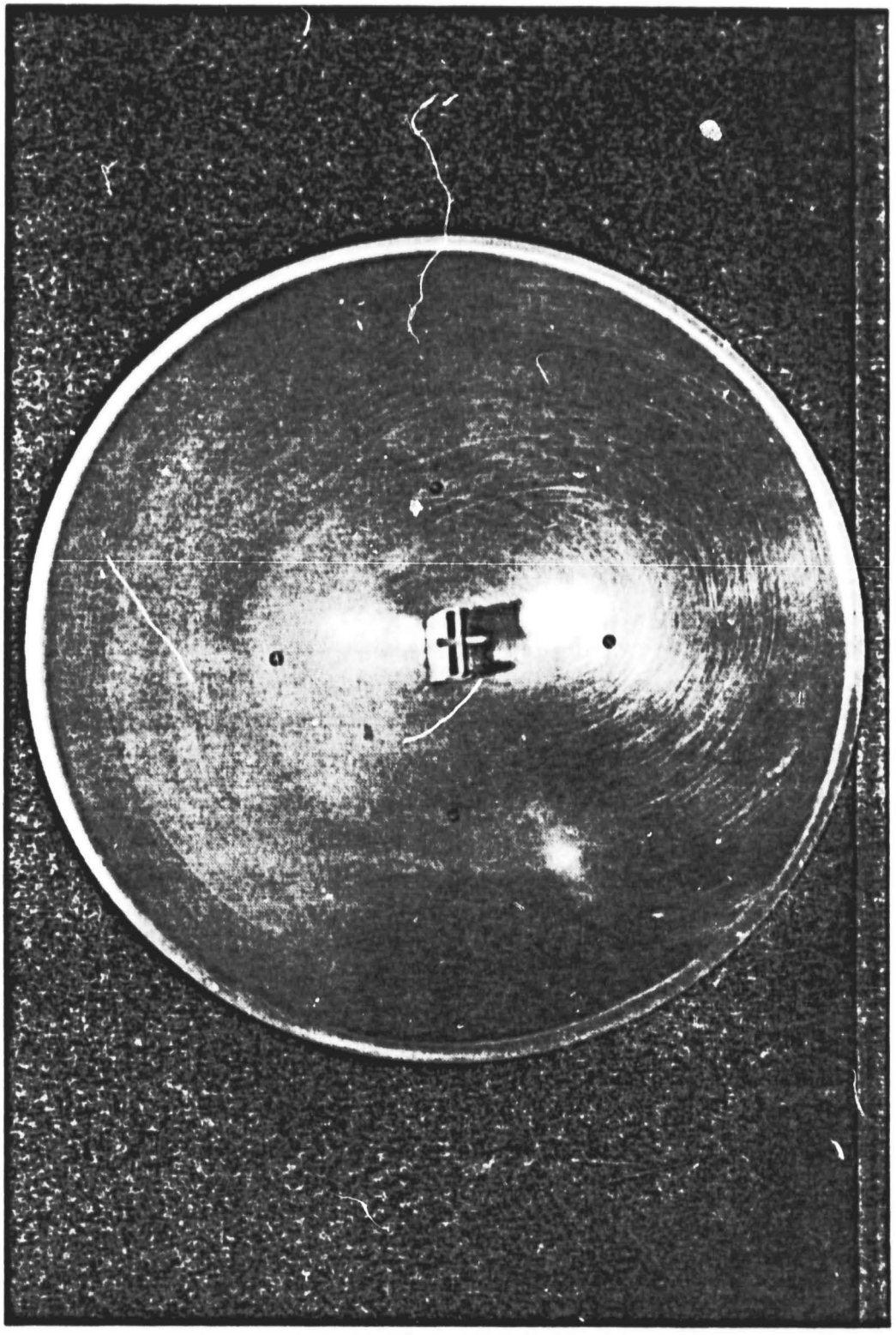

Figure A1. Transmit antenna.

Reflector Antenna Design

Since system costs were to be kept minimal and antennas are generally expensive devices, the option to custom-build an antenna in-house seemed appealing. The following design constraints were imposed in determing the final antenna form:

1. Inexpensive construction cost.
2. Design for a short far-field range since the system was to be portable and a high antenna structure would be prohibitive in cost.
3. Provide a narrow-beam antenna to minimize Doppler contributions and increase the number of spatially independent samples.
4. Give preference to a moderately high gain antenna to aid in handling system noise problems.
5. Operate at X-band.
6. Use low VSWR to minimize system noise due to internal reflections.

The constraints of high gain and narrow beamwidth pointed to the development of a reflector-type antenna. Silver [33] discussed a double dipole waveguide feed assembly that, when used in conjunction with a parabolic reflector [34] gave favorable results. Such a configuration was built and found to perform very well (Table A1).

Far-Field Range

If the antenna is operated in the far field, phase errors are negligible and the gain pattern can be treated as a range-independent function of θ. The far-field range criterion R_{ff} is given by

$$R_{ff} = \frac{2\,d^2}{\lambda} \tag{A1}$$

where

d = aperture effective diameter.

Beamwidth

As a first-order approximation, the beamwidth of an antenna can be fairly accurately predicted by

$$\beta = \frac{\lambda}{d} \tag{A2}$$

where

β = half-power beamwidth (radians)

λ = free-space wavelength.

From (A1) and (A2) we see that there is an inverse relation, for a given d, between beamwidth and far-field requirements. Therefore, some compromise is needed. The 30-cm reflector turned out to be a good compromise.

Figure A2 shows the final dimensions used and Figure A3 shows the results of return-loss tests on the feed with and without the reflector. This feed has a large radiation beamwidth that allows for full aperture illumination at a relatively short focal length. Excessive illumination, or spillover, tends to raise the sidelobe level and should be avoided.

The antenna was next tested at the Remote Sensing Laboratory antenna range to focus the feed properly and to cut patterns. The results are shown in Figures A4 and A5.

Product Patterns

It is necessary to find the product or multiplication patterns of the antennas in order to calculate the area on the ground that contributes to the radar backscatter. One way to calculate the product beamwidths with good accuracy is to use the Gaussian approximation. This states that, for a single antenna, the one-way gain distribution is described by

$$G = G_0 \, e^{-a\theta^2/\beta^2} \qquad \text{(A3)}$$

where

G_0 = boresight gain

β = half-power beamwidth

a = scale factor of 0.693

θ = angle away from boresight

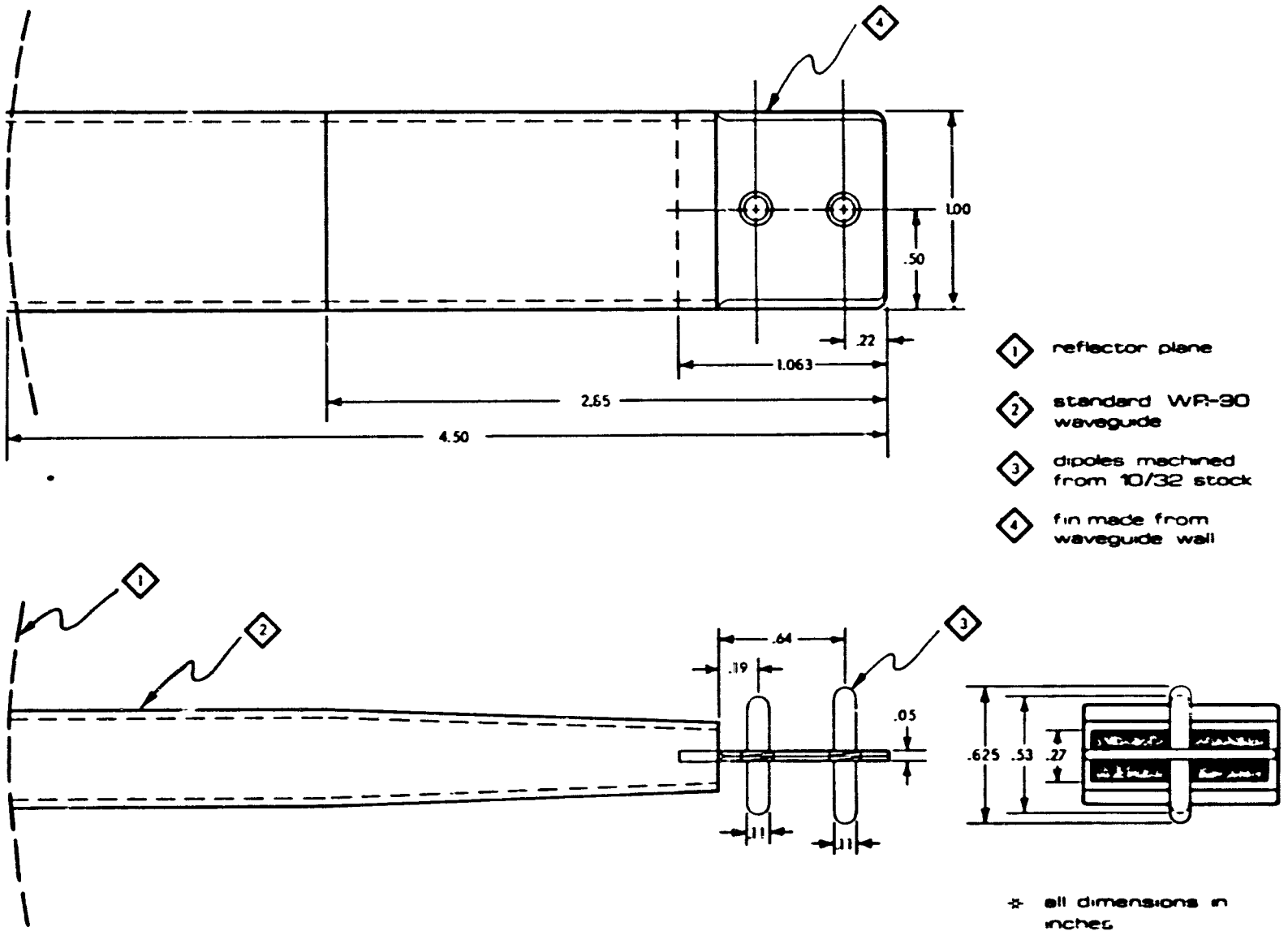

Figure A2. Double dipole feed assembly.

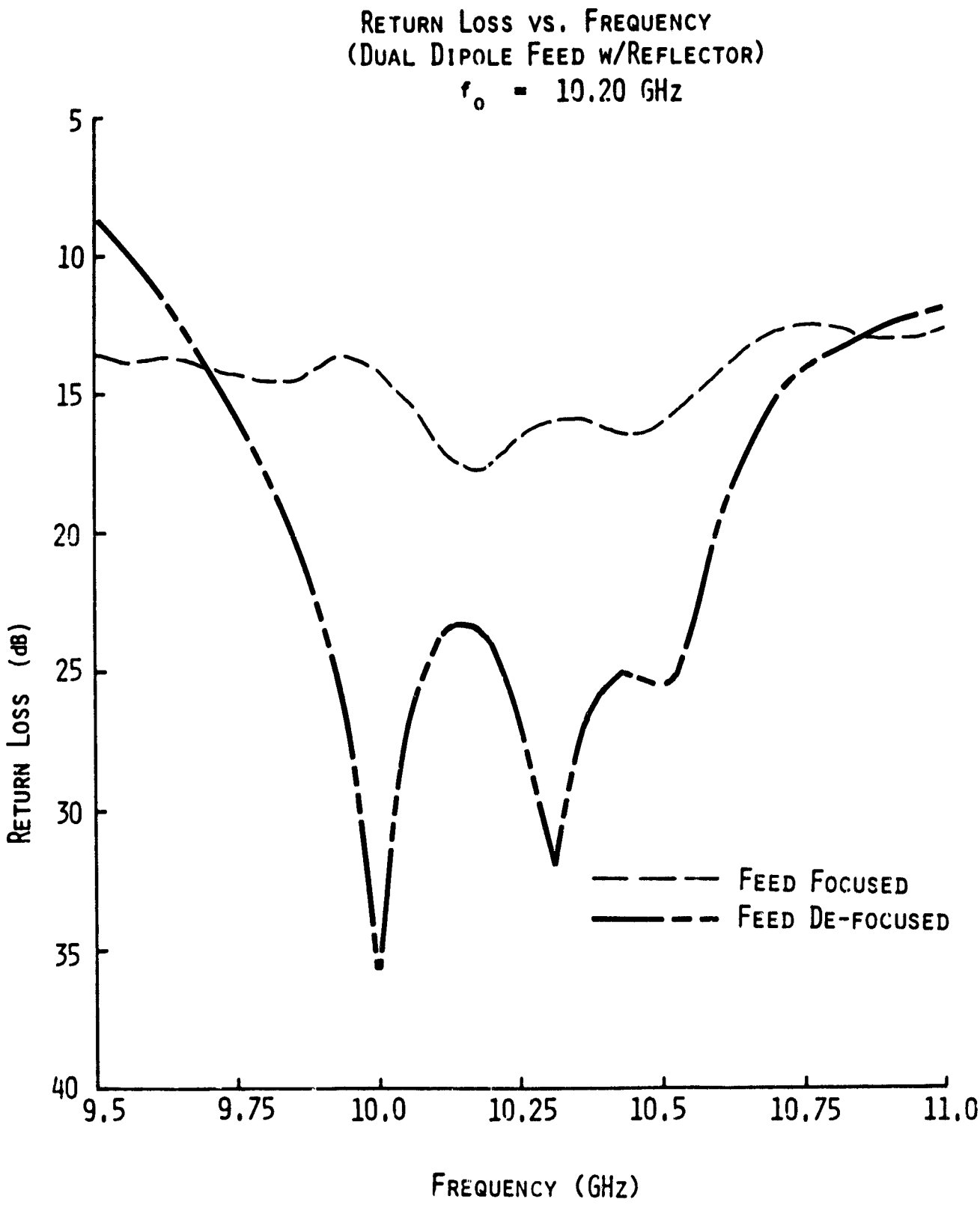

Figure A3. Reflector antenna return loss as a function of frequency.

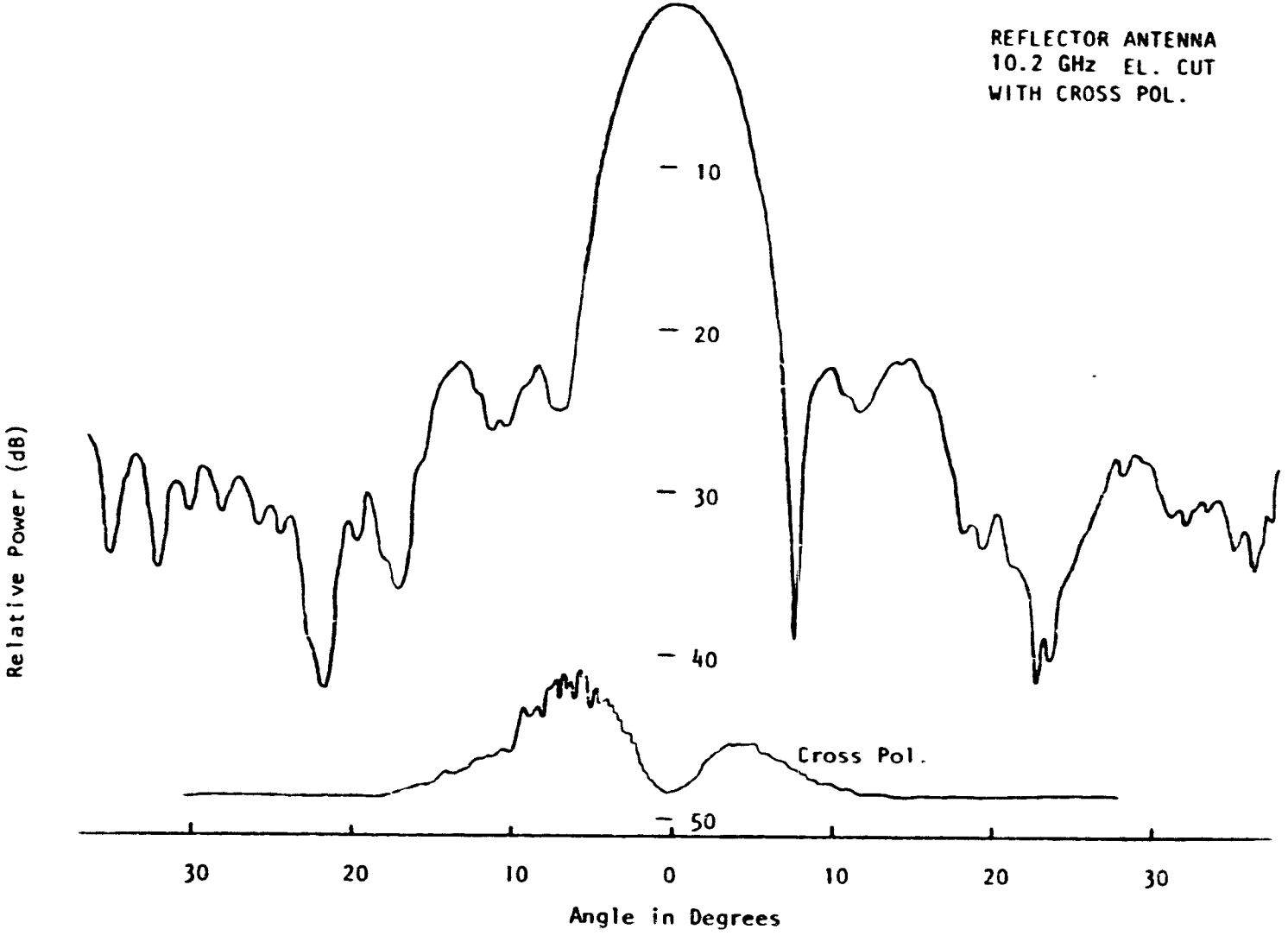

Figure A4. Reflector antenna elevation pattern with cross-polarization pattern.

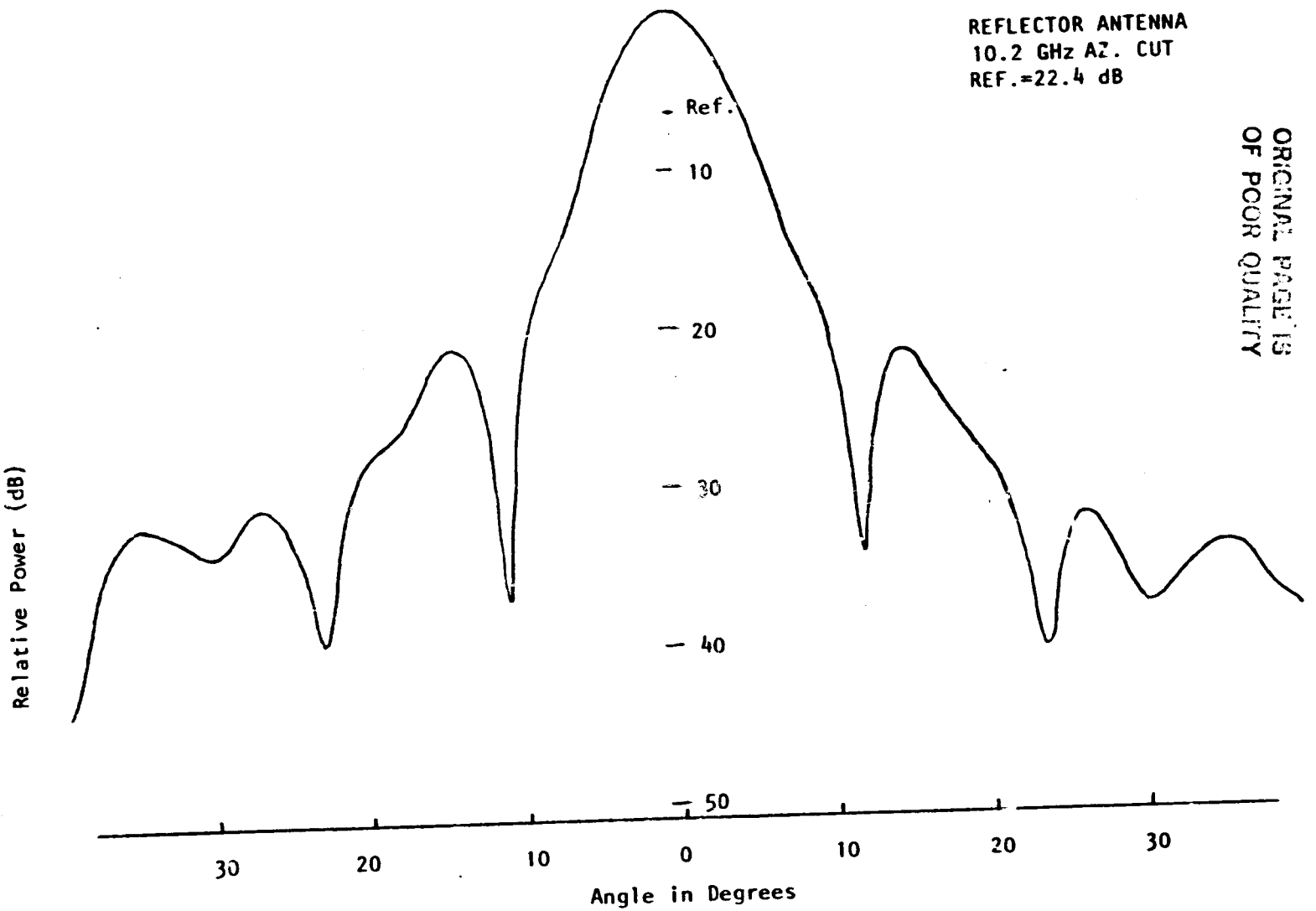

Figure A5. Reflector antenna azimuth pattern.

For a single antenna, the round-trip or two-way gain distribution is described by

$$G^2 = G_o^2 \, e^{-2a \cdot \theta^2/\beta^2} \, . \tag{A4}$$

If we take (A4) and define a new beamwidth β_{eq} such that

$$G_o^2 \, e^{-2a\theta^2/\beta^2} \triangleq G_o^2 \, e^{-a\theta^2/\beta_{eq}^2} \, , \tag{A5}$$

then we see

$$\beta_{eq} = \beta/\sqrt{2} \, . \tag{A6}$$

The equivalent beamwidth for a two-antenna system may be obtained using a similar procedure. For the two-way gain distribution of two separate antennas

$$G_1 \, G_2 = G_{01} \, e^{-a\theta^2/\beta_1^2} \cdot G_{02} \, e^{-a\theta^2/\beta_2^2} \tag{A7}$$

$$= G_{01} \, G_{02} \, e^{-a\theta^2 \, (1/\beta_1^2 \, + \, 1/\beta_2^2)} \, . \tag{A8}$$

Once again defining the equivalent beamwidth as β_{eq}, (A8) is

$$G_1 \, G_2 \triangleq G_{01} \, G_{02} \, e^{-a\theta^2/\beta_{eq}^2} \tag{A9}$$

from which we get the result

$$\beta_{eq} = \left(\frac{\beta_2^2}{\beta_1^2 + \beta_2^2} \right)^{\frac{1}{2}} \qquad \text{(A10)}$$

Table A2 shows the resultant product beamwidths for the two antennas used in the MARS system.

TABLE A2

MARS Product Beamwidths
and Product Gain

Polarization	Gain	$\beta_{Elevation}$	$\beta_{Azimuth}$
VV	28.8 dB	3.96°	4.31°
VH	25.6 dB	5.44°	5.14°

The previous derivation assumes that there is no pointing error between the two antennas, a case that obviously cannot be true for all angles of incidence. However, if there is significant pattern overlap and very small gain perturbations in the product patterns, the approximations are correct.

To verify this point, the product patterns were calculated to ± 8° from the boresight angle. This angular range was used because the reflector antenna gain drops off rapidly past 3° and tends to dominate the product result. Figure A6 shows the antenna

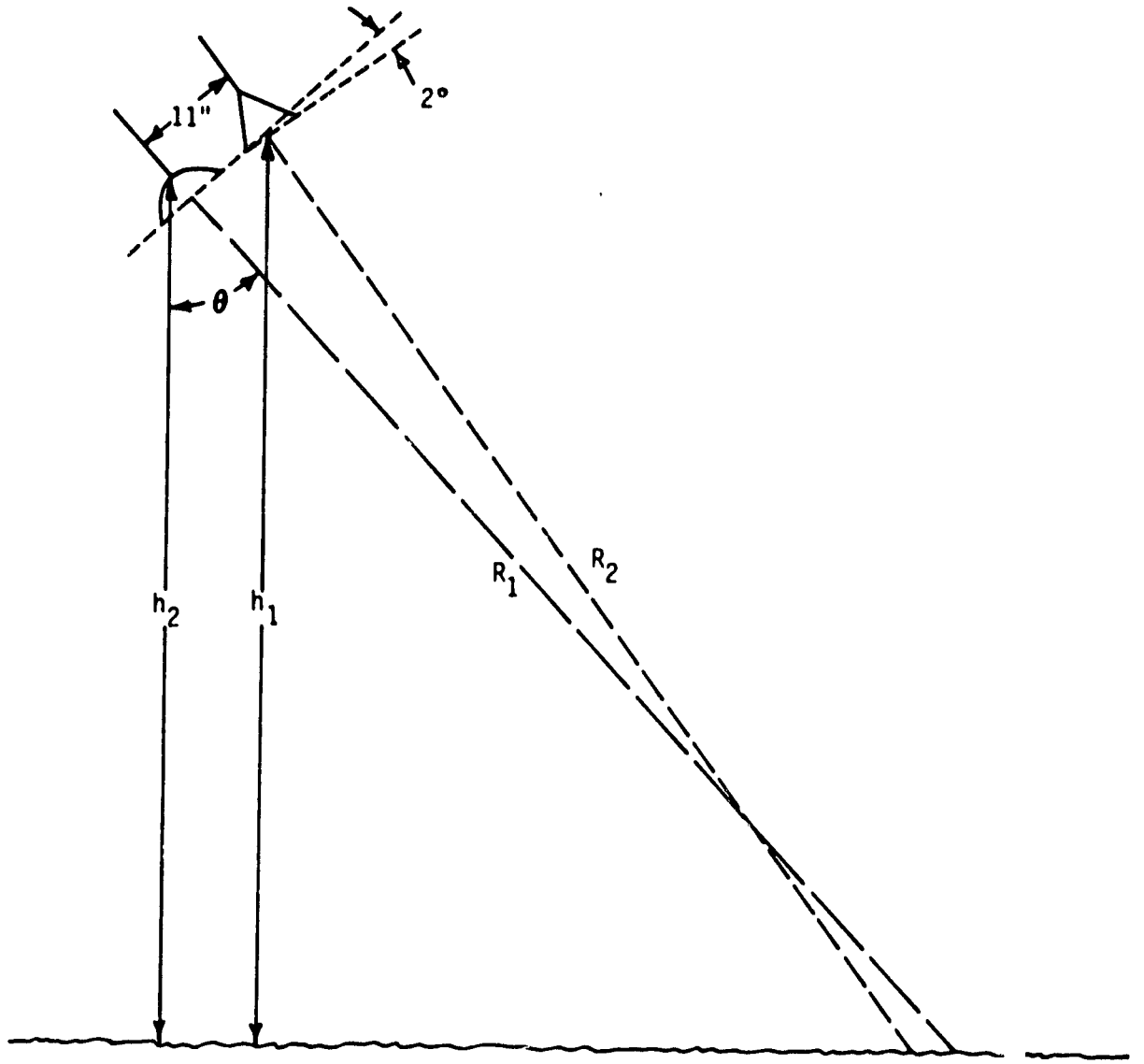

Figure A6. Geometry used to find antenna pointing error.

gecmetry that was used to determine the pointing error. Figures A7 through A12 show the one-way and product patterns for the various angles of incidence as indicated. Since the antennas are aligned in the H-planes, only one pattern need be calculated for the VH, Az orientation. The pointing error, as seen from the product patterns, is essentially negligible. This is due to the fact that the horn antenna has a beam-width approximately twice that of the refelctor antenna. The measured error due to pointing problems was 0.1 dB measured from the lens at a range corresponding to 70° incidence angle.

As a final note, the assumptions that were made concerning the relationship of the Gaussian approximations to the beamwidth calculations must be correct since the product patterns match the Gaussian results exceptionally well.

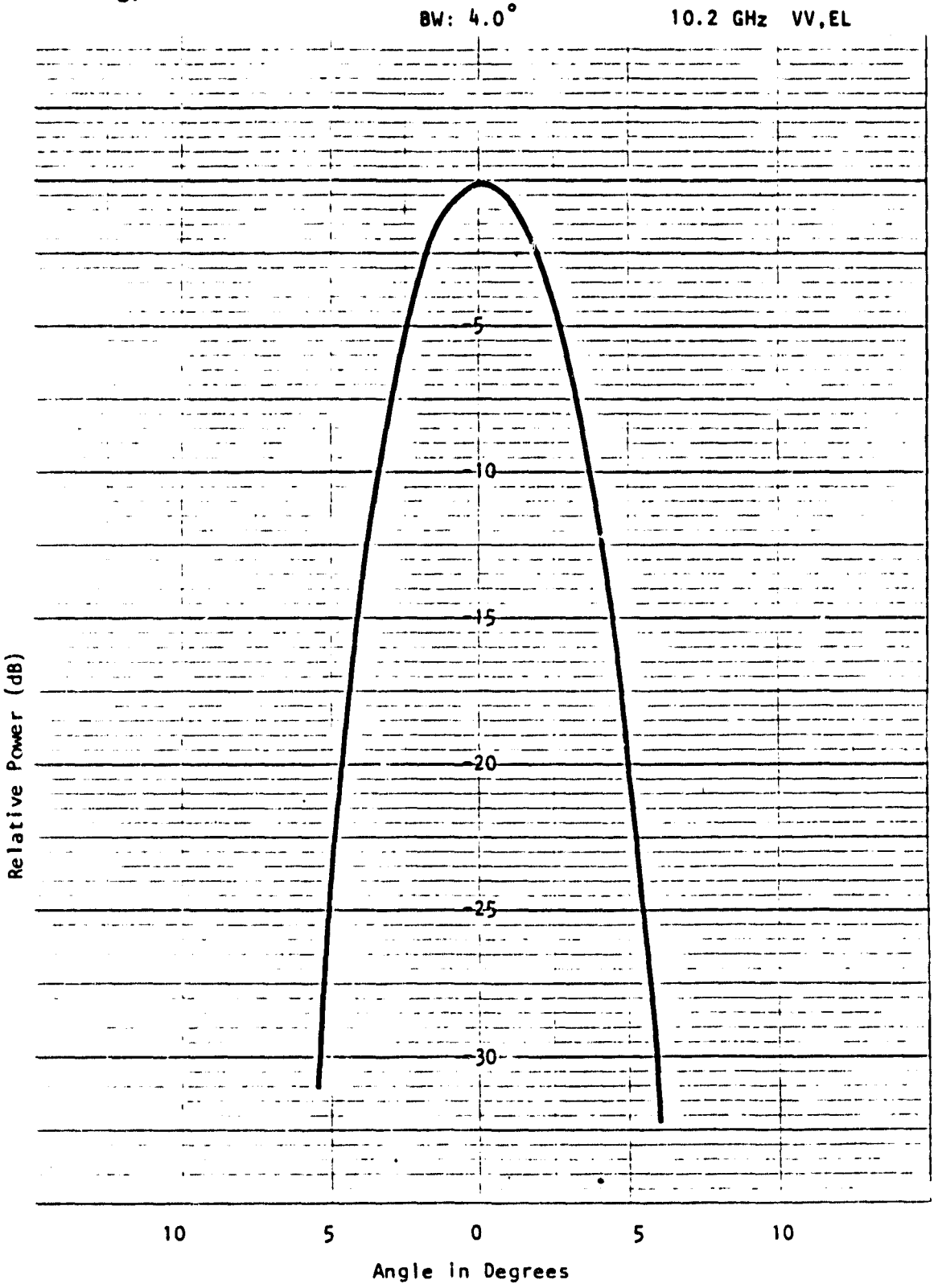

Figure A7.

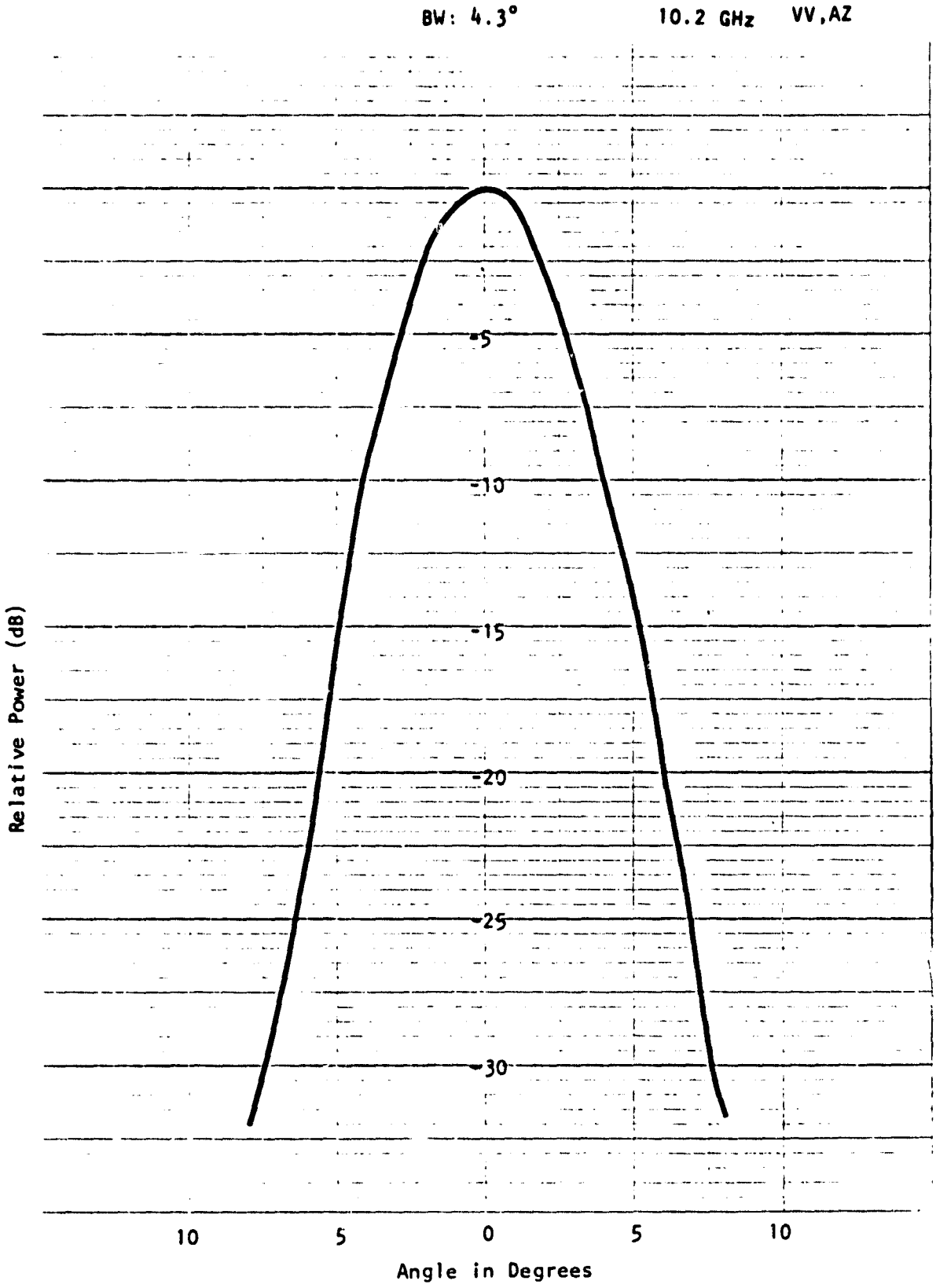

Figure A8.

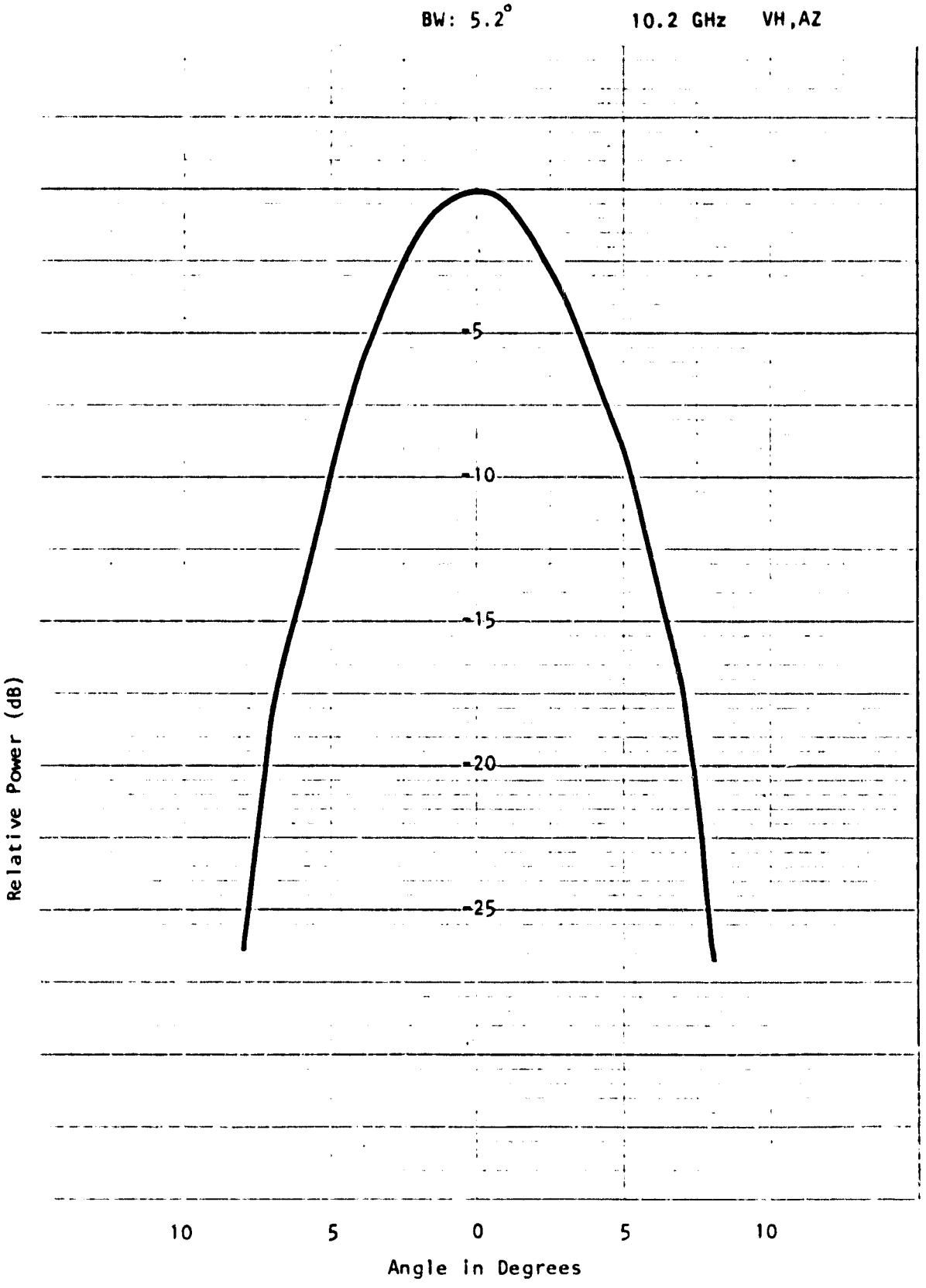

Figure A9.

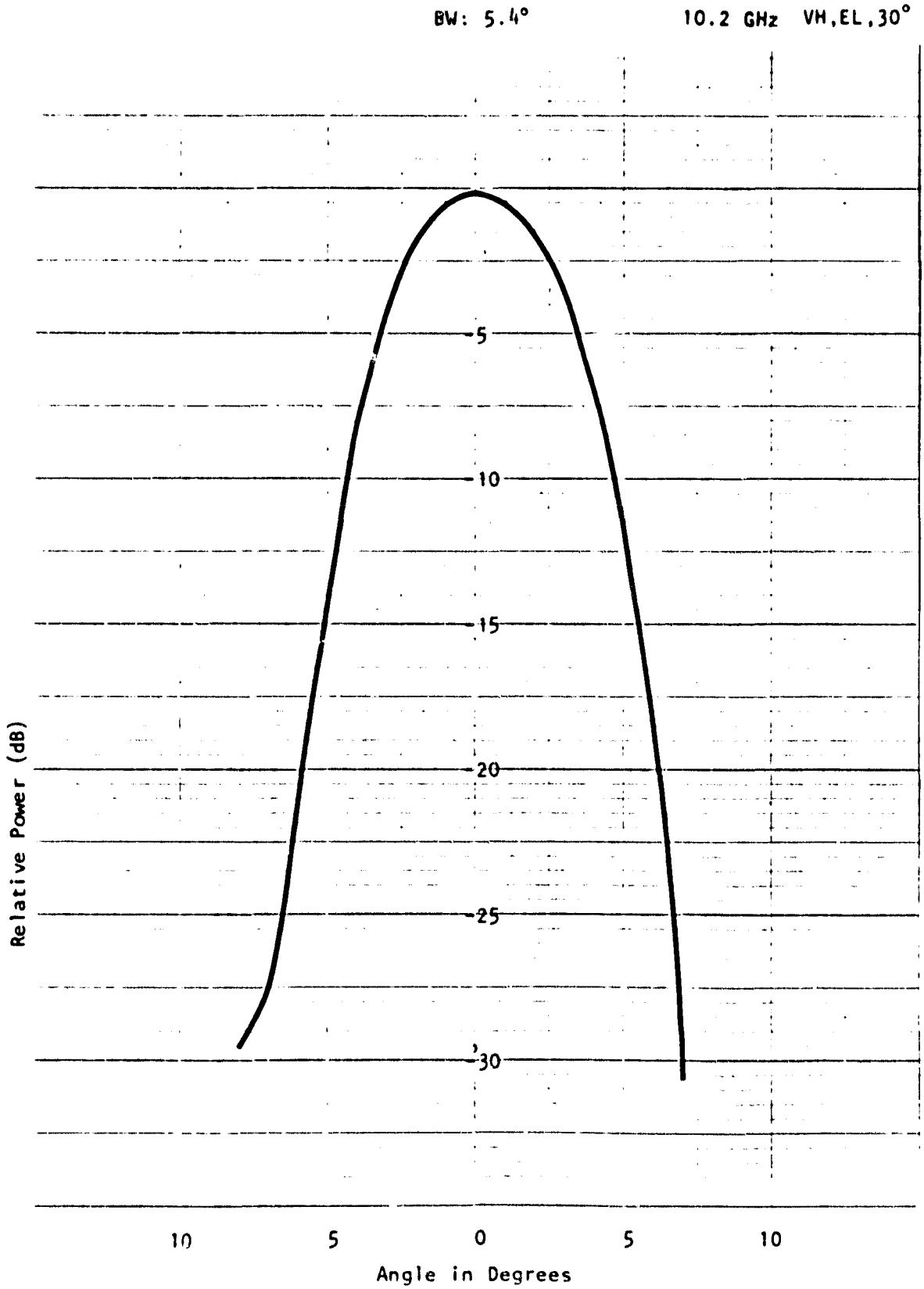

Figure A10.

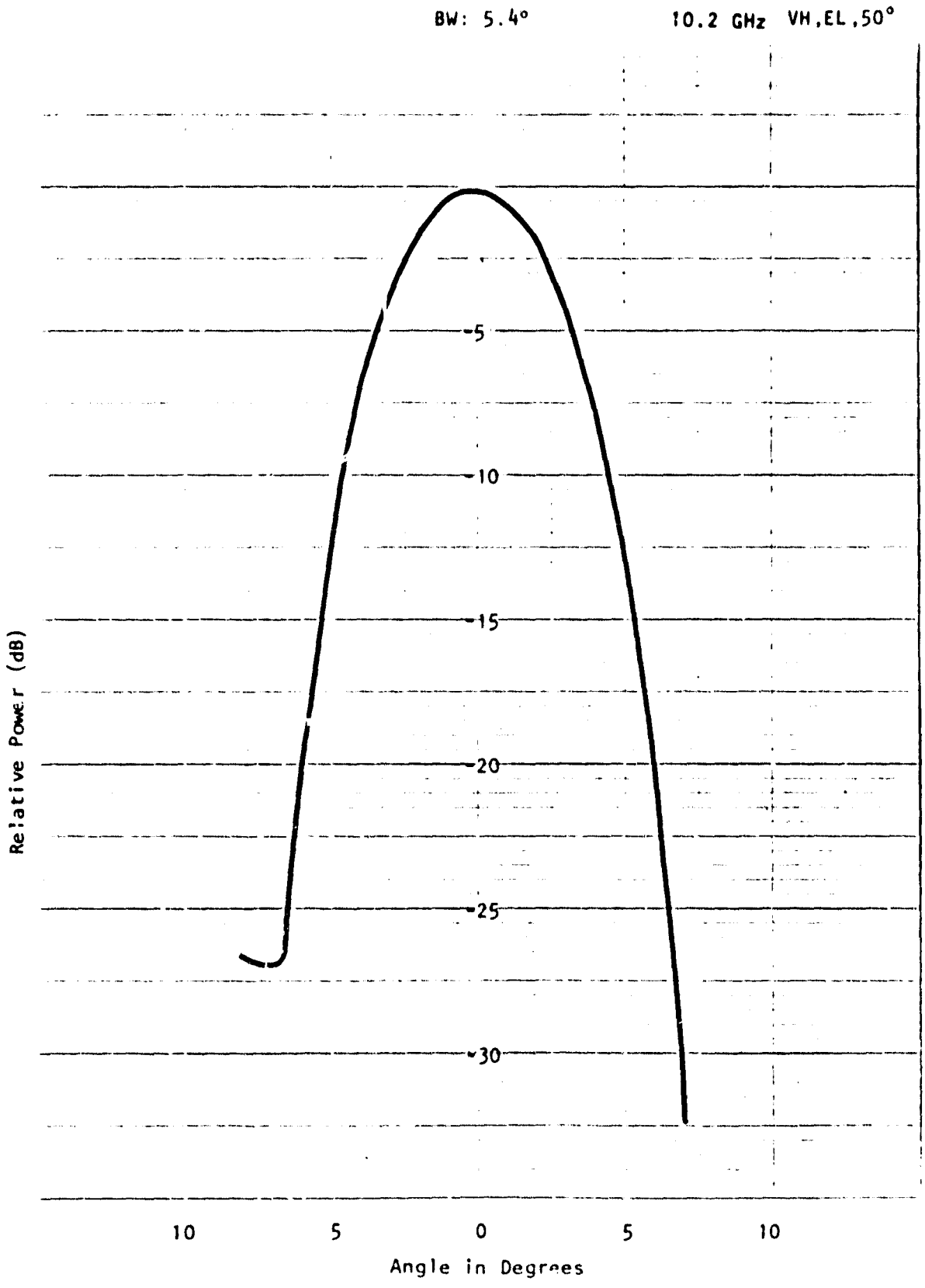

Figure A11.

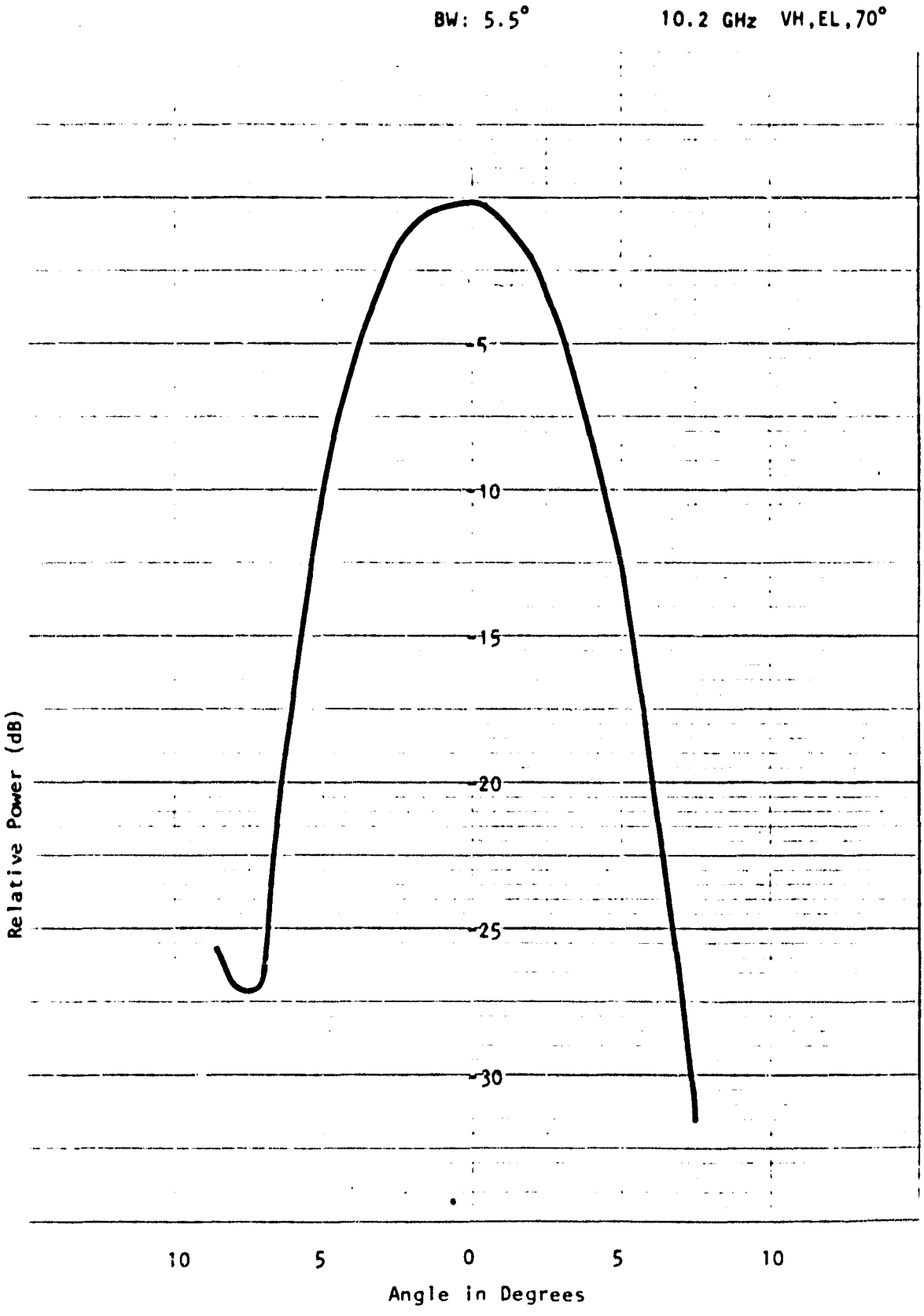

Figure A12.

APPENDIX B

CIRCUIT-BOARD DOCUMENTATION AND TUNING

Bus Board

The bus board is shown mounted in the mainframe with edge connectors in Figure B1. A listing in the lower left corner of the board gives a listing of the test jacks on the bus and their functions. Communication between individual cards was necessary and a bus approach was used for three reasons:

1. To minimize stray wires.
2. Because it is a simple, modular concept.
3. Because of the flexible order of car locations.

The first reason is self-evident due to the fact that stray capacitance and signal crosstalk can be minimized with short, isolated wires. Isolation is obtained by using a bus structure with widely spaced traces.

The second concept, modularity, seemed to be a good design point because it aided in overall system simplification. There are six card slots for the six cards, each of which performs one basic function. This modular construction had sturdy structural characteristics which were good for a system that was likely to be bounced around rather roughly during experiments.

The last point is one of convenience. With the exception of the power board, any board can work in any card slot and perform well. This eliminates the potential problems brought about by someone inadvertently putting a card in the wrong connector. Table B1 lists all lines, functions, and boards, and designates a line as input I, or output O, for a particular card. Figure B2 shows the points to which all lines physically conect.

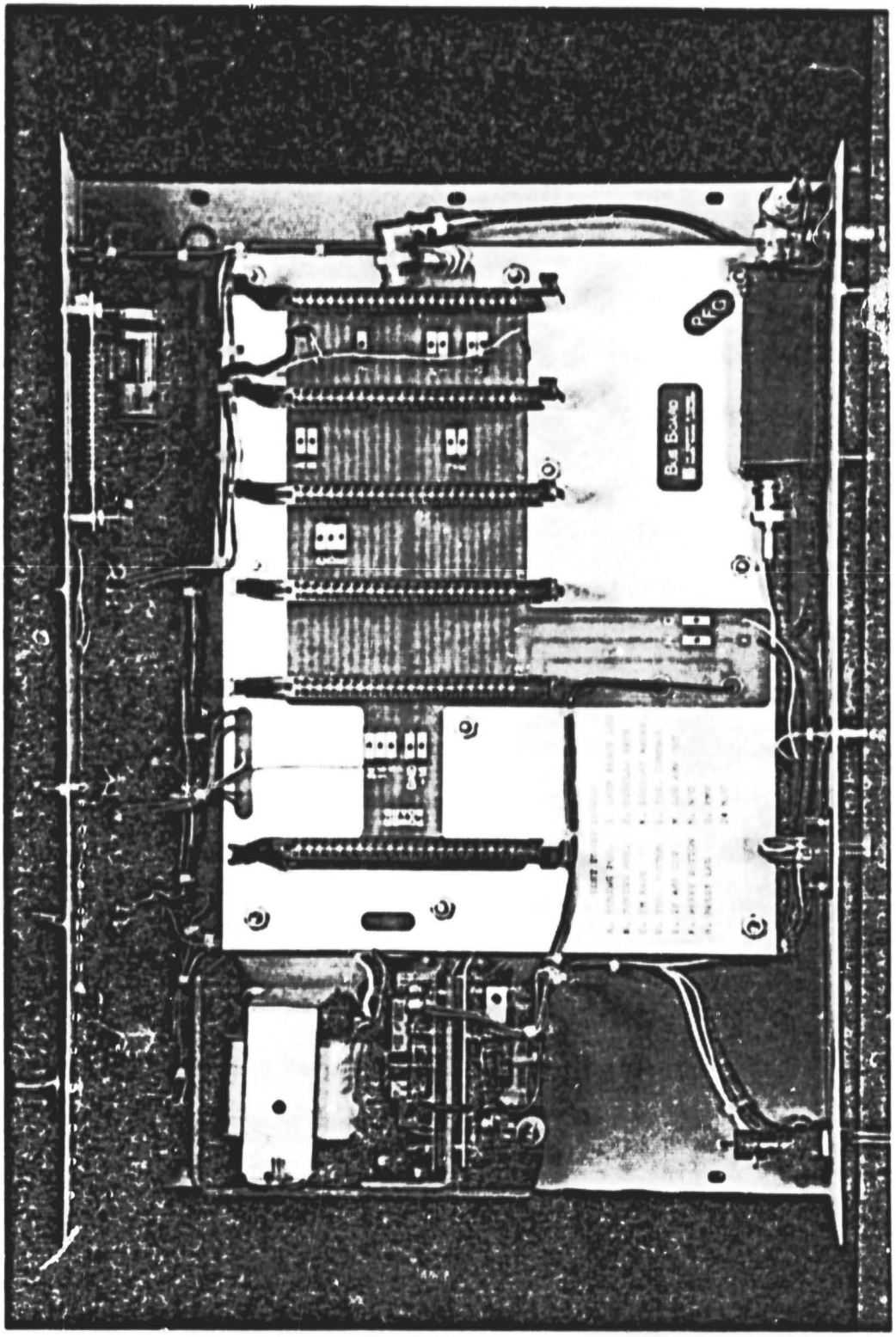

Figure B1. Bus board layout.

TABLE B1

Bus Pin Functions

Pin No.	Function	IF Amp	Detector	Signal	Control	FM
1	N/C					
2	Tune Pot. Voltage					I
3	FM Rate			I		O
4	Integrate Button				I	
5	IF Amp Out	O	I			
6	Integrate Button				I	
7	Reset Button				I	
8	N/C					
9	+15VDC	I	I	I		I
10	+5VDC				I	
11	GROUND	I		I		I
12	GROUND		I		I	
13	-15VDC	I	I	I		I
14	Reset Indicator				O	
15	Integrate Indicator				O	
16	V_{freq}			O		
17	V_{signal}			O		
18	Integrate Signal		I		O	
19	Log Amp Out		O	I		
20	N/C					
21	N/C					
22	FM Tuning Voltage					O

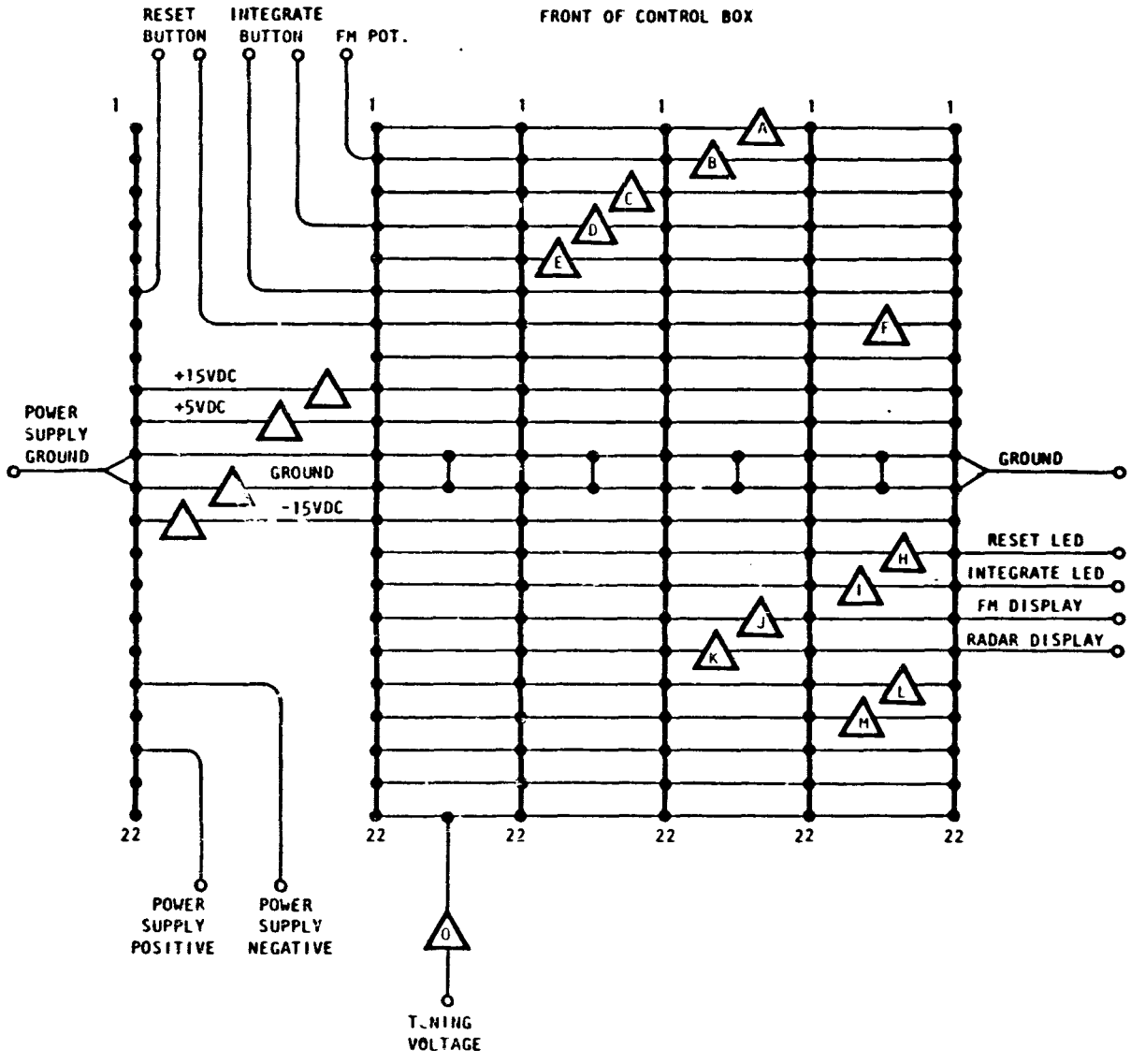

Figure B2. Bus board connections and layout.

IF Amplifier

A three-stage, transformer-matched input amplifier is used in this system. The three stages are comprised of cascaded operational amplifiers with the first stage configured in a differential mode while the last two are configured to be inverting and single-ended. The transformer at the input serves to match the input stage with the bandpass filter and to provide gain. Reasonably low noise performance was obtained by using bi-FET op-amps and film resistors in conjunction with lowpass filtering of the power supply inputs to each IC. As a final measure to minimize 1/f noise common to many monolithic amplifiers, the output of the amplifier and the input of the detector board serve as a 6-kHz highpass filter. Figure B3 is a photograph of the board and Figure B4 shows the schematic. The gain-frequency characteristic curve is shown in Figure B5; note how the gain is maximized in the region used as the IF passband. This aids somewhat in the signal peaking process and is a result of the high-pass filter at the amplifier output working in conjunction with the low-pass characteristic of the transformer at the input.

Detector/Integrator

The board shown in Figure B6 is comprised of three basic blocks. IC1 is the RMS-to-DC connector and serves to detect the signal from the IF amplifier. IC4 is the heart of the integrator network while IC5 is the log amplifier. IC2 is a scale adjusting amplifier and IC3 is an analog switch that controls the mode of the integrator, with either a integrate-and-hold command, or a reset command. Figure B7 shows a photograph of this board.

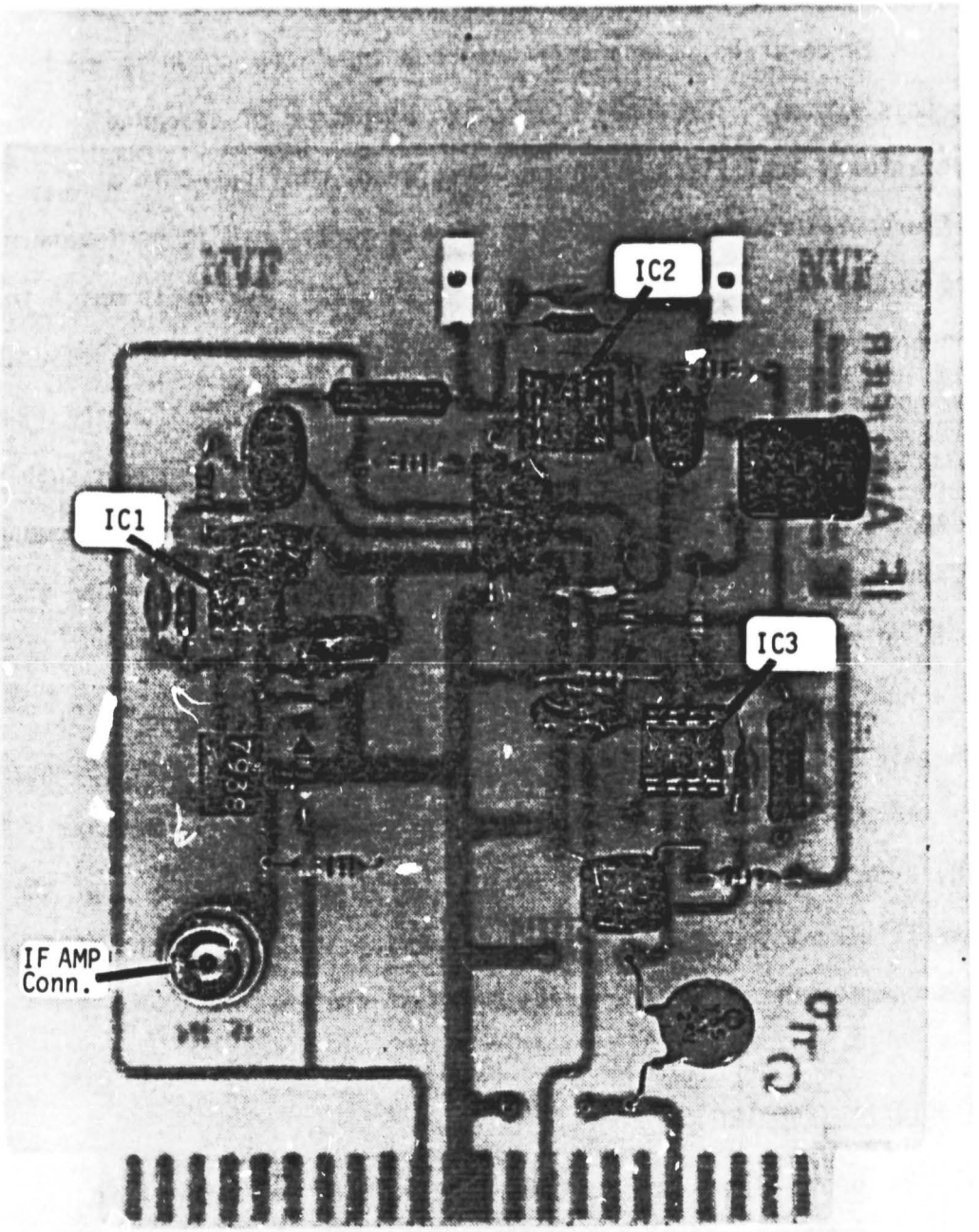

Figure B3. IF amplifier board layout.

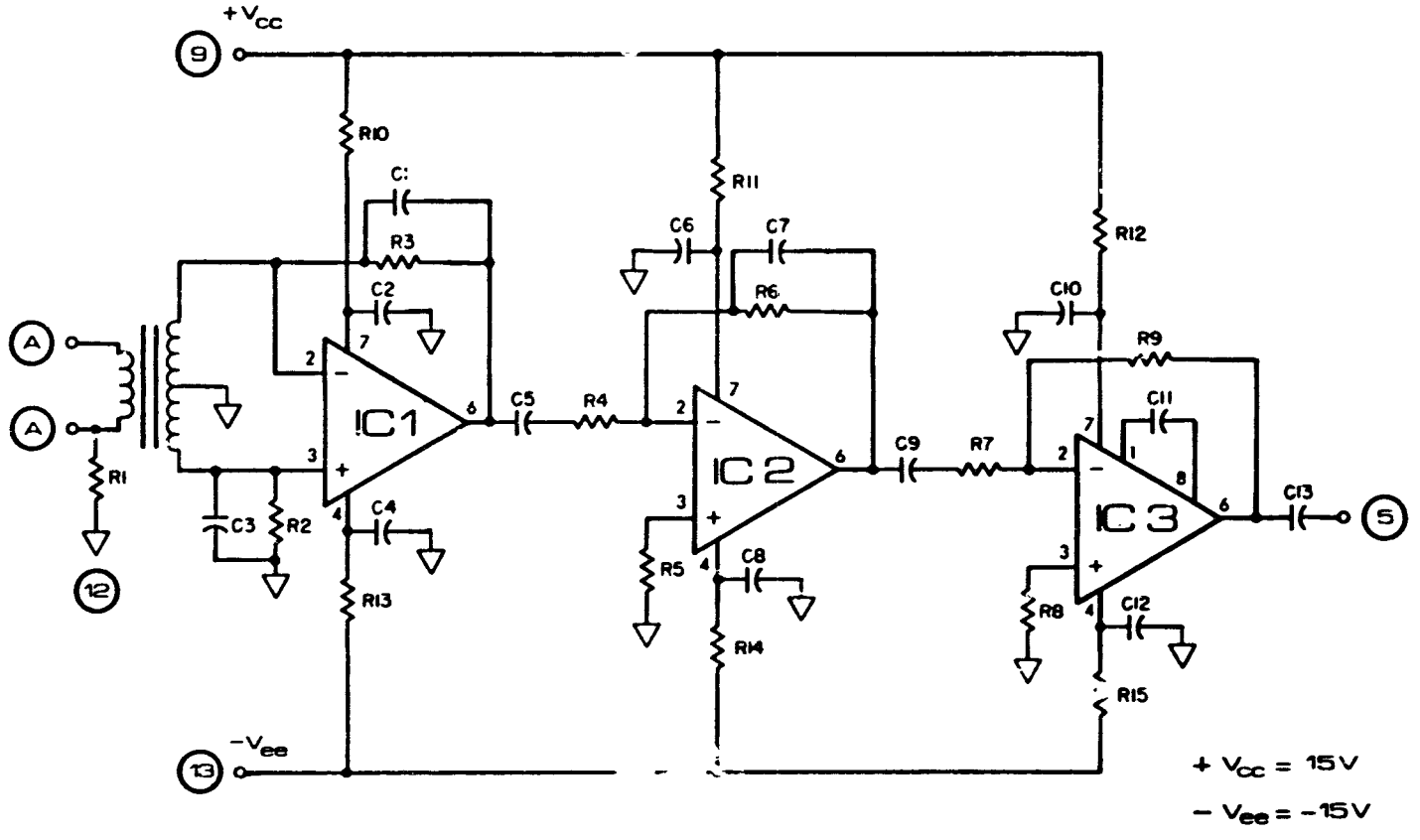

Figure B4. IF amplifier.

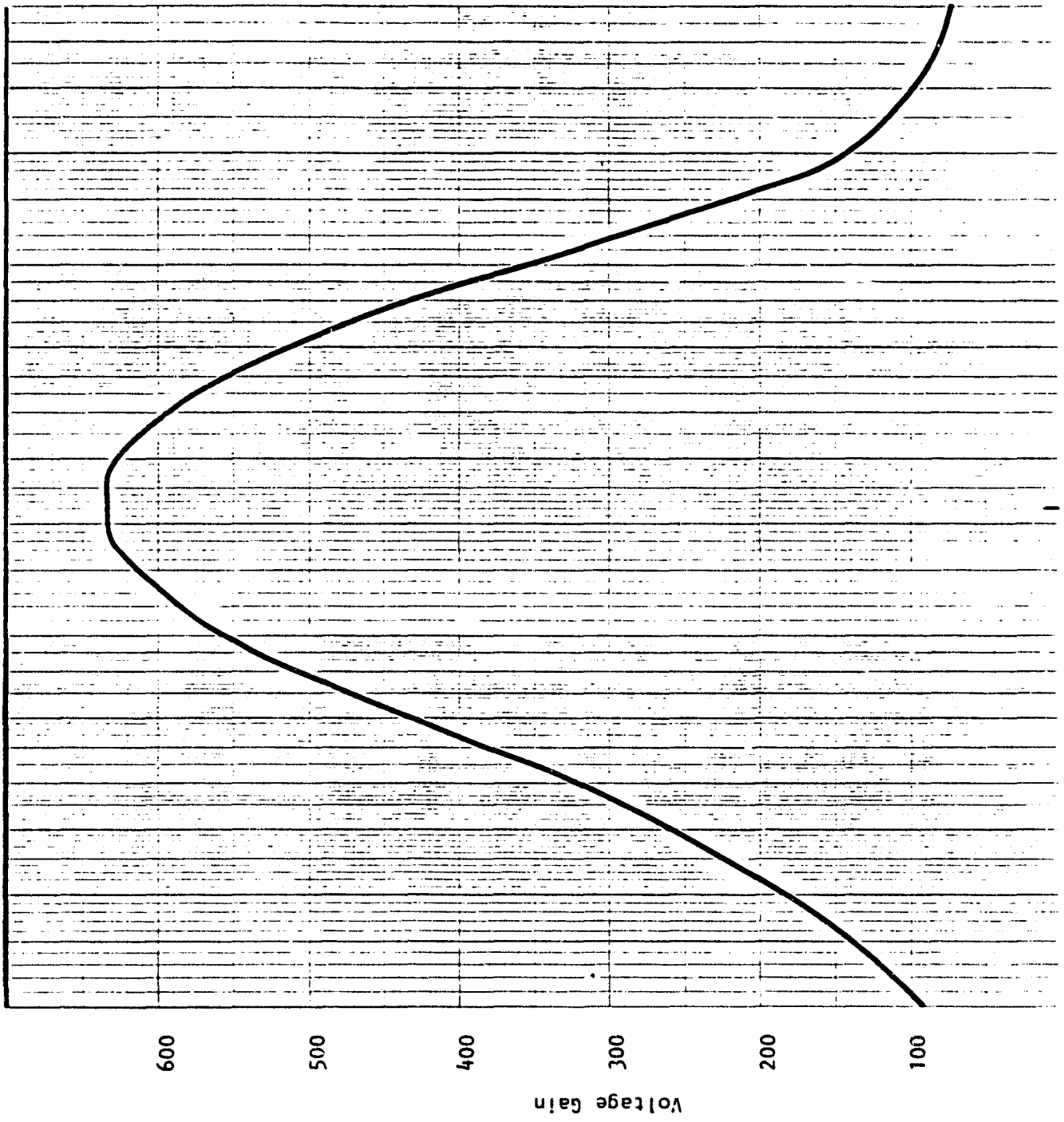

Figure B5. IF amplifier gain as a function of frequency.

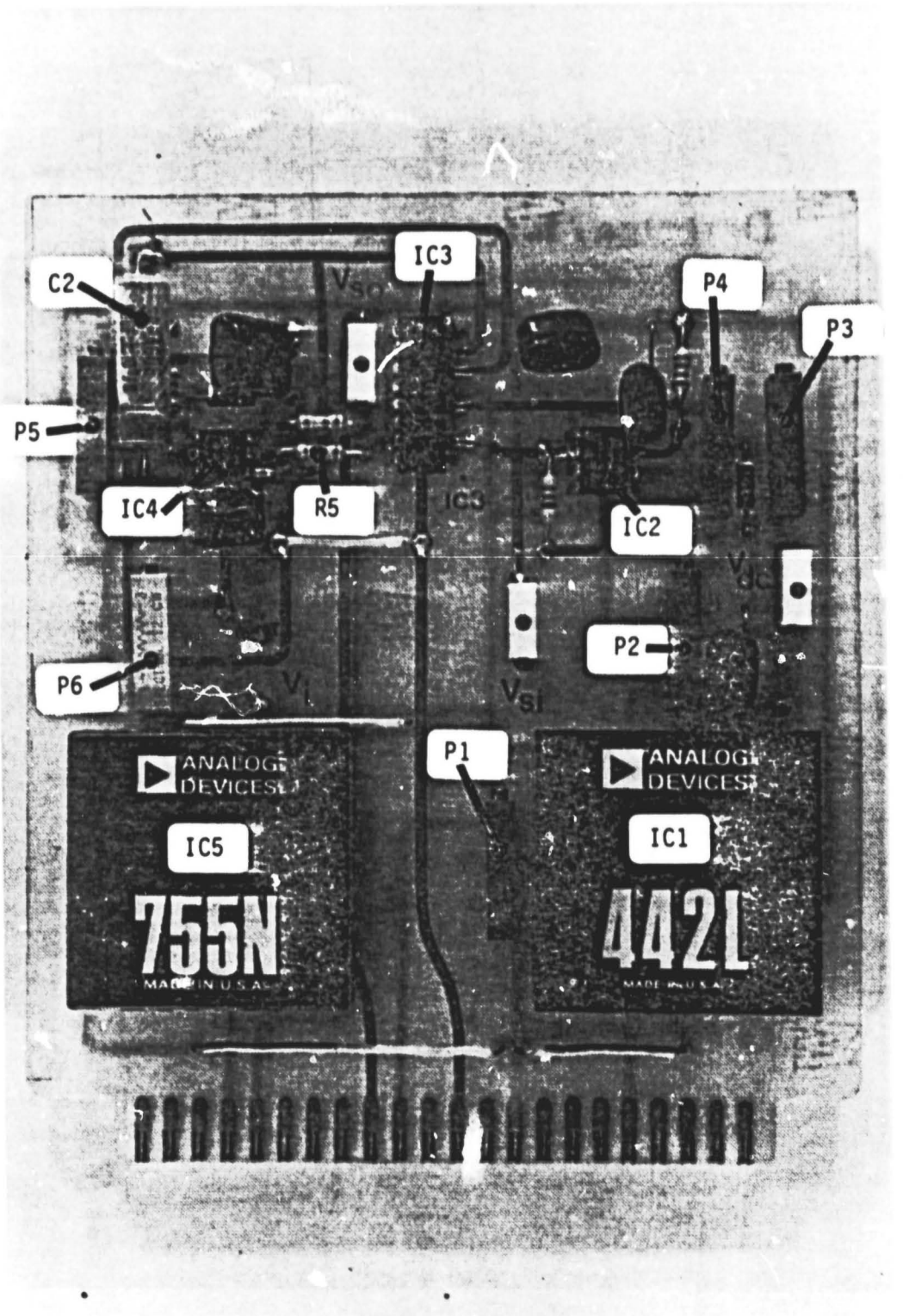

Figure B6. Integrator/detector board layout.

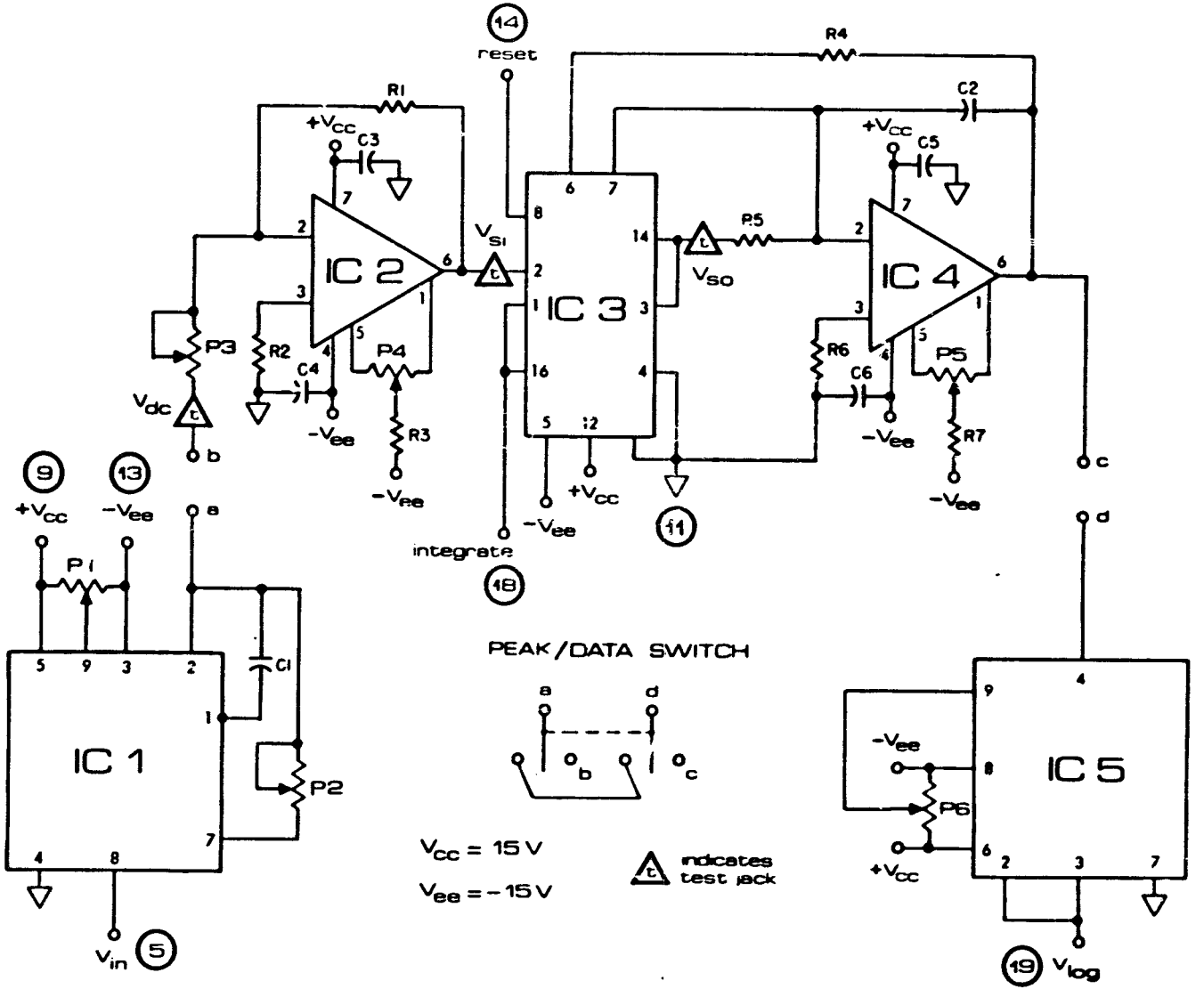

Figure B7. Detector/integrator board.

Since this card performs a critical role in the data-acquisition process, periodic tuning should be performed to maintain high reliability in the system. Table B2 describes the procedure for tuning the detector/integrator board.

TABLE B2

Integrator/Detector Board Tuning

I. RMS/DC Converter
(with IF amp removed and data switch in "PEAK" mode)

a. apply 10.0 mV RMS @ 22 kHz to PIN 5

b. adjust P2 for 10.0 mV DC at V_{DC} jack

c. apply 1.000V RMS @ 22 kHz to PIN 5

d. adjust P2 for 1.00V DC at V_{DC} jack

II. Log Amplifier
(data switch in "PEAK" mode)

a. adjust P4 until V_{sf} jack = 0.00V DC

b. depress "INTEGRATE" button and allow for one complete timing cycle

c. adjust P5 until PIN 6 of IC4 = 0.00V DC

d. with PIN 4 of IC5 grounded, adjust P6 until PIN 19 of bus = 5.4V DC

III. Integrator
(data switch in "DATA" mode)

a. apply 1.00V RMS @ 22 kHz into PIN 5

b. adjust P3 until V_{sf} = 1.00V DC

The integrator used in this circuit is linear and its configuration is shown in the schematic of Figure B8. The integrator output voltage V_i is described by

$$V_i = \frac{-1}{R5 \cdot C2} \int_0^T V_{so}\, dt \qquad (B1)$$

where T is the timing interval set by the timing chip and R2 and C1 of the control board. If we perform the integration of (B1) the result becomes (assuming $V_i = 0$ initially)

$$V_i = \frac{T}{R5 \cdot C2} V_{so} \qquad (B2)$$

where

$$T = R2 \cdot C1 .$$

If $R2 \approx R5$ and $C1 \approx C2$, as can be the case if the components come from the same lots, then (B2) becomes

$$V_i \approx V_{so} . \qquad (B3)$$

This procedure is used in the system and an error, which corresponds to component mismatch, of <2% was measured.

Figure B9 shows the error curve for the RMS to DC converter while Figure B10 shows the logging response of the logarithmic amplifier.

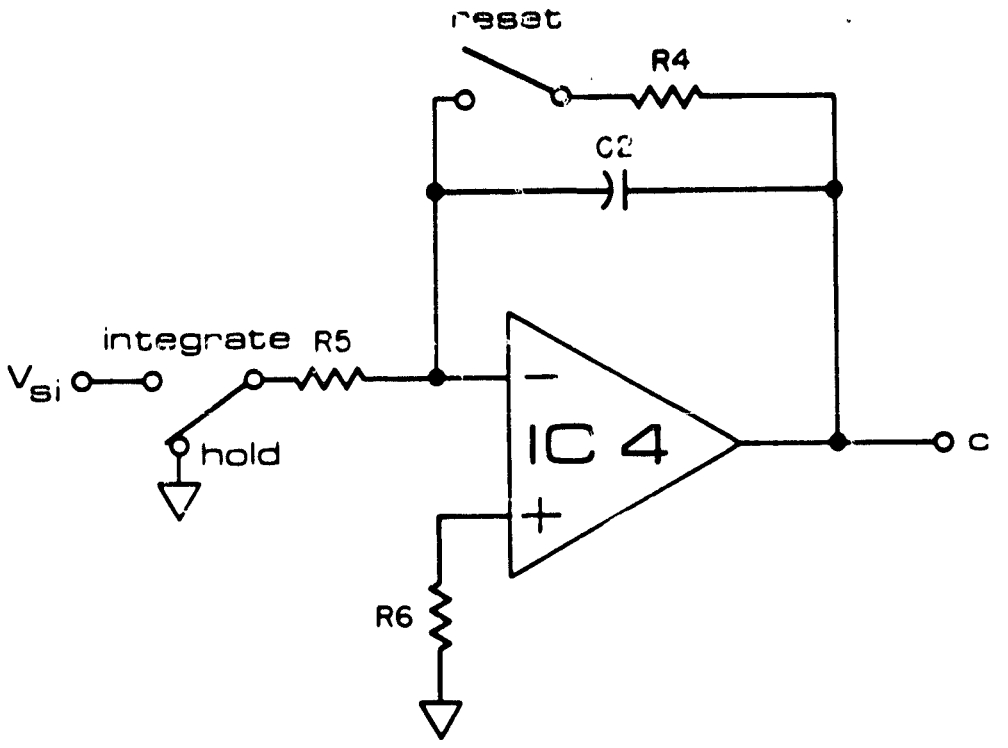

Figure B8. Schematic of MARS linear integrator.

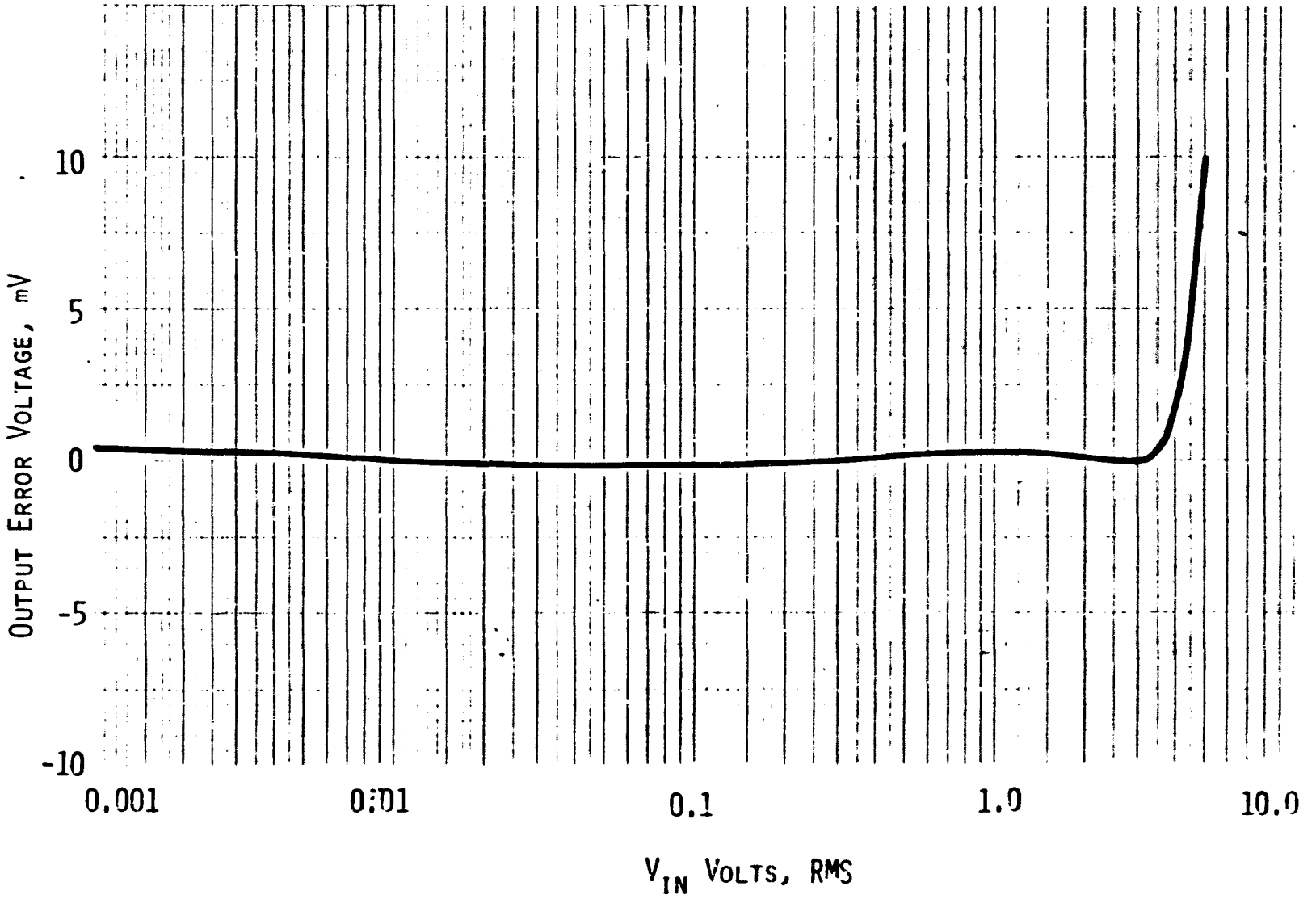

Figure B9. Error curve for 442L RMS to DC converter.

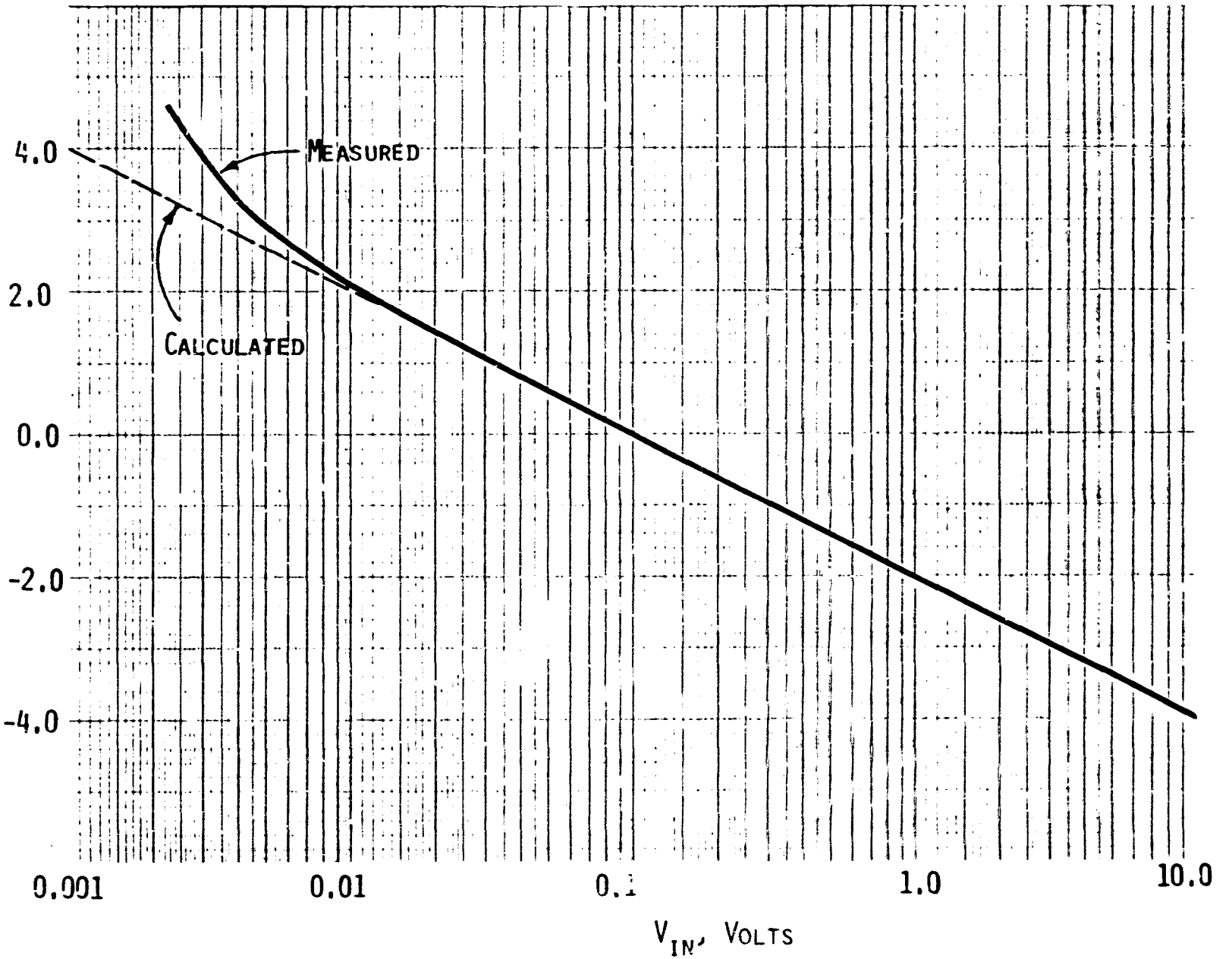

Figure B10. Characteristic curve of 755N logarithmic amplifier.

Signal Board

The signal board performs the final signal processing functions and serves as the source to the digit panel meter. The two inputs to this board are the radar signal from the logarithmic amplifier and a frequency input from the function generator chip equal to the FM rate.

Figure B11 shows this board and identifies the key components. IC1 is a frequency-to-DC-voltage converter that accepts the sinusoid output of the 8038 function generator and in turn converts the frequency input to a DC voltage designated as V_{FREQ}. This voltage is input to IC2 which is used as a scaling amplifier to convert V_{FREQ} to a signal that is displayed by the digit panel meter. The display then is equal to the FM tuning rate in hertz and is needed to determine the range to target. Figure B12 shows the error in these two components as a function of input frequency over the band used in this system.

The radar signal is input to IC3 where another scaling function is performed. This is necessary because the panel meter range is ± 2V and the log amp is capable of ranging ± 4V, hence the scaling amp was necessary. To minimize offset errors, an offset network is included. To cancel offset in the amplifier remove the detector/integrator board and adjust P2 such that PIN 17 - 0.00V.

Figure B13 shows the schematic and pin connections for this board.

C-2

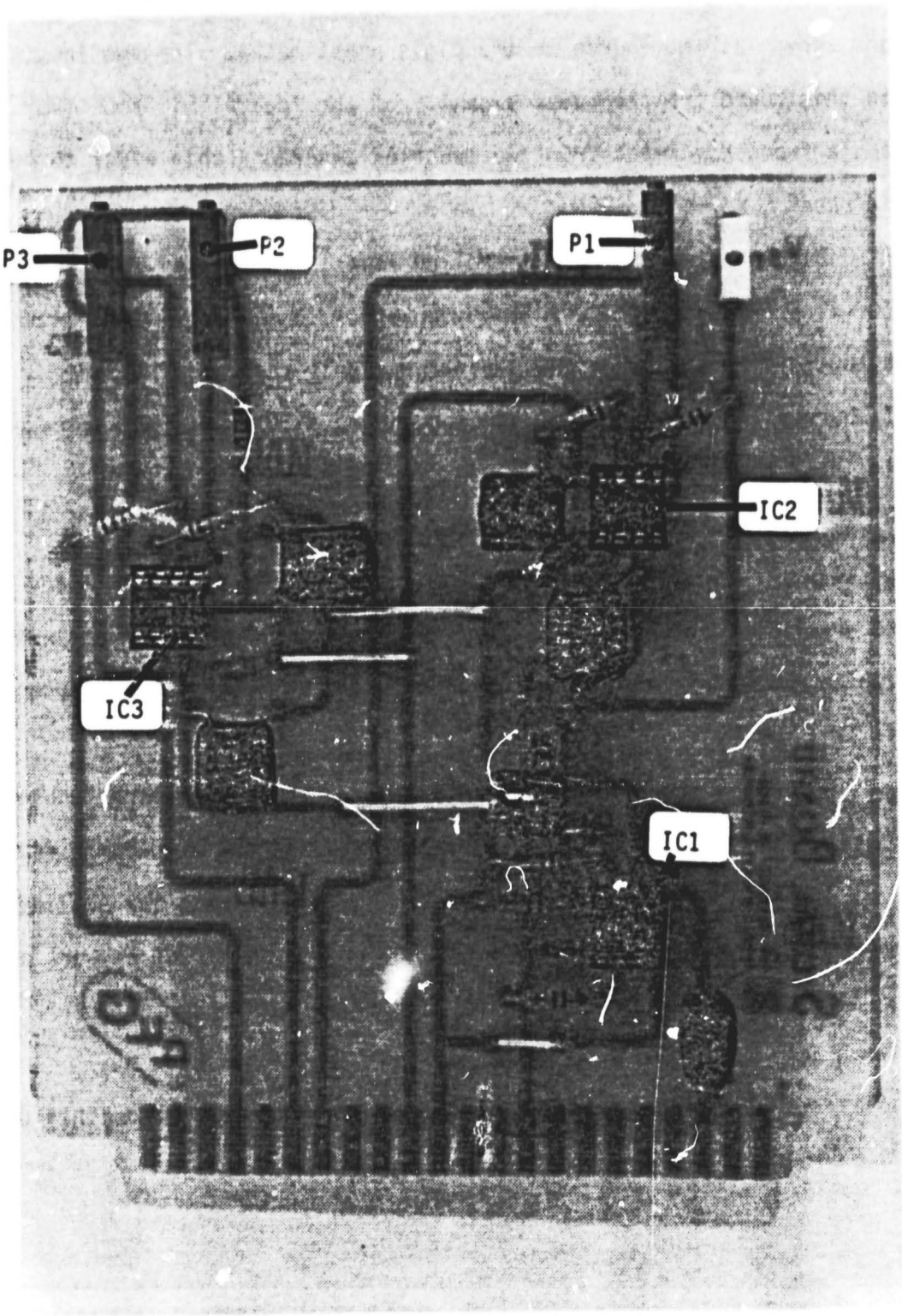

Figure B11. Signal board layout.

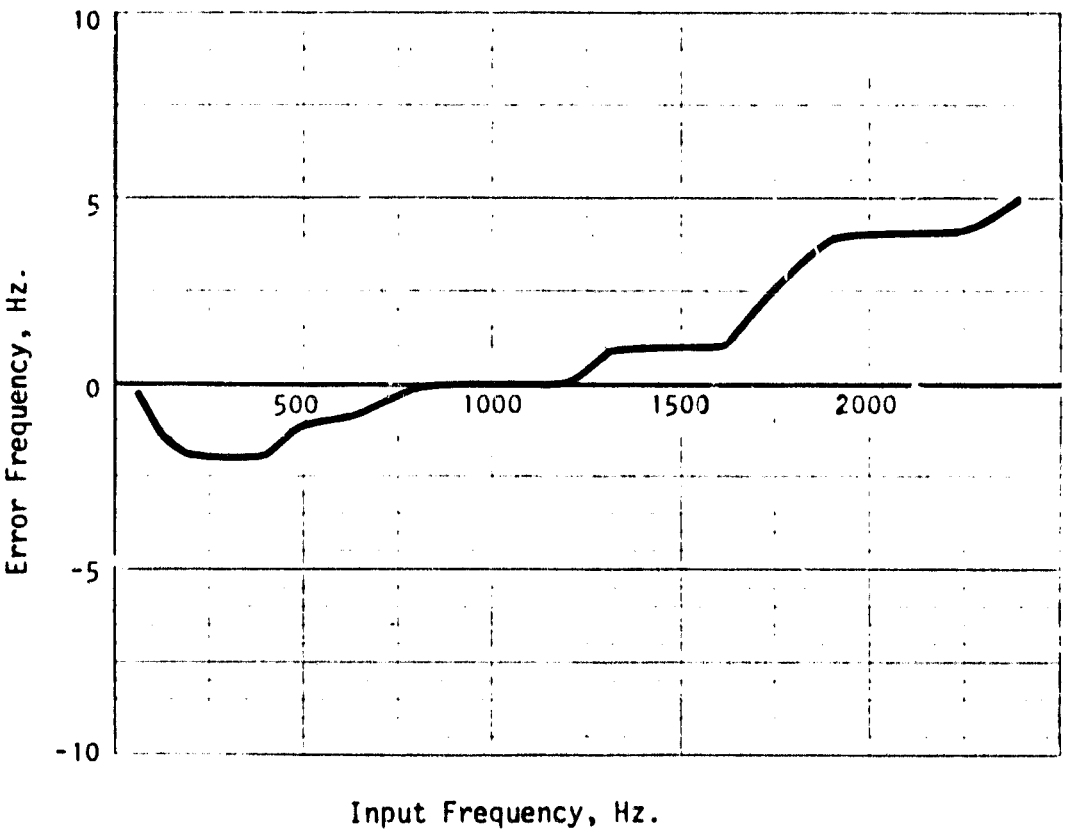

Figure B12. Output error frequency of LM2917N-8 frequency-to-voltage converter.

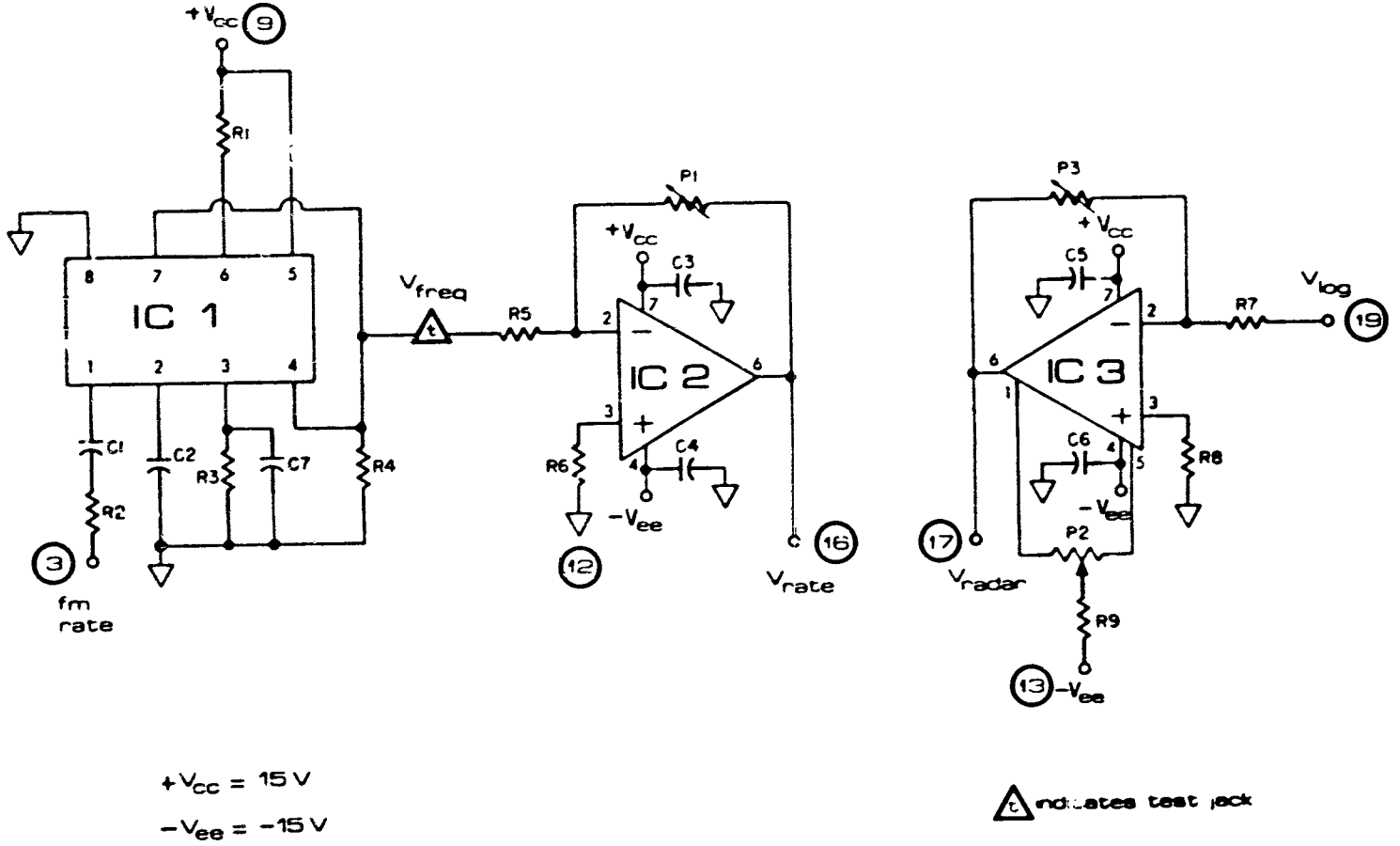

Figure B13. Signal board.

FM/Linearizer Board

Originally the MARS system was to have used a varactor tuned Gunn oscillator as a microwave power source. For this reason a five-stage resistive ladder network was designed to linearize the non-linear tuning characteristic of the varactor. However, due to RF bandwidth limitations encountered, a VIG (Yttrium-Iron-Garnet) oscillator was chosen. These devices have an inherently linear relation between output frequency and tuning current that rendered the linearizer unnecessary. This feature was left on the board, however, in the event that a non-linear source be used in the future.

The chief function of this board is to create a triangle tuning voltage that serves to shift the IF spectrum in the frequency domain to some desired location. That location is set at 22 kHz for this system, which is the center of the bandpass filter. The process of moving the spectrum is what is actually happening during the peaking procedure as the spectrum is shifted into the bandpass filter.

IC1 is the function generator chip which has three output waveforms: sine, square, and triangle. The frequency of these waveforms is a function of the DC voltage applied to the chip from the FM tuning potentiometer. A 10- to 15-V range in DC voltage corresponds to a frequency range of 40 to 1600 Hz. The sine output is processed by the signal board and displayed on the panel meter while the triangle wave is used to tune the radar. The square wave is not used.

ORIGINAL PAGE
BLACK AND WHITE PHOTOGRAPH

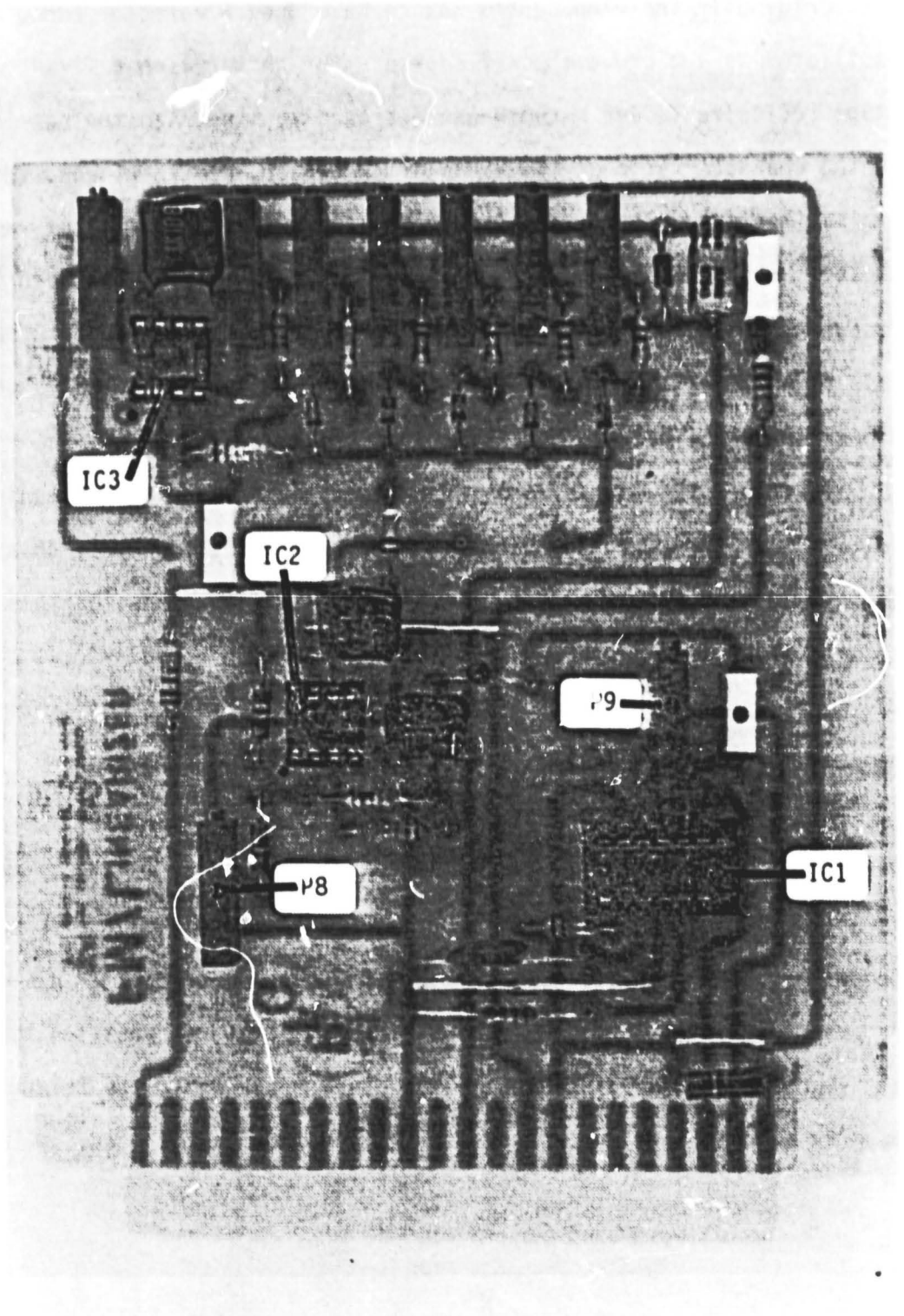

Figure B14. FM/linearlizer board layout.

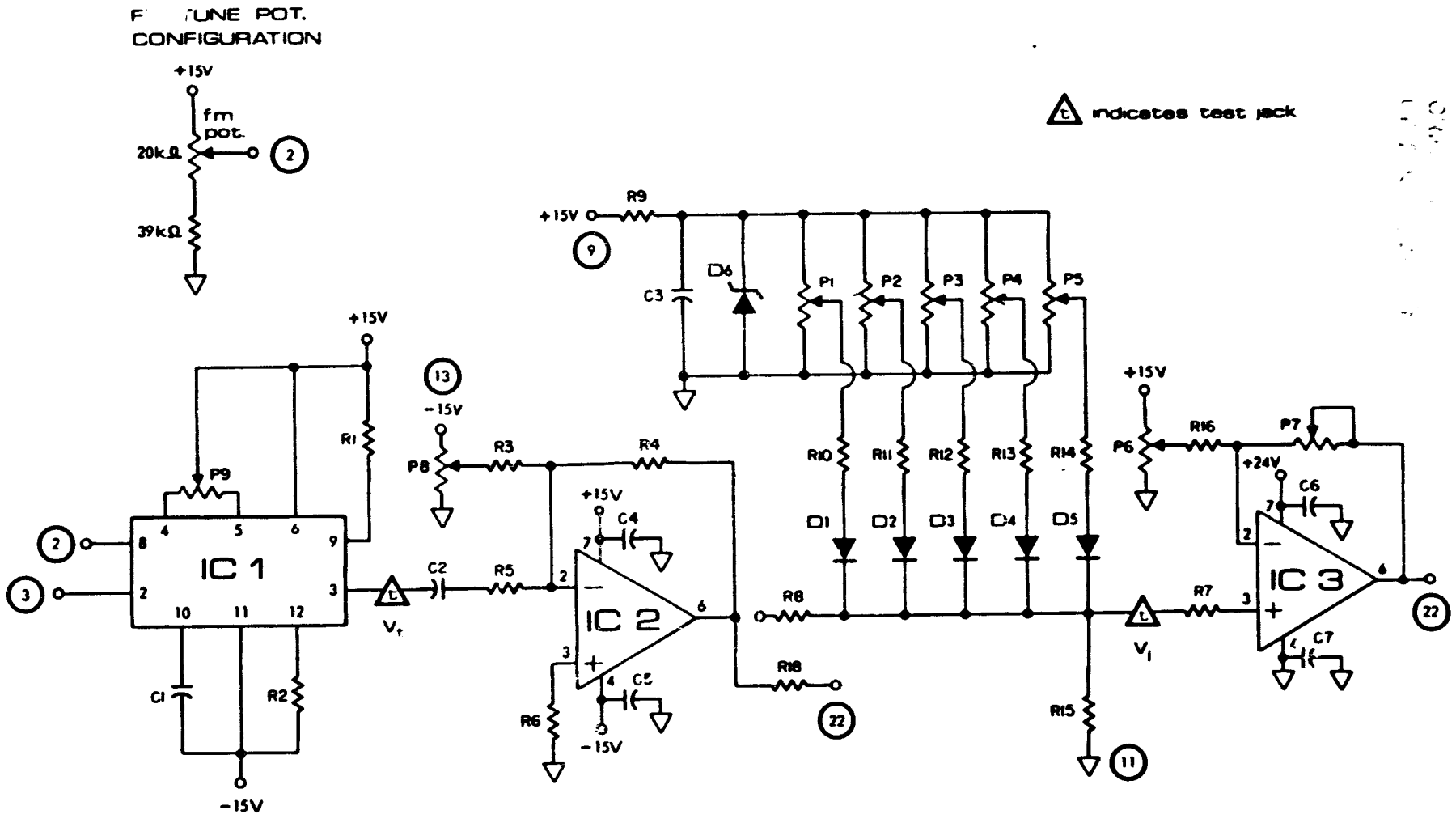

Figure B15. FM/linearizer schematic.

The triangle wave is fed into IC2, which scales it and adds an offset DC value. These two components of the tuning voltage have distinct functions that are worth mentioning. The offset determines the center frequency for the YIG oscillator. To operate at 10.2 GHz, the DC component of the tuning voltage should be equal to 5.08 V and is adjusted by P8. The AC component controls the RF bandwidth used in the system. This is not adjustable but a .327 V_{RMS} signal corresponds to 420 MHz of bandwidth. These levels should be checked periodically to insure proper operation and should be measured while being loaded by the oscillator. Measurements taken in an unloaded state will be faulty. P9 controls the triangle symmetry. Asymmetry will cause the IF spectrum to have a double peak and will make peaking more difficult.

Figure B15 shows the schematic and indicates pin outs and test points.

Control Board

The control board houses the integrator timing circuitry and the logic that drives the "RESET" and "DATA READY" LEDs.

IC1 is an analog timer whose time duration is set by the product R2 and C1, which are equal to R5 and C2 of the integrator circuitry. When PINS 2 and 3 are momentarily shorted, a logic high appears on PIN 9 for one timing interval. This signal is connected to the but PIN 18 and services the integrator through IC3 of that board.

IC2 and IC3 are simple gate packages that are configured to enable and disable certain commands from the console at the appropriate time.

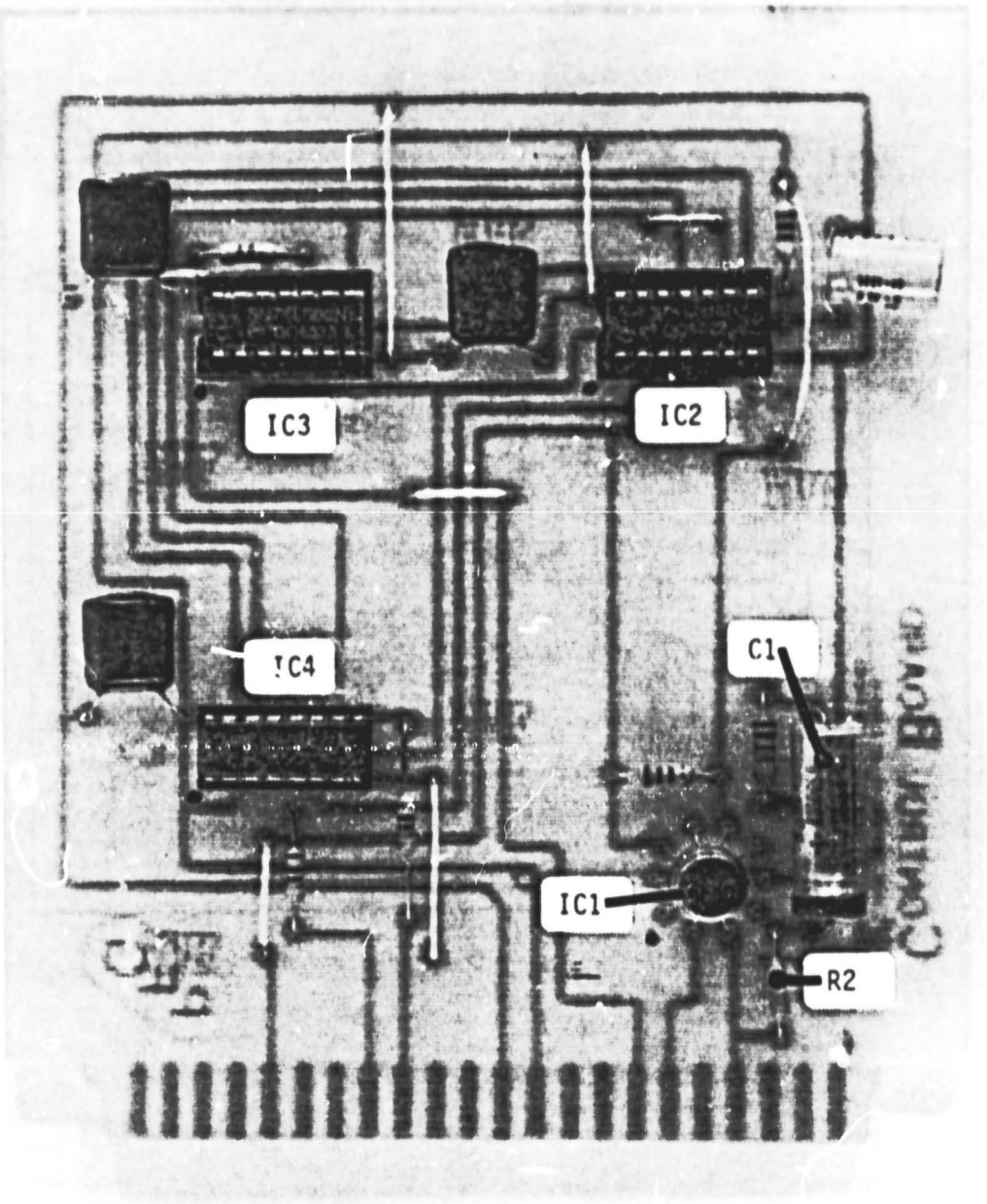

Figure B16. Control board layout.

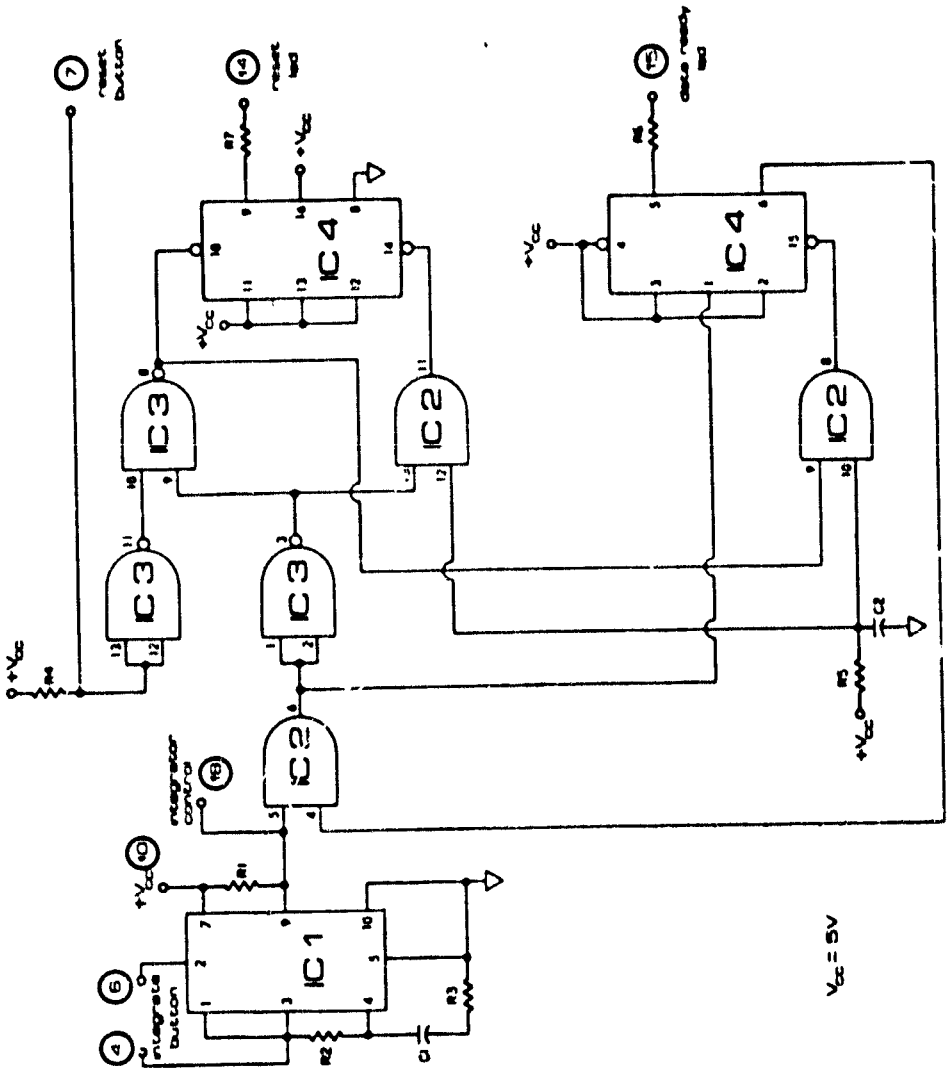

Figure B17. Control board.

IC4 is a dual J-K flip-flop that drives the small LEDs on the console's left side. Figure B16 shows the board and identifies components while Figure B17 shows the schematic.

Upon start-up of the system, IC1 will always cycle through one timing interval. For this reason, the first number displayed after power-up has no significant meaning.

Power Board

The function of this board is to provide a regulated 5 VDC source for all TTL components and protection for all mainframe-mounted cards connected to the ± 15 VDC supplies.

IC1 is a 1.5 A-regulator whose output is controlled by P1. Adjust P1 such that PIN 10 of the bus is 5.0 VDC. In the event this output should exceed 5 V by a moderate amount, Z1 begins to draw current in an attempt to bring the voltage down to the proper level. If the output continues to rise, Z1 will draw current until fuse F1 blows and opens this line. Z1 is a transient suppressor device and is configured here as protection against overvoltage.

Z2 and Z3 serve the same purpose for the -15 V and +15 V supply lines, respectively. Figure B18 shows all components and Figure B19 gives the schematic for this board.

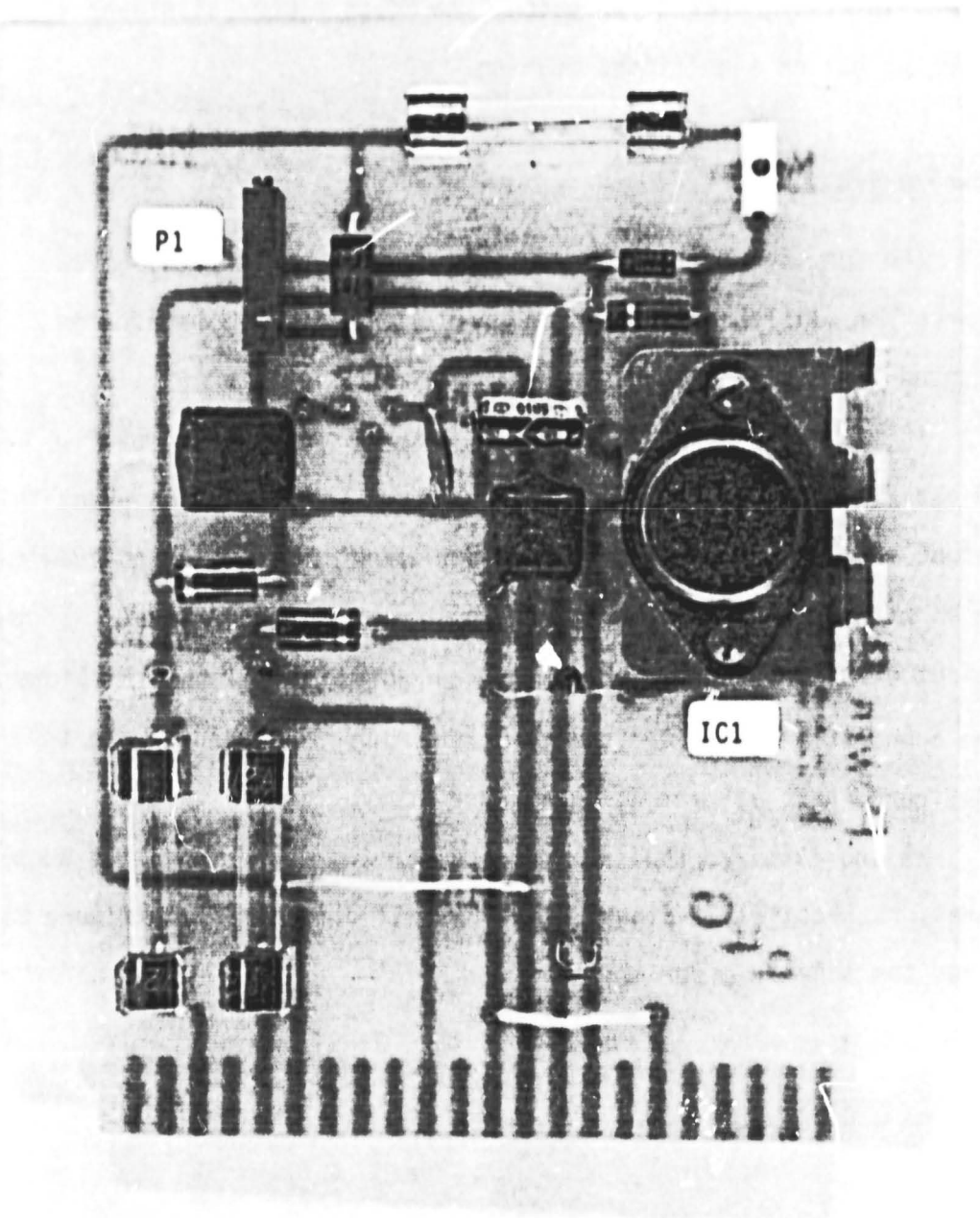

Figure B18. Power board layout.

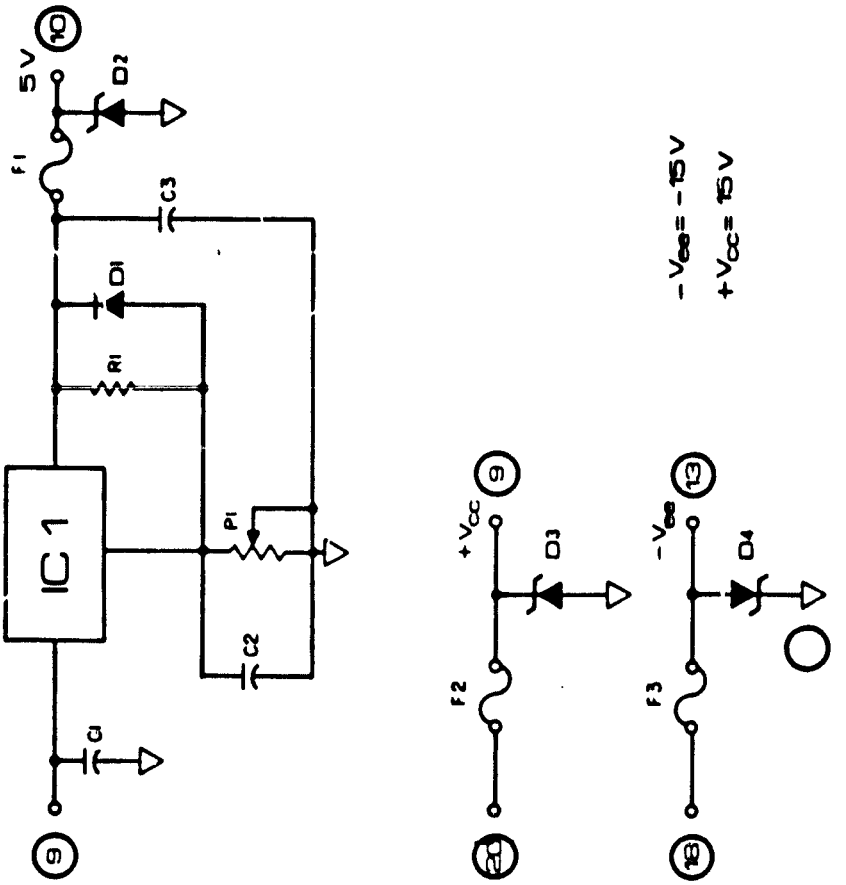

Figure B19. Power board.

PARTS LISTING

Bus Board

Edge connectors (6) Elco 22 pin	6022-022-938-002
PC test jacks (19) E.F. Johnson	105-0751-001 WHT

IF Amplifier

Transformer T1 Litton Triad -4 trad	SP-4		
IC's:			
IC1, IC2, IC3	TL071 CP	T.I. OP-AMP	
Resistors			
R1	10Ω		
R2, R3, R6	1.1KΩ	low noise	Dale
R4, R5	5.62KΩ	low noise	Dale
R7	6.8KΩ		
R8	5.6KΩ		
R9	27.4KΩ	low noise	Dale
R10 - R15	18Ω		
Capacitors:			
C1, C3, C7, C11	5pF	ceramic	
C2, C4, C6, C8, C10, C12	.1μF	polyester, 35V	
C5, C9	.22μF	polyester, 35V	
C13	.01μF	polyester, 35V	

Integrator/Dectector

IC's:

IC1	442L	RMS/DC Converter	ANALOG DEVICES
IC2, IC4	TL071	T.I. OP-AMP	
IC3	LF13333	Analog Switch	National
IC5	755N	Log Amplifier	ANALOG DEVICES

Resistors (¼ W):

R1	47KΩ
R2	22KΩ
R3, R7	9.1KΩ
R4	10Ω
R5, R6	330KΩ

Potentiometers:

P1, P4, P5	20KΩ	20 TURN	3005P	Bourns
P2	5KΩ	20 TURN	3005P	Bourns
P3	50KΩ	20 TURN	3005P	Bourns
P6	100KΩ	MODEL 70	20 TURN	Spectral

Capacitors:

C1, C3, C4, C5, C6	.1μF polyester, 35V
C2	10μF Type 630D Extralytic Sprague

Test jacks (3) 104-0751-001 EF Johnson

Signal Board

IC's:

IC1	LM2917N-8	National Freq/Voltage Converter
IC2, IC3	TL071CP	T.I. OP-AMP

Resistors: (¼ W)

R1	470Ω
R2, R4	100KΩ
R3, R7	56KΩ
R5	5.6KΩ
R6	3.9KΩ
R8	15KΩ
R9	9.1KΩ

Potentiometers:

P1, P2	20K	20 turn	3005P	Bourns
P3	50K	20 turn	3005P	Bourns

Capacitors:

C1	.22μF polyester, 35V
C2	1100pF ceramic
C3, C4, C5, C6	.1μF polyester, 35V

Test Point: (1) 105-0751-001 E.F. Johnson

FM/Linearizer Board

IC's:

IC1	ICL8038CC	Intersil Function Generator
IC2, IC3	TL071CP	T.I. OP-AMP

Resistors: (¼ W)

R1, R8, R15	100KΩ
R2, R5	82KΩ
R3, R5	10KΩ
R4	12KΩ
R7, R11	15KΩ
R9	1KΩ
R10	6.2KΩ
R12	56KΩ
R13	120KΩ
R14	220KΩ
R16	33KΩ
R18	2.2KΩ

Potentiometers:

P1	2KΩ	20 turn	3005P	Bourns
P2, P3, P6, P8	10KΩ	20 turn	3005P	Bourns
P4, P5, P9	50KΩ	20 turn	3005P	Bourns
P7	500KΩ	MODEL 70	20 turn	Spectrol

Capacitors:

C1	.02μF, ceramic
C2	1.0μF, tantalum, 35V
C3	10μF, electrolytic, 16V
C4, C7	.1μF, polyester, 35V

Diodes:

D1-D5	IN914
D6	IN5530 10V Zener

Control Board

IC's:

IC1	LM122H	Precision Timer	National
IC2	SN74LS08	Quad AND gate	
IC3	SN74LS00	Quad NAND gate	
IC4	SN74LS112	Dual J-K Flip-Flop	

Resistors: (¼ W)

R1	560Ω
R2	330KΩ
R3	100Ω
R4, R5	4.7KΩ
R6, R7	2.2KΩ

Capacitors:

C1	10μF	Type 630D Extralytic Sprague
C2	22μF	Electrolytic, 10V

Power Board

IC2	LM317K	Adjustable Regulator, National	
R1	220Ω	½ W	
P1	5K	20 turn	3005P Bourns

Capacitors:

C1, C3	1μF, tantalum 16V
C2	10μF, electrolytic 16V

Diodes:

D1	1N4001			
D2	ICTE-5	;D3,D4-ICTE-15	transzorb	International Rectifier

Fuses:

F1	1A	3AG	;F2, F3	2A	3AG

Control Box:

Enclosure		Type TV2157 Bud Box
Panel Meter		ICL 7106EV Intersil
Power Supply		540D-12/15 Standard Power
Bandpass Filter		522 22kc Case 30
		1k = Z_{in} = Z_{out} TT Electronics
LED Displays		5mA w/Mount Radio Shack
FM Pot.		20K 10 turn Bourns
Fuse Holder		Radio Shack
FMV & IF Connector		BNC Bulkhead Mount
Control Connector		MS TYPE 3102A-165-015
Switches		
ACT/CAL	SPDT	Radio Shack
DATA/PEAK	DPDT	Radio Shack
POL.	SPDT	Radio Shack
Display	DP3T	Radio Shack
Power	SPDT	LComp
Reset	momentary push button N.O.	
Integrate	momentary push button N.O.	

Power Inverter:
Model PV-400 Tripplite

Microwave Parts

ACT/Cal Switch
X-band Waveguide Switch, MDL, 90SR46-1E
X-band Transitions (3) MDL, 90AC86-1E
8.0 - 12.4 Gc YIG Tuned GaAs Oscillator WJ-5008-310DF Watkins-Johnson
1 - 18 Gc Double Balanced Mixer, RHG
4015C-10 10dB Coupler Narda
A31-8010 Isolator (2) Aertech
8.2 - 12.4 Gc Standard Gain Horn Scientific-Atlanta 12 - 8.2
Butt Cover, WR90 Waveguide MDL, F90BBC
Bronze Waveguide, WR90 MDL, WR90 90/10
Integrated Receiver Unit, Microwave Assoc., MA87127-1
IF Switch National Semiconductor, LF13333
Semi-Rigid Coax RG 402/W
30 cm Parabolic Reflector

OSM Plug Short	Omni Spectra	2021-1314-00
20 dB Attenuator	Omni Spectra	2082-6184-20
SMA Cable Plugs (5)	Omni Spectra	2001-5003-00
SMA Cable Jack (1)	Omni Spectra	2002-5015-00
RG-58 Cable Plug	Omni Spectra	2031-5002-00
Plug-to-Plug Adapter (3)	Pasternack	PE 9069
Plug-to-Jack Adapter (3)	Pasternack	PE 9068

APPENDIX C

C(R) PROGRAM AND DATA FORMS

The program SIGMA is used to calculate values of $C(R)_{VV}$ and $C(R)_{VH}$ for the generation of σ^{o} from experimental measurements. To use the program, only three DATA statements need be altered to calculate C(R) for any given angle. The procedure to make these changes as well as to document the results is outlined below.

Line 460 DATA ANGL/___./

This line declares the angle of incidence to be used. The value in the delimiters is a floating point number with Fortran format of F3.0.

Line 540 DATA NFM/ /

This line specifies the beginning FM rate value to be used for C(R) calculations. Since an interval of 145 hz is used, NFM is determined by finding the mean FM and subtracting 70 from it. The value in the delimiters in an integer number with format I3.

Line 550 DATA LFM/ /

This is similar to 540 in use except this specifies the last value of the FM rate to be used in the interval. It can be calculated LFM = NFM + 145. Again format is I3.

```
.LIST SIGMA

00100      PROGRAM TO CALCULATE C(R) FOR THE GENERATION
00200       OF SIGMA0 WHERE C(R) IS FOUND IN THE EQS.
00300
00400      FOR LIKE POL.
00470
00440                 SIGMA0(DB)=A-B*C(R)
00460
00480      FOR CROSS POL.
00500
00520                 SIGMA0(DB)=D+E*C(R)
00540
00560      WHERE:
00700          A=(POWER TARGET -POWER DELAY LINE)DB
00800          B=(POWER LENS-POWER DELAY LINE/DB
00900          D=(POWER TARGET(VH)-POWER TARGET(VV))/2
00940          E=SIGMA0 VV(DB)
00950
00980      C(R) TAKES ON TWO DISTINCT FORMS DEPENDING
00970          ON WHICH POLARIZATION IS USED.
00980
00990          FOR LIKE:
01000          C(R)=SIGMA(LENS)DB-10LOG(AREA ILLUM.)
01020              +40LOG(RANGE TARGET)-40LOG(RANGE LENS)
01050
01080          FOR CROSS:
01100          C(R)=10LOG(AREA ILLUM.(LIKE))-10LOG(AREA ILLUM.(CROSS))
01150              +DIFF
01180
01200                                  --P.F.GABEL
01300
01400      DEFINITION OF VARIABLES
01500
01600       NFM:  RADAR MODULATION RATE
01700       SIGL: SIGMA OF LUNEBERG LENS AT 10.25GC.
01800       RC:   RANGE TO LENS   SET AT 45 FEET
01900       RT:   RANGE TO TARGET
02000       AREA: RESULTANT AREA OF RADAR ILLUMINATION
02100       ANGL: INCIDENCE ANGLE IN DEGREES
02200       LFM:  LAST FM VALUE USED IN LOOP
02300       NFM:  FIRST FM VALUE USED IN LOOP
02400       DIFF: OFFSET CONSTANT BETWEEN LIKE AND CROSS POLS.(DB)
02500             (DUE TO GAIN & CONVERSION LOSS DIFF. IN 2ND MIXER)
```

```
0260C
0270C      ANTENNA VARIABLES
0280C
0290C       BWED:  E-PLANE 3DB BEAMWIDTH OF DISH
0300C       BWHD:  H-PLANE 3DB BEAMWIDTH OF DISH
0310C       BWEH:  E-PLANE 3DB BEAMWIDTH OF HORN
0320C       BWHH:  H-PLANE 3DB BEAMWIDTH OF HORN
0330C       GAIND: DISH ANTENNA GAIN(DB)
0340C       GAINH: HORN ANTENNA GAIN(DB)
0350C       NP:    POLARIZATION(VV=1 OR VH=2)
0360C      ANTENNA PARAMETERS ARE MEASURED AT 10.2GC.
0370C
0380C      BEGIN INITIALIZATION
0390C
0400       DIMENSION RT(30),JFM(30),CR(30),AREAL(2,30)
0410C
0420C      INPUT PARAMETERS
0430C
0440       DATA SIGL/6.7/
0450       DATA RC/45.0/
0460       DATA ANGL/30.0/
0470       DATA BWED/5.6/
0480       DATA BWHD/6.1/
0490       DATA BWEH/12.0/
0500       DATA BWHH/13.0/
0510       DATA GAIND/28.8/
0520       DATA GAINH/22.4/
0530       DATA DIFF/15.0/
0540       DATA NFM/270/
0550       DATA LFM/415/
0560C
0570       PI=3.1415927
0575       RANGL=ANGL
0576       ANGL=ANGL*PI/180.
0580C
0590C      BEGIN MAIN PROGRAM
0600C
0610C      BEGIN POLARIZATION LOOP  (VV=1,VH=2)
0620       DO 110 NP=1,2
0630       IF(NP.EQ.2) GO TO 10
0640C
0650C      CALCULATE ANTENNA MULTIPLICATION BEAMWIDTHS
0660C       USING THE GAUSSIAN APPROXIMATION
0670C       LIKE -POL. HERE
0680       BETAE=(BWED/(SQRT(2)))*PI/180.
0690       BETAH=(BWHD/(SQRT(2)))*PI/180.
```

```
0700        GO TO 20
0710C
0720C       CROSS-POL. HERE
0730   10   BETAE=(SQRT((BWEH**2)*(BWHD**2)/
0740      $       (BWEH**2+BWHD**2)))*PI/180.
0750        BETAH=(SQRT((BWHH**2)*(BWED**2)/
0760      $       (BWHH**2+BWED**2)))*PI/180.
0770   20   CONTINUE
0780C
0790C       BEGIN FM RATE LOOP, CALC. RANGE AND AREA
0800        I=0
0810        DO 30 MFM = NFM,LFM,5
0820         I=I+1
0830         JFM(I)=MFM
0840C
0850C       ENTER CURRENT RANGE EQUATION (5/6/81)
0860        RT(I)=3423.5/MFM-0.106
0870C
0880C       CALCULATE HEIGHT OF ANTENNA(METERS)
0900        HT=RT(I)*COS(ANGL)
0910C
0920C       CALC. AREA OF RADAR ILLUMINATION
0930        XTANBE=(SIN(BETAE/2.))/(COS(BETAE/2.))
0940        XTANBH=(SIN(BETAH/2.))/(COS(BETAH/2.))
0950        COSTHE=COS(ANGL)
0960        SINTHE=SIN(ANGL)
0970        B=(HT*XTANBH)/COSTHE
0980        A=(HT*XTANBE)/COSTHE
0990        YY=(HT*HT-A*A*SINTHE*SINTHE)
1000        CAPB=SQRT((HT**4)*(XTANBH**2)/(((COSTHE**2)*YY)))
1010        CAPA=A*HT*HT/(COSTHE*YY)
1020        AREA=PI*CAPA*CAPB
1030        AREAL(NF,I)=10*(ALOG10(AREA))
1040        RANGET=40*(ALOG10(RT(I)))
1050        RANGEL=40*(ALOG10(RC*12./39.37))
1060       CR(I)=SIGL-AREAL(NF,I)+RANGET-RANGEL
```

```
1070  30   CONTINUE
1080C
1090C      BEGIN HEADER OUTPUTTING
1100       WRITE(6,40)RANGL
1110  40   FORMAT(5X,"INCIDENCE ANGLE : ",F3.0)
1120C
1130C      TEST FOR VV OR VH POLARIZATION
1140       IF(NP.EQ.1) GO TO 70
1150C
1160C      ADD CONVERSION/GAIN CONSTANT TO THE
1170C         CALC. VALUES OF VH C(R).
1180       DO 50 K=1,30
1190       CR(K)=AREAL(1,K)-AREAL(2,K)+DIFF
1200  50   CONTINUE
1210C
1220       WRITE(6,60)
1230  60   FORMAT(5X,"POLARIZATION:VH"///)
1240       GO TO 90
1250  70   WRITE(6,80)
1260  80   FORMAT(5X,"POLARIZATION:VV"///)
1270  90   WRITE(6,100)((RT(I),JFM(I),CR(I),RT(I+15),
1280      $            JFM(I+15),CR(I+15)),I=1,15)
1290 100   FORMAT(5X,"C(R) AS A FUNCTION OF FM RATE"/
1300      $       5X,"RANGE(M)",3X,"FM RATE",3X,"C(R):(DB)",
1310      $       5X,"RANGE(M)",3X,"FM RATE",3X,"C(R):(DB)"/
1320      $       15(6X,F6.2,5X,I3,6X,F7.2,7X,F6.2,7X,I3,4X,F7.2/)///)
1330 110   CONTINUE
1340       STOP
1350       END
```

LIKE POLARIZATION SIGMA-0

$A = P_{tar}(dB) - P_{dl}(dB)$ $B = P_{lens}(dB) - P_{dl}(dB)$ C(R) = TABLE VALUE

FIELD	DATE	ANGLE	A	-	B	+	C(R)	=	SIGMA-0(VV)

CROSS POLARIZATION SIGMA-O

$D = P_{tar}VH(dB) - P_{tar}VV(dB)$ E = SIGMA-O VV(dB) C(R) = TABLE VALUE

FIELD	DATE	ANGLE	D	+	E	+	C(R)VH	=	SIGMA-O(VH)

SKY NOISE TEST

DATE

CAL FM _____ P_{dl} _____

		P_{VV}	P_{VH}
30 FM	_____	_____	_____
40 FM	_____	_____	_____
50 FM	_____	_____	_____
60 FM	_____	_____	_____
70 FM	_____	_____	_____

LENS SET TEST

DATE

CAL FM _____ P_{dl} _____

RANGE = 45 FEET

FM	P_{VV}	P_{VH}
_____	_____	_____
_____	_____	_____

AVERAGE:

P_{VV} = _____

P_{VH} = _____

($P_{VV} = P_{lens}$)

SKY NOISE TEST

DATE

CAL FM _____ P_{dl} _____

		P_{VV}	P_{VH}
30 FM	_____	_____	_____
40 FM	_____	_____	_____
50 FM	_____	_____	_____
60 FM	_____	_____	_____
70 FM	_____	_____	_____

LENS SET TEST

DATE

CAL FM _____ P_{dl} _____

RANGE = 45 FEET

FM	P_{VV}	P_{VH}
_____	_____	_____
_____	_____	_____

AVERAGE:

P_{VV} = _____

P_{VH} = _____

($P_{VV} = P_{lens}$)

APPENDIX D

BANDPASS FILTER RESPONSE

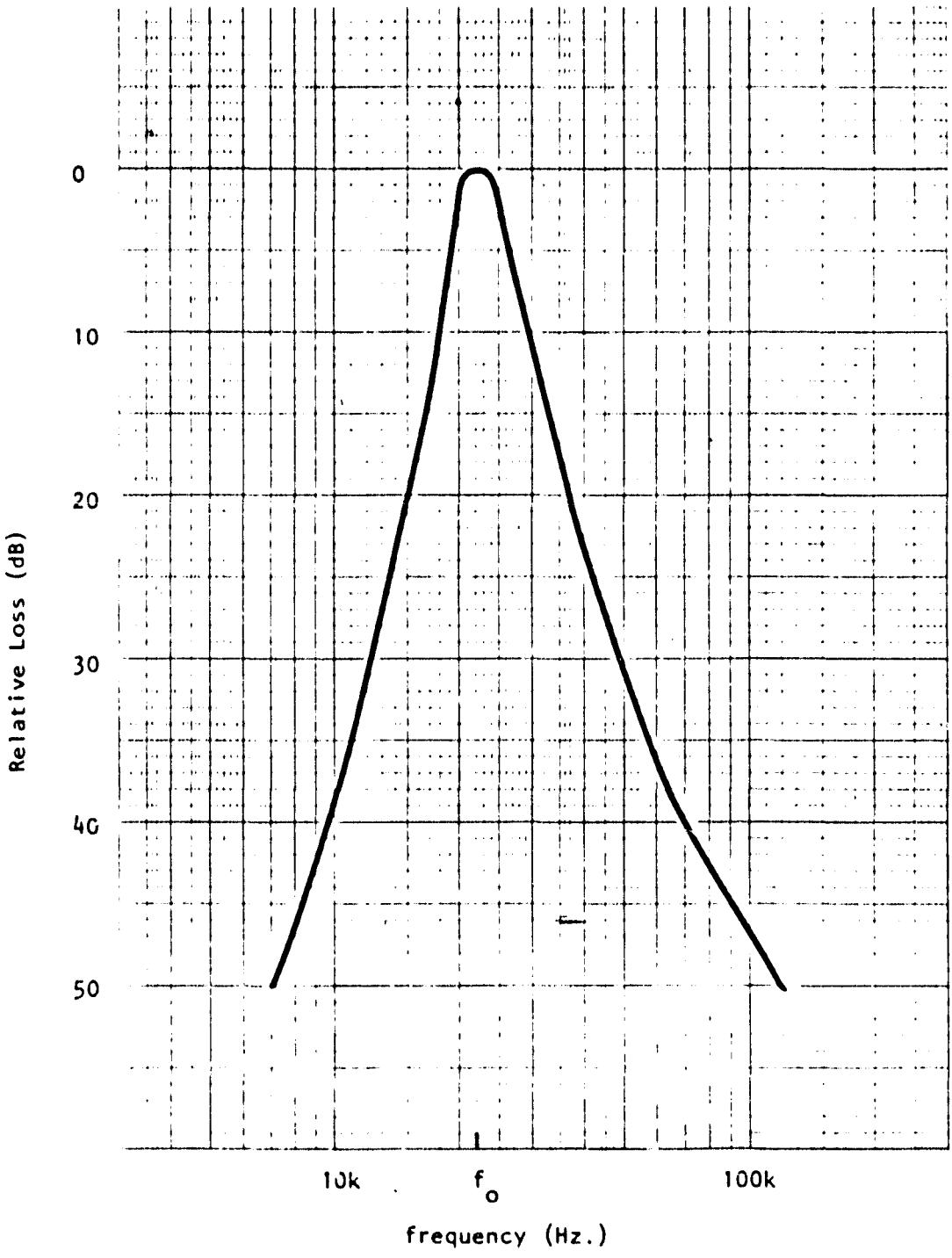

Figure D1. Bandpass filter response with load impedance = 2.2KΩ.

APPENDIX E

CABLE AND CONNECTOR SETS

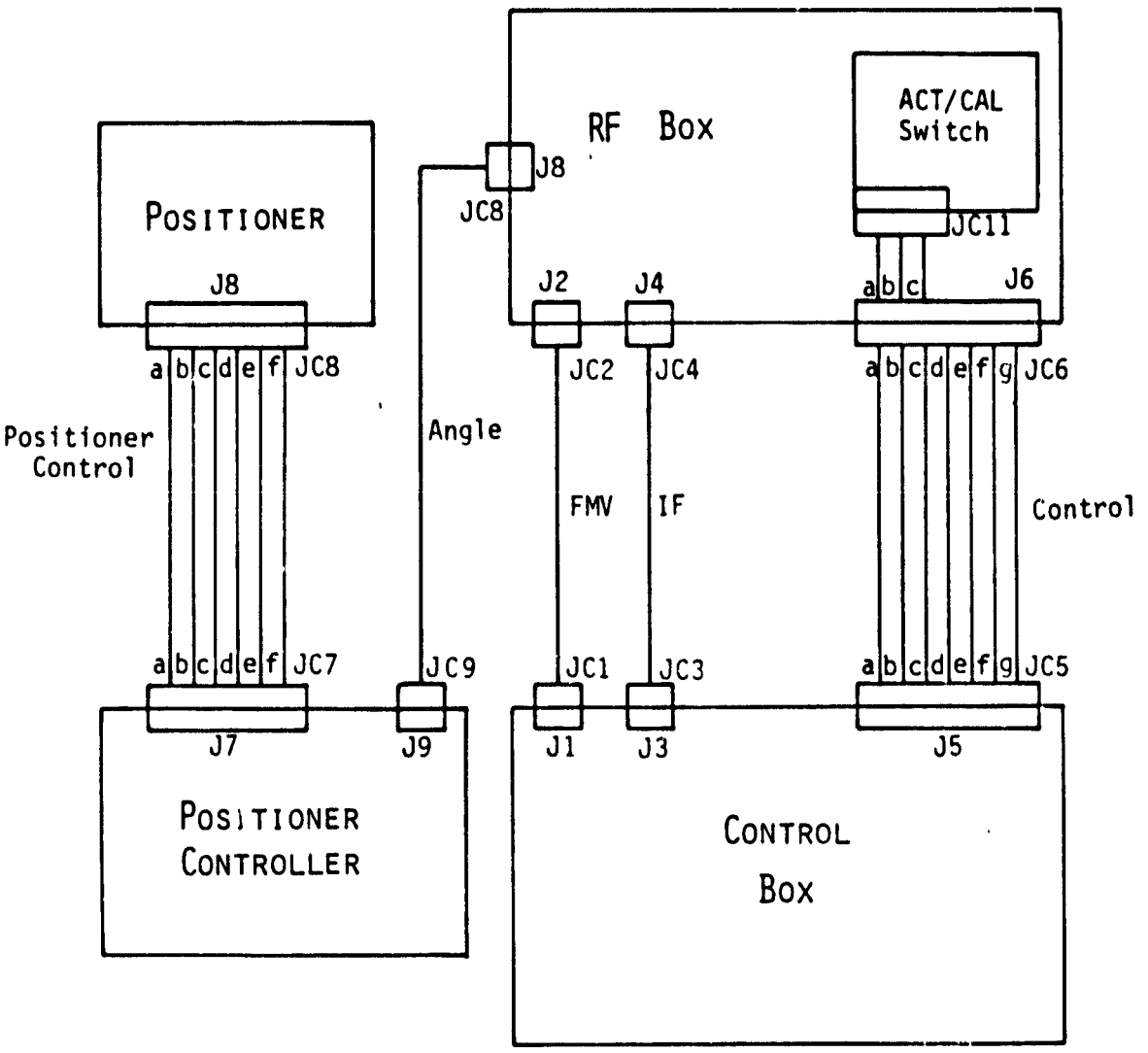

Figure E1: MARS cable diagram.

GENERAL SET LISTING

RF Box/Control Box Cable Set

Control End Connector	Name	Type	RF End Connector
JC1	FMV	RG-58	JC2
JC3	IF	RG-58	JC4
JC5	CONTROL	8 CONDUCTOR 20 GA.	JC6

Positioner/Controller Cable Set

Controller End Connector	Name	Type	Positioner End Connector
JC7	POSITIONER CONTROL	8 CONDUCTOR 20 GA.	JC8
JC9	ANGLE	RG-58	JC10

Waveguide Switch Cable

Name	Type	Switch Connector
ACT/CAL.	3 CONDUCTOR 18 GA. SHIELDED	JC11

Cable Functions and Connector Types

Control Cable Pin	Function
A	Act/Cal Com. (110 VAC)
B	Act/Cal Cal. (110 VAC)
C	Act/Cal Act. (110 VAC)
D	Like/Cross IF
E	+ 15V DC
F	- 15V DC
G	Ground
JC5	MS 7 PIN Male 3106A - 16S - 01P
JC6	MS 7 PIN Female 3106A - 16S - 01S

Act/Cal Cable Pin	Function
A	Com. (110 VAC)
B	Cal. (110 VAC)
C	Act. (110 VAC)
JC11	Bendix Twist-Lock PT06A - 10 - 6S (SR)

Positioner Control Cable

Pin	Function
A	(YEL) Line Voltage (50 VAC)
B	(RED) Direction
C	Limit Override
D	Limit Override
E	(BL) Field Winding
F	(BLK) Field Winding
JC7	MS 6 PIN Male 3106A - 14S - 06P
JC8	MS 6 PIN Female 3106A - 14S - 06S

FMV Cable

JC1, JC2	BNC Male, King Corp. KC - 59 - 291

IF Cable

JC3, JC4	BNC Male, King Corp. KC - 59 - 291

Angle Cable

JC9, JC10	BNC Male, King Corp. KC - 59 - 291

APPENDIX F

POSITIONER/CONTROLLER

Positioner and Controller/Indicator Units

It was decided that a positioning unit for antenna angular adjustment with a remote controller and indicator would ease the data-collection process. However, a positioner costing several hundred dollars would not follow the economic trend established for this system. Using spare parts and a simple pulley-and-belt drive system, the positioner shown in Figure F1 was designed and built. Absolute accuracy is about 1.5°, which is acceptable when dealing with vegetation in the 30° - 70° interval. Mr. Dennis Anderson of the Remote Sensing Lab is credited with the design and construction of this positioner.

The heart of this unit is a motor whose direction of rotation is alterable by switching two field windings. Switch S2 controls the direction of rotation. A 1732:1 gearbox allows for proper rotation speed but was deemed slightly fast so a further reduction of 2:1 pulleys was installed. Thus the overall speed reduction of 3464:1 works well.

Limit switch S3 was installed to prevent possible damage to cables or antennas due to operator neglect. In the event a limit is encountered, switch S1 can be used to override S3 and to bring the antennas back into the normal operating range.

Transformer T1 serves as another means to slow the motor down and allow for reasonable rotation speed.

The angle indicator is comprised of a calibrated current meter, a potentiometer, and a pendulum. As the positioner rotates the antennas, the pendulum, which is mounted on the RF box, causes the potentiometer to rotate and the center tap voltage to vary. Resistors R1 and R2 are fixed to change this voltage into a current that is within the operating range of the meter. The meter, S1, and S2 are

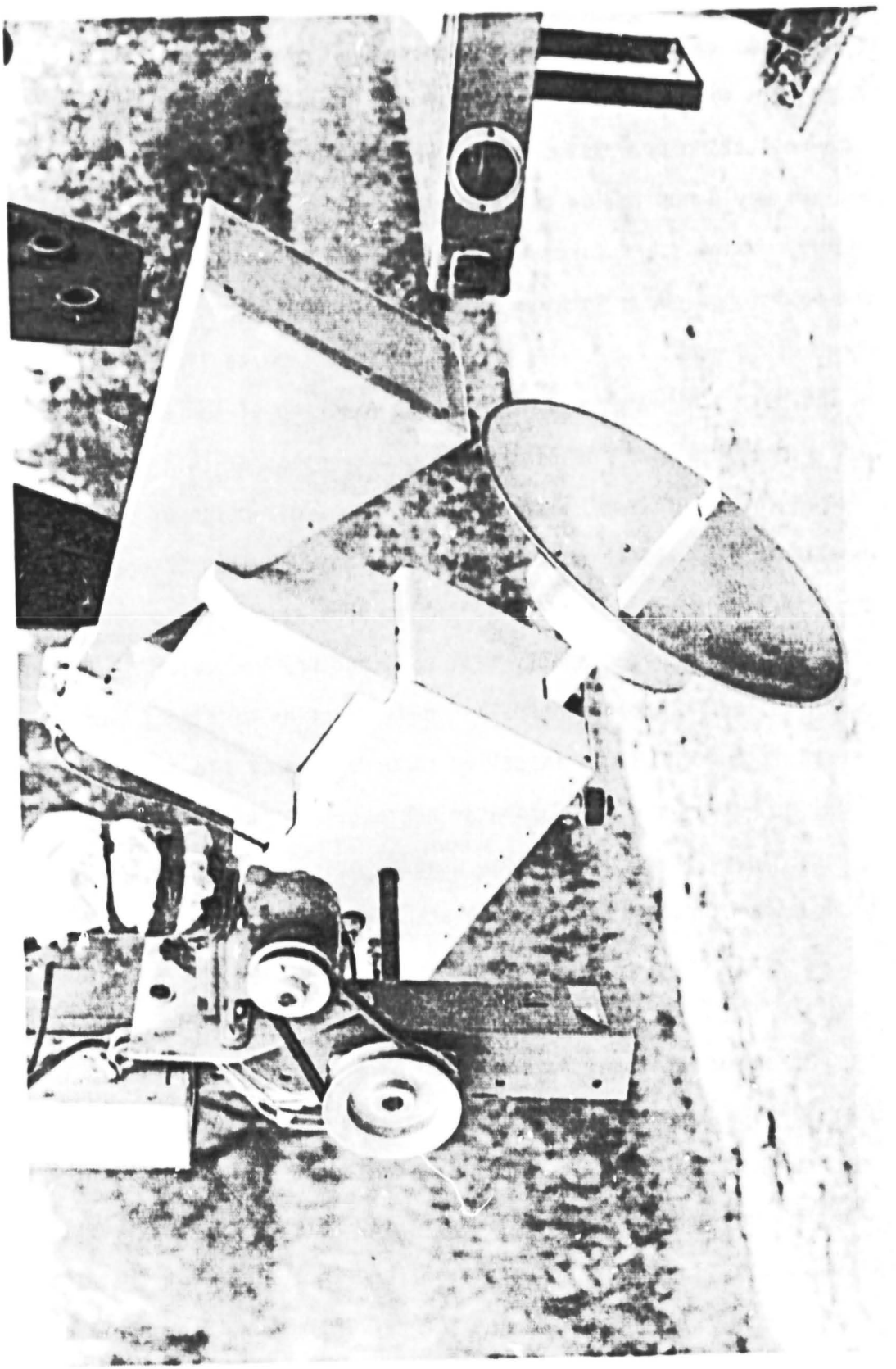

·Figure F1. RF positioning unit.

are mounted in a hand-held unit such that remote operation from the truck cab is possible. Figure F2 shows the positioner and indicator schematic.

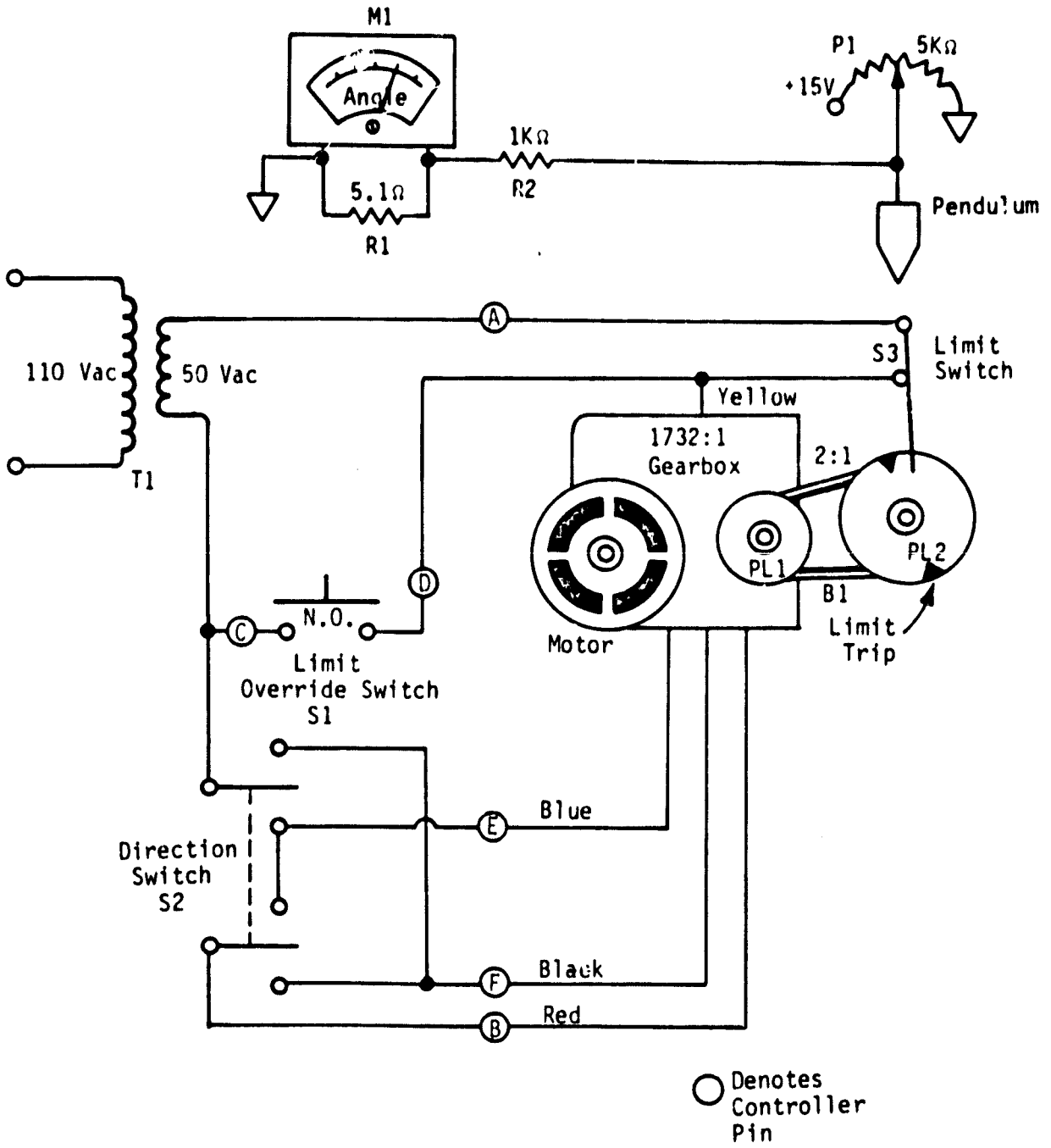

Figure F2: Positioner and angle indicator schematic.

APPENDIX G

COST ANALYSIS

RF Subsystem Cost

Antennas:	
Standard Gain Horn and Transition	357.00
Double Dipole Feed, Reflector and Flange	48.50
10 hours labor (tech.)	
Oscillator:	2,070.00
Microwave Components:	
Mixer (Double Balanced)	250.00
Isolators (2)	338.00
10 dB Coupler	179.00
Waveguide Switch X-band WR90	545.00
Transitions (2)	184.00
20 dB Attenuator	35.00
Integrated Receiver	55.00
Miscellaneous:	
IF Switch	6.00
SMA Plug-to-Plug Adapters (3)	23.85
SMA Plug-to-Jack Adapters (3)	33.40
SMA Cable Plugs (5) (.141)	16.25
SMA Cable Jack (.141)	4.75
SMA Short .141	5.95
SMA RG-58 Cable Plug	6.00
5.5 m .141 Semi-Rigid Coaxial Cable	27.00
Chassis (RF Box)	15.00
16 hours labor (tech.)	
	$4,199.30

IF/Controller Subsystem Cost

Control Box:

Enclosure	32.21
Panel Meter	34.45
Power Supply	65.00
Switches	21.00
Connectors	14.25
LED Displays	1.99
FM Pot.	12.25
Fuse Holder and Line Cord	5.00
Bandpass Filter and Mount	97.00
	$283.15

Bus Board:

Connectors	30.66
Test Jacks	3.99
Hardware	2.00
P.C. Board	20.00
	$ 56.65

IF Amplifier:

Connector	4.99
Components	25.50
P.C. Board	4.89
	$ 35.38

Integrator/Detector:

RMS/DC Converter	184.00
Log Amplifier	69.00
Components	28.50
P.C. Board	6.15
	$287.15

Signal Board:

Components	15.50
P.C. Board	4.89
	$ 20.39

FM/Linearizer Board:	
Components	40.18
P.C. Board	4.89
	$ 45.07
Power Board:	
Components	19.00
P.C. Board	4.89
	$ 23.89
Control Board.	
Components	13.67
P.C. Board	4.89
	$ 18.56
Cable Assemblies:	
FMV	11.50
IF	11.50
Control	13.70
Positioner Control	13.35
Angle	11.50
Act/Cal	23.00
	$ 84.55
Total IF/Controller Construction Cost	$855.29
24 hours labor (tech)	
16 hours tuning (eng.)	
Positioner:	
Indicator Unit	13.75
Motor/Gearbox	135.00
Hardware	18.00
	$166.75
Power Inverter:	$119.00
SYSTEM TOTAL	$5,340.70

* U.S. GOVERNMENT PRINTING OFFICE 1982—869-011/47